The functional blood platelet and its biogenesis: Biochemical and cell biological analysis of thrombopoiesis in vitro, in situ and in vivo

Dissertation zur Erlangung des akademischen Grades des
Doktors der Naturwissenschaften (Dr. rer. nat.)

eingereicht im Fachbereich Biologie, Chemie, Pharmazie
der Freien Universität Berlin

vorgelegt von

IMKE MEYER
aus Solingen

Berlin, September 2012

Die vorliegende Arbeit wurde von Februar 2009 bis September 2012 unter der Leitung von PD Dr. Harald Schulze im Labor für Pädiatrische Molekularbiologie der ehemaligen Klinik für Allgemeine Pädiatrie, Charité – Universitätsmedizin Berlin angefertigt.

1. Gutachter/in: Prof. Petra Knaus
2. Gutachter/in: PD Dr. Harald Schulze
Disputation am: 04. Februar 2013

„Es wird ja fleißig gearbeitet und viel mikroskopiert, aber es müsste mal wieder einer einen gescheiten Gedanken haben.“

Rudolf Virchow (1821 - 1902)

Acknowledgements

An dieser Stelle möchte ich allen danken, die zum Gelingen dieser Arbeit beigetragen haben.

Herrn PD Dr. Harald Schulze danke ich für das Überlassen und die erstklassige Betreuung eines breiten und nach wie vor spannenden Promotionsthemas, dessen Produktivität nie gedachte Formen angenommen hat.

Silke Schwiebert gilt mein besonderer Dank für ihre tatkräftige Unterstützung, den Rückhalt in jeder Labor- und Lebenslage und die ausgezeichnete Zusammenarbeit. Bei Stefan Kunert möchte ich mich nicht nur für die Hilfe und Zusammenarbeit, sondern auch für die daraus entstandene Freundschaft bedanken.

Meinen herzlichsten Dank möchte ich außerdem Janine Fiedler, Sarah Kottnik und Katja Henning ausdrücken: Für eine unvergessliche Zeit im und außerhalb des Labors. Für fachliche und produktive Diskussionen, sowie besonders für die, die es nicht waren!

Den Mitarbeitern des LPMB unter Leitung von Professor Dr. Christian Hagemeier danke ich für das fröhliche Arbeitsklima, spannende Tipp-Spiele und den ein oder anderen Kuchen.

Allen Mitarbeitern der AG Hauser am DRFZ möchte ich für ihre Hilfsbereitschaft danken. Insbesondere Frau Professor Dr. Anja Hauser, für fachliche Diskussionen und Anregungen, Motivation und zunehmende Begeisterung für riesige, autofluoreszente Zellen. Katrin Roth danke ich für die Einführung am Mikrotom und 2-Photonen-Mikroskop und für eine tolle Zusammenarbeit, die ihresgleichen sucht. Sandra Zehentmeier danke ich nicht nur für die fachlichen Diskussionen und Anregungen. Bei Dr. Raluca Niesner möchte ich mich für die Hilfe am 2-Photonen-Mikroskop und bei den Auswertungen bedanken. Außerdem ein großes Dankeschön für die lehrreichen biophysikalischen Erklärungen.

Professor Dr. Bernhardt Nieswandt, Dr. Ina Hagedorn und Dr. Sebastian Dütting, des Rudolf-Virchow-Zentrums in Würzburg, danke ich für spannende und produktive Kollaborationen und einen immer wieder stimulierenden Austausch.

PD Dr. Oliver Meyer danke ich für die Zusammenarbeit und für die klinische Sicht der Dinge, sowie für die Organisation und Bereitstellung von Patientenmaterial.

Für die Übernahme des Koreferats und die Organisation der Dokrorandensymposien, die immer wieder angeregt und motiviert haben, möchte ich mich herzlich bei Frau Professor Petra Knaus bedanken.

Patrick, dessen Geduld endlos scheint, danke ich für „Web- und Life-Administration“. Vielen Dank für alles!

Index

Acknowledgements I

Glossary VI

1. Introduction 1

1.1. Megakaryocyte origin and fate 1

1.1.1. Hematopoiesis 1

1.1.2. From hematopoietic stem cell to megakaryocytes: megakaryopoiesis 2

1.1.3. Thrombopoiesis - the terminal differentiation step 3

1.2. Blood platelets 3

1.3. Platelet intrinsic factors sustaining platelet function 4

1.3.1. The role of β1-tubulin cytoskeleton in platelet formation and activation 4

1.3.2. Identification and characterization of RanBP10 a β1-tubulin binding protein 5

1.3.3. Platelet signaling in thrombus-formation 5

1.3.4. Platelet function tests 8

1.4. Extrinsic factors influencing megakaryocyte biology in BM 9

1.4.1. The bone marrow niche concept 10

1.4.2. Immune thrombocytopenia modeling bone marrow dynamics 11

1.4.3. Visualization of in vivo MK-dynamics in BM 12

1.5. Specific aims 15

2. Materials and Methods 16

2.1. The microtubule modulator RanBP10 plays a critical role in regulation of platelet discoid shape and degranulation 16

2.1.1. Mouse husbandry, MK culture, and 5-bromo-4-chloro-3-indolylbeta-D-galactopyranoside (X-Gal) staining 16

2.1.2. Reverse transcription–polymerase chain reaction, polymerase chain reaction, cloning, and sequencing 16

2.1.3. Antiserum, platelet activation, and immunoblot analysis 17

2.2. Altered microtubule equilibrium and impaired thrombus stability in mice lacking RanBP10 17

2.2.1. Animal husbandry 17

2.2.2. Megakaryocyte ploidy and immunohistochemistry 17

2.2.3. Gene expression quantification via real-time PCR 18

2.2.4. Platelet isolation and analysis 18

2.2.5. Flow-chamber, platelet spreading and in vivo thrombus formation 19

2.2.6. Mepacrine assay, Modified Tubulins, Aggregometry and dense granule release 20

2.2.7. Statistical analysis 21

2.3. Effect of an anti-GPIb-platelet antibody on bone marrow megakaryocytes in a mouse model of passive immune thrombocytopenia 21

2.3.1. Animal husbandry 21
2.3.2. Platelet depletion and hemograms 21
2.3.3. Tissue preparation and staining 21
2.3.4. Apoptosis detection assay 22
2.3.5. Multiphoton Microscopy 22

2.4. Future directions: Development of a MK BM atlas 23

2.4.1. Preparation, staining and analysis of cryosections 23
2.4.2. Fetal liver cell culture 23
2.4.3. BSA-gradient enriched MKs 24
2.4.4. Flow cytometry 24
2.4.5. Adhesion experiments 24
2.4.6. Proplatelet formation assay 25
2.4.7. Zymography 25

3. Results and Discussions 27

3.1. RanBP10 27

3.1.1. The microtubule modulator RanBP10 plays a critical role in regulation of platelet discoid shape and degranulation 27
3.1.1.1. In vivo disruption of RanBP10 by gene trap 27
3.1.1.2. MT filaments in MKs from RanBP10-null mice 28
3.1.1.3. RanBP10 ablation leads to reduced proplatelet-forming MKs 28
3.1.1.4. Loss of RanBP10 results in a disordered platelet marginal band 30
3.1.1.5. Defective hemostasis, platelet activation, and aggregation in RanBP10-deficient mice 31
3.1.2. Altered microtubule equilibrium and impaired thrombus stability in mice lacking RanBP10 33
3.1.2.1. RanBP10 depletion is partially compensated for by overexpression of RanBP9 33
3.1.2.2. Slightly altered platelet adhesion under shear and normal spreading 35
3.1.2.3. Thrombus formation is impaired in RanBP10-/- mice 37
3.1.2.4. RanBP10 is not essential for δ-granule number, composition or release but for platelet shape change 39
3.1.2.5. RanBP10 is crucial for marginal band contraction after platelet activation 42
3.1.2.6. RanBP10 modulates the tubulin-equilibrium 43
3.1.3. Discussion 46

3.2. Effect of an anti-GPIb-platelet antibody on bone marrow megakaryocytes in a mouse model of passive immune thrombocytopenia 49

3.2.1. Diametral affect of platelet depletion on MK homeostasis 49
3.2.2. The depletion antibody decorates MKs in BM and does not lead to apoptosis 51

3.2.3. Studies on MK proliferation after platelet depletion 53
3.2.4. Antibody decorated MKs give birth to pro- and pre-platelets 56
3.2.5. Discussion....59

3.3. Future directions: Development of a MK BM atlas....62

3.3.1. Identification and distribution of BM MKs in situ....63
3.3.2. In situ distribution of BM ECMs and factors of the vascular BM niche 65
3.3.3. MKs are embraced by collagen IV and fibronectin fibers in situ 67
3.3.4. MKs in direct agonist contact express both collagen receptors 67
3.3.5. MKs adhere best in vitro onto ECMs of the vascular niche 69
3.3.6. MK adhesion on ECMs supports PPF 70
3.3.7. MMP2 and MMP9 are not active in MKs when seeded on ECM coated dishes 73
3.3.8. Summary....74
3.3.9. Future perspectives: Do different ECMs influence MK migration in vitro 75

4. Abstract 76

5. Zusammenfassung....77

6. References 79

7. Appendix VIII

7.1. Eidesstattliche Erklärung VIII

7.2. Curriculum Vitae....IX

Glossary

This abbreviation index contains no SI or therefrom derived units. The time units seconds, minutes and hours are abbreviated as sec, min, hrs respectively. Scientifically usual abbreviations are not indicated and plural forms are labelled by a suffixed „s“.

ADP	Adenosine diphosphate
ATP	Adenosine triphosphate
BM	Bone marrow
BMP	Bone morphogenetic protein
BSA	Bovine serum albumin
c-Mpl	Myeloproliferative leukemia virus proto-oncogene (TPO receptor)
CD	Cluster of differentiation
CLP	Common lymphoid progenitor
CMP	Common myeloid progenitor
COX	Cyclooxygenase
CXCL12	Chemokine (C-X-C motif) ligand 12
CXCR4	Chemokine (C-X-C motif) receptor 4
DMEM	Dulbecco‘s Modified Eagle Medium
ECM	Extracellular matrix molecule
EdU	5-ethynyl-2'deoxyridine
EHS	Engelbreth-Holm-Swarm
FcRγ	Fragment, crystallizable region receptor gamma
FGF-4	Fibroblast growth factor 4
FITC	Fluorescein isothiocyanate
GEF	Guanine nucleotide exchange factor
GMP	Granulocyte-macrophage progenitor
GP	Glycoprotein
GPCR	G protein coupled receptor
HSC	Hematopoietic stem cell
IF	Immunofluorescence
ITP	Immune Thrombocytopenia
LT-HSC	Long-term hematopoietic stem cell
MAP	Microtubuli associated protein

MEP	Myeloid-erythroid progenitor
MK	Megakaryocyte
MPM	Multiphoton microscopy
MSC	Mesenchymal stem cell
MT	Microtubule
PAR	Protease-activated receptor
PBS	Phosphate buffered saline
PCR	Polymerase chain reaction
PF4	Platelet factor 4
PFA	Paraformaldehyde
PMSF	Phenylmethylsulfonylfluorid
PPF	Proplatelet formation
PRP	Platelet rich plasma
RanBP10	Ran binding protein 10
SCID	Severe combined immunodeficiency
SHG	Second harmonic generation
SLPI	Secretory leukocyte protease inhibitor
TPO	Thrombopoietin
TPR	Thromboxane receptor
TXA2	Thromboxane A2
VEGF-A	Vascular endothelial growth factor A
vWF	Von Willebrand factor
x-gal	5-bromo-4-chloro-indolyl-β-D-galactopyranoside

1. Introduction

1.1. Megakaryocyte origin and fate

1.1.1. Hematopoiesis

Most somatic cells including differentiated blood cells are limited in their life span. Blood cells are mainly short lived and thus need to be replenished perpetually to sustain their population. They derive out of rare precursors so called hematopoietic stem cells (HSCs).[1] Whereas in adolescent mammals HSCs are located in their stem cell niche in the bone marrow, the localization during ontogenesis is highly dependent on the developmental stage. During the murine embryonic development HSCs circulate from the ventral mesoderm via the yolk sac, aorta-gonad mesonephros and placenta towards the fetal liver and thymus.[2,3] After birth they finally reach quiescence in the BM. HSCs can be classified into the most primitive precursor, the pluripotent long-term HSCs (LT-HSC, Figure 1) with the ability of self-renewal and the more developed multipotent short-term HSCs which are direct precursors of the lymphoid and myeloid progenitor cells: common myeloid and common lymphoid progenitors (CMP and CLP). In the myeloid lineage they further differentiate into the megakaryocyte/erythrocyte progenitors (MEPs) or the granulocyte/macrophage progenitors (GMPs). In the lymphoid lineage the activation of specific transcription factors leads to a direct development of B- and T-lymphocytes out of the CLP (Figure 1). Myeloid progenitor cells can be characterized in vitro by their developmental potency in clonal assays on semisolid media.[4,5]

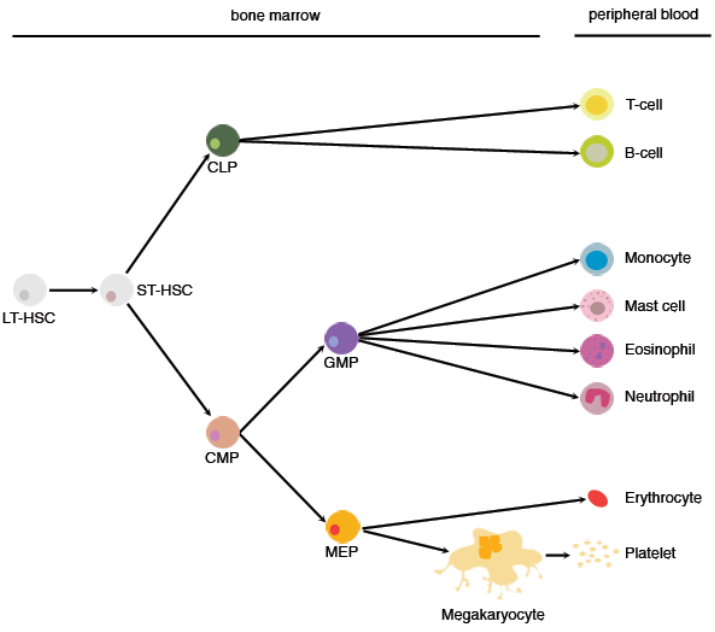

Figure 1 - Hematopoiesis Model. Lymphoid (CLP) and myeloid (CMP) progenitors derive out of HSCs in the BM and differentiate to mature blood cells. Abbreviation index: Long-term HSC (LT-HSC), short-term HSC (ST-HSC), granulocyte/macrophage progenitor (GMP), megakaryocyte/erythrocyte progenitor (MEP).

1.1.2. From hematopoietic stem cell to megakaryocytes: megakaryopoiesis

Megakaryocytes (MKs) are rare polyploid cells, located in the bone marrow (BM) with a frequency of 0.1% [6] and an average in situ cell size of about 25 μm in diameter (cf. chapter 3.3.1). The maturation process out of HSCs is called megakaryopoiesis. It can be characterized and followed by changes in morphology, classical histochemical Wright-Giemsa-staining and the serial expression of specific immunophenotypic markers, the cluster of differentiation (CD). The first cells of the megakaryocytic lineage are called megakaryoblasts. They show 2N ploidy levels and the expression of three specific and cardinal surface receptors: CD41, CD61 building the αIIbβ3-integrin receptor complex and CD110 (c-Mpl) the thrombopoietin receptor.[7,8] The next step in differentiation is the pro-megakaryocytic stage. Pro-MKs are bigger due to higher ploidy-levels and cytoplasma-maturation processes. At this stage many granules are formed. Younger pro-MKs show an azurophilic staining which shifts with granule formation to an acidophil staining. MK polyploidy evolves through endomitosis. During mitosis anaphase II and telophase are omitted and cells pass directly into G1-phase of the cell cycle.[9,10] Ploidy levels of up to 128N can be found in murine MKs, levels of 16N - 32N are the most common in mature MKs. Megakaryopoiesis is highly dependent on different humoral factors. The most important and essential one is thrombopoietin (TPO).[11] TPO is required for the MK maturation process and only the last step, the release of platelets, referred to as thrombopoiesis, is TPO-independent.[12-14] The ablation of TPO or c-Mpl leads to a platelet-production decline as a result of a 30% reduction in MK numbers and ploidy of remaining MKs.[15,16] Despite the importance of TPO for megakaryopoiesis other chemo- and cytokines as Chemokine (C-X-C motif) ligand 12 (CXCL12) and fibroblast growth factor 4 (FGF-4) together can transiently restore platelet levels in TPO or c-Mpl knock out mice.[17,18] Both chemokines are humoral components of the MK microenvironment in BM and mediate HSC and MK migration out of their corresponding niches to the BM vascularity and affect MK differentiation and thrombopoiesis (see chapter 1.1.3)[17,19] where terminal platelet biogenesis takes place.

1.1.3. Thrombopoiesis - the terminal differentiation step

During thrombopoiesis the entire MK cytoplasm reorganizes, including structural elements as the cell-membrane, actin- and tubulin-cytoskeleton and granules as well as macromolecular soluble factors to finally equip around 100 - 1000 anucleated uniform discoid platelets equally[20] with structure-giving factors and functional molecules. Thrombopoiesis typically starts at one cell pole with the formation of pseudopodial protrusions which branch and form at their very tips platelet-like swellings, called proplatelets.[21] This process is microtubule (MT)-driven which allows elongation and granule transport within the proplatelets.[22]

Proplatelets attain the blood stream by penetration of the BM-blood-barrier composed of extracellular matrix molecules (ECMs) building the basal lamina and endothelial cells. Final platelet formation occurs via an intermediate preplatelet stage and within the shear forces of blood stream.[23,24,25] Already in 1937 it has been described that higher platelet counts can be found in pulmonary vessels in comparison to prepulmonary vessels where platelet counts are elevated.[26] It has been believed that proplatelet formation (PPF) is a partly apoptotic process.[27,28] Recent analysis revealed that during proplatelet formation the intrinsic apoptosis caspase signaling pathway is not activated, MK rather block it for thorough PPF.[29,30]

1.2. Blood platelets

Blood platelets are anucleated cell fragments with a size of 2 - 3 μm. Their main function in hemostasis is the sealing of injured vessels to prevent the organism from blood loss. Therefore a stable homeostasis between platelet biogenesis out of MKs in BM, circulating platelets and functionality of activated platelets is necessary.

A massive variety of cell intrinsic and extrinsic factors are crucial for maintaining a stable and functional platelet population. The cytoskeleton, for instance, is pivotal for platelet formation and activation through a complex diversity of different signal-transduction pathways during activation and aggregation processes. Extrinsic BM niche factors influence MK differentiation, proliferation and maturation and hence platelet formation. A stable and functional MK population is *condicio sine qua non* for platelet biogenesis and thus their role in hemostasis.

In the next chapters an overview and introduction is given into main mechanisms regarding cell intrinsic factors as platelet biogenesis (chapter 1.3.1) and platelet function

(chapter 1.3.2 to 1.3.4). Cell extrinsic factors as the BM microenvironment; how fully equipped, functional, resting platelets are generated is introduced in chapter 1.4.

1.3. Platelet intrinsic factors sustaining platelet function

1.3.1. The role of β1-tubulin cytoskeleton in platelet formation and activation

During proplatelet formation MKs undergo striking cytoskeletal changes which are dependent on mechanisms underlying reorganization, growth and branching of microtubule filaments.[21,31] Megakaryocytic microtubule filaments are composed of α- and β1-tubulin heterodimers.[32,33] β1-tubulin is the most divers tubulin isoform and is exclusively expressed in the megakaryocytic lineage.[34,35] Ninety percent of β-tubulin in platelet microtubule filaments organized in the peripheral MT coil also referred to as *marginal band*, belong to the β1-isoform. β1-tubulin shows a sequence homology to other isotypes from only 70 - 80%, in contrast to all other β-tubulin isotypes that share homology about 90-95% on amino acid level.[36] Seven up to 12 microtubule filaments, consisting out of 13 protofilaments, are organized in the marginal band at the tip of proplatelets and in platelets, keeping them in their characteristic discoid shape (Figure 2).[37,38] In the absence of β1-tubulin, mice harbor severe thrombocytopenia with only 40% of normal platelet counts. The residual platelets show remarkable morphologic defects: the marginal band consists of only 2 to 3 microtubule coils and platelets show a spheric shape.[39]

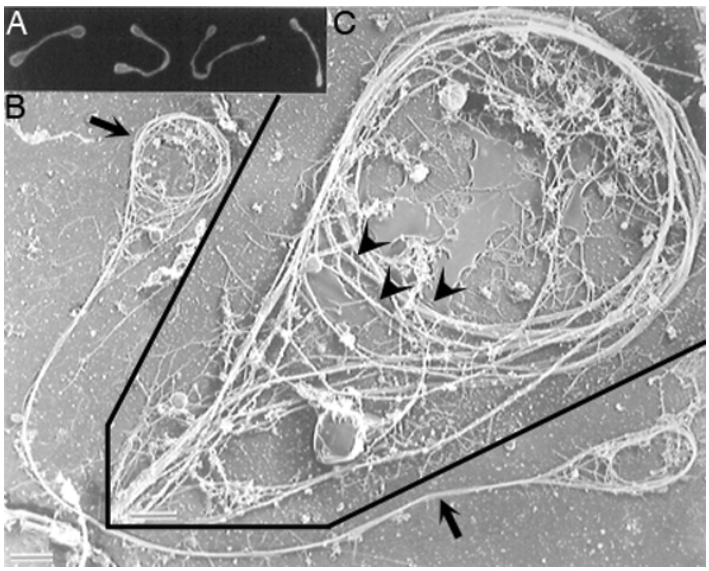

Figure 2 - MT cytoskeleton organization during thrombopoiesis. (A) Confocal microscopic picture depicting immunofluorescence stainings showing tubulin proplatelets connected with tubulin structures. (B) Scanning electron micrograph after platelet membrane permeabilization, showing MTs coiled to a marginal band in a proplatelet and a MT-lined shaft (arrows). (C) Higher magnification of (B) MTs are coiled several times at proplatelet-tips (arrow heads).[21]

The C-terminal region of the protein shows the most divergent amino acid sequence and can bind and interact with microtubule-associated proteins (MAPs).[40]

1.3.2. Identification and characterization of RanBP10 a β 1-tubulin binding protein

To find new essential β1-tubulin microtubule interacting partners a yeast two hybrid Screen was performed in a murine megakaryocytic cDNA library. The proteins secretory leukocyte protease inhibitor (SLPI) and Ran binding protein 10 (RanBP10, NCBI database: EU281316) were identified.[41,42]

Besides its capacity to bind β1-tubulin, RanBP10 also interacts with the small GTPase Ran. The biochemical characterization revealed that RanBP10 is specifically expressed in organs of hematopoiesis (BM, liver and spleen) and immunofluorescence stainings showed that the protein is located in the cytoplasm of mature MKs and platelets in a close association with MT filaments. Its influence on MT equilibrium is clearly seen when the protein is depleted in MKs by shRNA. Only short rudimentary MT-filaments are detected. When, in contrast, RanBP10 is ectopically overexpressed in MKs, augmented microtubule bundling is observed. Based on sequence homology analogies, a Rho-GEF-consensus domain was identified and led to unexpected cytoplasmic guanine nucleotide exchange-factor (GEF) activity toward Ran.[42] This detrimental influence of RanBP10 knock-down and overexpression on the MT-cytoskeleton, the binding ability towards β1-tubulin and the GEF-activity led to the assumption that RanBP10 might play a pivotal role in platelet generation, biogenesis or function.

Therefore a transgenic mouse model lacking RanBP10 was generated. For analysis results cf. chapter 3.1.[43]

1.3.3. Platelet signaling in thrombus-formation

Plug-formation, the sealing of vascular injuries by platelet clotting, underlies sensitive multistep processes with a highly specialized interaction of signaling molecules and different agonists. It is divided into three stages: **(1)** *Initiation* - with platelet adhesion and activation, **(2)** *Extension* - the phase of granule secretion and platelet accumulation **(3)** *Perpetuation* - wherein platelet-aggregation, stabilization and final plug-formation occur.

Due to their size as smallest cellular components in peripheral blood, platelets are hemodynamically forced to the endothelial vessel barrier. The monolayered endothelial

cells secrete and express antagonists of platelet activation as nitric oxide (NO), prostacyclin PGI_2, or the ADPase CD39.

(1) In case of vascular trauma the constant exposure to blocking molecules is interrupted and the subendothelial ECMs are exhibited whereby the initial phase of plug-formation starts. Molecules as collagen, von Willebrand factor (vWF), fibronectin and others are exposed. Under high shear conditions as in arterioles, platelet activation is mainly initiated by collagen- and vWF-binding. Platelets express high (50,000) copy numbers of the vWF receptor complex GPIb/V/IX wherein mostly the GPIbα subunit supports adherence under shear.

(2) Two collagen receptors are expressed on cells of the megakaryocytic/platelet lineage, α2β1-integrin and GPVI, the latter one is the most potent collagen receptor, but is unable to mediate platelet adhesion.[44] After collagen binding GPVI clusters, which leads to Fc receptor γ-chain (FcRγ) phosphorylation. The following signaling cascade triggers Ca^{2+}-influx across the platelet plasma membrane and from the platelet dense tubular system. A stable very low Ca^{2+}-concentration is maintained in resting platelets[45], once activated the rising cytosolic Ca^{2+}-concentration leads to adenosine diphosphate (ADP) secretion from δ-granules, generation and release of thromboxane (TXA_2) via the cyclooxygenase (COX) pathway and additional αIIbβ3-integrin activation and cytoskeletal reorganization referred to as *shape change*. Taken together those signaling cascades lead to signal amplification.

Platelet shape change is a rapid process during which the actin network is reorganized and filopodia are formed, myosin-dependent contractions are stimulated and the circumferential microtubule coil centralizes and platelet shape finally changes from discoid to spherical.[46,47]. Platelet shape change is required for optimal granule secretion and supports platelet-platelet and platelet-matrix interactions and tethering. Platelets posses three different kinds of secretory organelles, which release their procoagulant and thrombosis supporting molecules after platelet activation: α-granules and δ-granules (or dense-granules) are specific for MKs and platelets, the third group, lysosomal granules are ubiquitously found in cells.[48] α-granules are the storage-pool for different kinds of platelet-specific proteins as platelet-factor 4 (PF4), vWF, fibrinogen or factor V, which are synthesized by MKs or endocytosed from plasma and stored inside the granules.[49,50] The smaller and sparsely distributed δ-granules store nucleotides, as ADP and ATP, Ca^{2+}- and Mg^{2+}-cations and serotonin.[51,52] Lysosomes contain

transmembrane proteins as CD63, which can be also found in δ-granules.[53,54,55] Stored membrane proteins, as CD62P, also referred to as P-selectin (mainly in α- but also found in δ-granules), further serve as platelet activation marker, when sequestered and exposed on platelet surface.[20] The exocytosis leads to signal amplification and the so called *second wave* which together form the basis of thrombus extension.

The stabilization **(3)** of plug formation includes the recruitment of additional circulating platelets. This is achieved by release of potent agonists from already activated collagen-bound platelets. ADP, thrombin and TXA_2 mainly act via G protein-coupled receptors (GPCRs), in particular members of the G_q and $G_{12/13}$ family, respectively. They trigger shape change, degranulation and platelet aggregation.[56] GPCR signal transduction is very potent because no complex recruitment is required as in integrin signaling and each receptor can reach various effector pathways.[57] Thrombin receptors belong to the protease-activated receptors (PAR) family. In humans PAR1 and PAR4 are responsible for thrombin signaling in platelets, in mice PAR3 and PAR4 can be found, with the latter one being the main receptor. The PARs and TXA_2 receptor (TPR) are coupled to the $G_{12/13}$ family and trigger shape change by activation of the Rho-kinase pathway.[58] ADP triggers shape-change via its $G_q\alpha$ bound $P2Y_1$ receptor.[59] The absence of the second ADP receptor $P2Y_{12}$ does not influence shape change but aggregation. Thus both ADP receptors are essential for complete ADP response.

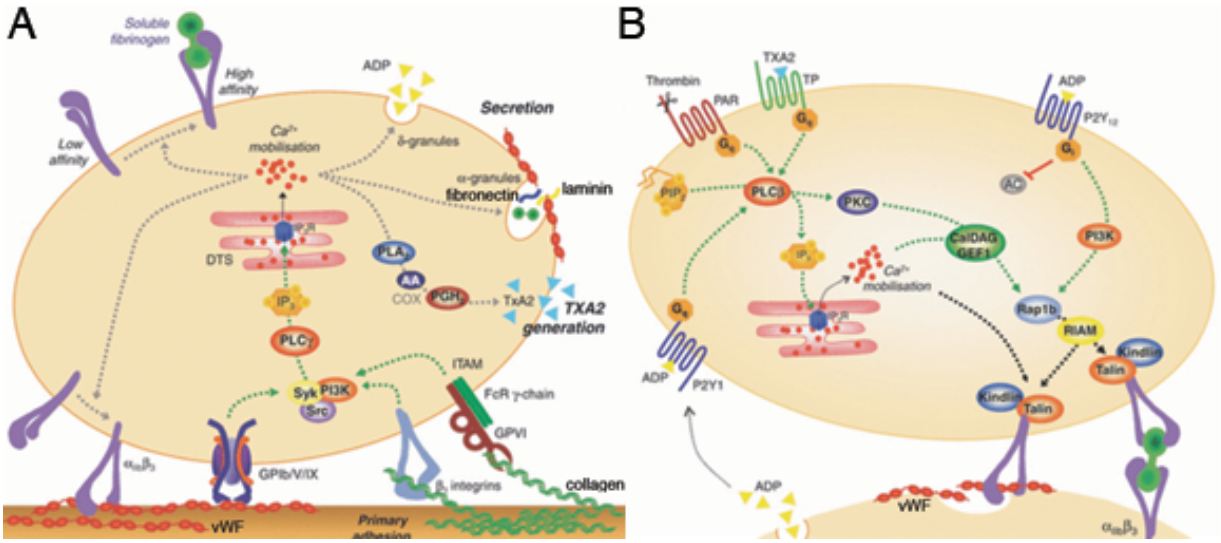

Figure 3 - Overview of platelet signal transduction. (**A**) Signaling model of platelets during adhesion to exposed ECM. Signal amplification via inside-out signaling is followed by Ca^{2+} mobilization and subsequent granule secretion. (B) After aggregation activated platelets release ADP and TXA_2 and recruit and activate further platelets. Adopted from Wei 2009.[60]

In early activation processes the main target for signal amplification is the β3-cytoplasmic chain of the receptor αIIbβ3-integrin, also denominated as GPIIb-IIIa-complex or CD41a.[61] The binding of talin and kindlins to the cytoplasmic tail results in conformational changes of the receptor which in resting platelets resides in a low affinity state towards its ligands fibrinogen, fibronectin and vWF. Once activated the receptor binds with high affinity,[62] a process referred to as inside-out-signaling. αIIbβ3-integrin ligand binding and subsequent signaling, or outside-in signaling, can occur via 80,000 receptor copies on the surface of one platelet and further copies stored in α-granules waiting for release.[63] Outside-in signaling is crucial for thrombus extension through platelet spreading and further granule secretion and platelet aggregation.[64,65,66] The binding of fibrinogen and other macromolecular structures via αIIbβ3-integrin results in cross linking of platelets and thus thrombus-formation.[67] Platelets in aggregates can interact directly or through a simultaneously bound adhesion molecule. No interaction via typical cell junctions is described for platelets.[68] Tight aggregates on one hand prevent the diffusion of activating molecules and on the other hand do not allow the cleavage of thrombus components by plasma molecules. Further thrombus stabilization is attained by incorporation of fibrin. Thrombus constitution can be discriminated between the vessels where it is formed in. A venous thrombus is rich in fibrin and their main cellular components are erythrocytes (red thrombus), thrombi in arteries are rich in platelets with a low fibrin content (white thrombi).[69]

1.3.4. Platelet function tests

Platelet function tests are potent tools to monitor response to agonist and give information for platelet diagnostics and function in men and mice. Therefore different methods have been established based on platelet aggregometry measurements and flow cytometry. Aggregation can be measured photometrically as light-transmission through platelet rich plasma (PRP)[70] or in whole blood by electrical impedance. Platelets in suspension as in PRP have a characteristic light scatter behavior, light beams are diffracted by cells and the detectable light is set as 0% light transmission and defined as 0% aggregation. When exogenous platelet agonists are applied and platelets respond by activation, platelet-aggregates are formed and light scattering changes, more light is transmitted through the sample and aggregation can be measured. When physiological agonist concentrations are used, a first and a second wave response can

be observed. The first wave response is based on the applied agonist, the second wave or amplification of signal is mainly due to δ -granule release of platelets. Additional cytoskeletal changes and hence shape change can also be monitored by aggregometry. Whole blood aggregometry measurements are based on accumulation of activated platelets at electrodes in suspension and thus resulting in a gain of impedance across those electrodes.[71] Further specialized methods have been established for instance to analyze δ -granule secretion, the so called luminoaggregometry.[72] When ATP released from activated platelets reacts with exogenous firefly luciferase bioluminescence occurs and can be quantified.

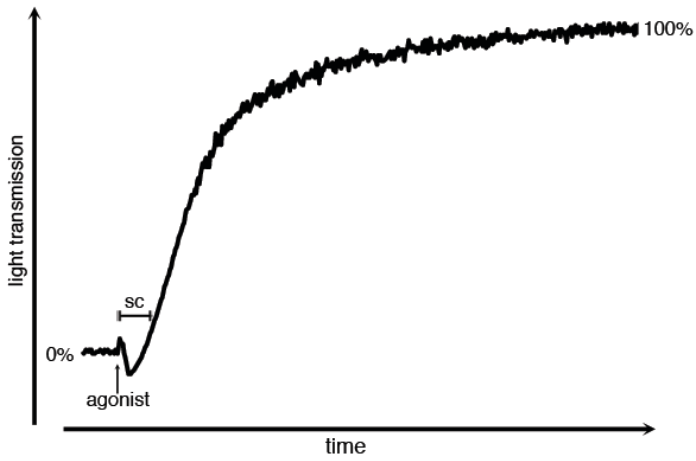

Figure 4 - Standard aggregation curve. Platelet response to agonist stimulation. From a light transmission baseline (0% aggregation) the platelet shape change (sc) can be observed followed by an increase in light transmission reaching a plateau of maximum aggregation.

In addition to aggregometry, flow cytometry offers a broad range of methods to examine platelet counts, platelet reactivity (calcium flux, granule release), surface-marker expression (indication for disease diagnosis), thrombopoiesis (bigger, reticulated platelets) and is therefore essential for platelet studies and diagnosis. Detailed description of relevant applications can be found in chapter 2.

1.4. Extrinsic factors influencing megakaryocyte biology in BM

The destination of every cell in the body is dependent on intrinsic and extrinsic factors, as for instance transcription factors or chemokines. This is especially true for stem cells. HSCs are located in the bone marrow and highly dependent on their microenvironmental surrounding the so called “niche“.

The concept of a niche in early studies was understood as a three-dimensional anatomic structure of heterologous cell types creating an architectural recess for stem cells. Now the idea of a dynamic regulatory microenvironment, consisting not only of

heterologous cell types but structural and humoral factors which can enforce fate of stem cells becomes implemented.[73] The niche thus becomes functional.

The composition of the HSC niche determines the fate of the cell: quiescence, self-renewal, apoptosis or differentiation. The niche concept was already proposed in the late seventies by R. Schofield.[74] By now three key components and their three dimensional composition can be distinguished: **(1)** cellular elements, **(2)** structural factors as ECM and **(3)** humoral factors as cyto- and chemokines.

1.4.1. The bone marrow niche concept

The bones give structure and shape to the mammalian body and are indispensable for body movement. They enclose BM completely and therefore form a protective barrier. Bone rigidity is based on hydroxylapatite formed out of the accumulation of the mineral components calcium and phosphate. Bones contain different cell types and their precursors as osteoblasts, osteoclasts and structural proteins as collagen type I fibers or proteoglycans and molecules as osteopontin or osteocalcin.[75,76] Anatomically can be discriminated between BM within the trabecular bones in the epiphysis of long bones and BM in the cavity situated in the long bone diaphysis. Homing experiments gave evidence that the bone lining endosteal region in BM is the habitat for HSCs.[77] In 2003 the identification of the HSC niche was proposed with an essential role for osteoblastic cells for HSC proliferation through bone morphogenetic protein (BMP) signaling[78] which was refuted recently.[79] Further studies propose an essential role for Notch-signaling and the Wnt/β-catenin pathway for the maintenance of primitive HSC populations and the self-renewal potency respectively.[80,81] Although HSCs are the best analyzed stem cell population, an in situ characterization of the niche architecture is still incoherent, what is also true for their progeny.

(1) The BM parenchyma consists beside blood precursor cells and lymphatic cells mainly out of mesenchymal cells as fibroblasts, adipocytes, myocytes, pericytes, chondrocytes, osteoblasts, osteoclasts and endothelial cells. Mesenchymal stem cells (MSCs) show full reconstitutive potential and are able to restore this heterologous cell population after transfusion.[82] BM stromal cells, another MSC-derived cell population, are known to be a functional part of BM niches. Their specific impact still remains elusive as this cell population is poorly characterized regarding surface molecules, biochemical processes and main function in BM.

In between the BM parenchyma every kind of maturation stage of blood cell lineages can be identified. In 1975 it was proposed by Shackney that a developmental gradient exists within the BM. Primitive undifferentiated cells are located in the proximity of bone lining cells, the endosteal region or osteoblastic niche, favoring cell quiescence. In contrast, maturating, more differentiated hematopoietic cells are found close to the sinusoids, also referred to as the vascular niche.[78,80,83] It is still ill-defined whether differentiation of MKs takes place during migration from the endosteal region to the vascular niche or whether the niche itself favors differentiation and HSC migrate towards BM-sinusoids and fully differentiate at the vascular niche. The direct cell-cell interaction, the expression of chemokines and ECMs are known to have a substantial impact on proliferation and differentiation.[84,85,86].

(2) The influence of niche factors as ECMs on megakaryopoiesis and platelet biogenesis still remains to be elucidated. Collagen type I, proposed to be component of the osteoblastic niche inhibits proplatelet formation in vitro, whereas type III and IV collagen, known to be factors of the vascular niche, promote platelet biogenesis with different kinetics, as do fibronectin, fibrinogen and vWF.[87] All those molecules are strong agonists for platelet activation but neither leads to a premature cell differentiation and platelet generation within the BM or to activation events. The actual in situ distribution of ECM-molecules, co-localization and interaction with MKs remains elusive.

(3) MK differentiation is TPO-dependent and the chemokine receptor CXCR4 and its ligand CXCL12 not only play a crucial role in HSC homing,[88] but also in MK biogenesis and thrombopoiesis. It has been proposed that CXCL12 augments cell motility and transendothelial migration and fibroblast growth factor 4 (FGF-4) additionally enhances the adhesion of MKs to endothelial cells.[17] MKs themselves secrete VEGF-A and constitute a pro-survival environment for endothelial cells.[89] How precise adjustment of MK- and niche factor-interactions are mastered and what happens when this susceptible system is disrupted is subject of the next chapter and chapter 2.3.

1.4.2. Immune thrombocytopenia modeling bone marrow dynamics

Homeostasis of BM environment and microarchitecture are laid out to be susceptible to react on smallest changes in the need of myeloid or lymphoid blood cells. A disrupted equilibrium of either cellular, structural or humoral factors has an impact on BM and blood cells, leading to further consequences in blood cell generation. The cellular

equilibrium within BM is not only dependent on endogenous factors, invading molecules as for instance antibodies can markedly influence BM homeostasis and dynamics. Autoantibodies recognizing surface molecules on platelets and MKs cause severe thrombocytopenia due to accelerated platelet clearance in the reticuloendothelial system. This autoimmune disease is referred to as immune thrombocytopenia (ITP).[90,91,92] It has been reported that BM of patients reacts on platelet destruction with a compensatory increase in MK numbers even though they are described to be (para-) apoptotic and just able to produce less platelets.[93] Auto-antibodies present in plasma of some patients can bind to MKs and inhibit MK differentiation and maturation in vitro,[94,95] although early studies reported normal to increased platelet production in patients suffering from ITP.[96,97] Despite lacking platelets in the peripheral blood and altered MK numbers, TPO serum levels from ITP-patients are normal or only slightly increased.[98,99] The dynamics in ITP-BM regarding the feedback mechanisms of the MK-platelet axis remain ill-understood as so far no in situ techniques could display the kinetics of MK numbers, maturation stage and reactivity towards anti-platelet auto-antibodies. Mouse models for analysis of autoimmune diseases are due to the multiplicity of those disorders so far unfrequent. However, a recent study using a severe combined immunodeficiency (SCID) mouse model describes the generation of real platelet auto-antibodies in mice.[100] Beside the interesting findings that platelet destruction is based on both humoral and cellular immune response, the observed BM alterations including depleted or morphological abnormal MKs remain elusive as BM histology is often from poor quality and difficult to evaluate. Thus in situ BM dynamic-analyzation is ambiguous. Here, a simple mouse model for passive immune thrombocytopenia has been described. Serial analysis of hemograms, BM homeostasis, in situ analysis of MK morphology and apoptotic state and in vivo observation of MKs all describing BM-dynamics after platelet depletion were performed and examined.

1.4.3. Visualization of in vivo MK-dynamics in BM

Standard confocal microscopy is a substantial tool to analyze tissues, single cells or structural elements within or outside cells. Even time-lapse live-cell imaging can be performed by confocal laser scanning microscopy. However, data on dynamic intravital analysis in intact tissue association, confocal microscopy reaches it limits due to resolution and penetrance restrictions.

In standard immunofluorescence (IF) microscopy methods, high light energies (beamed from laser or Mercury-lamps) are needed to generate adequate images due to energy loss via light scattering. The higher the excitation energy needed, the more phototoxicity occurs and leads to damage of the analyzed tissue and only shallow tissue penetrance is achieved due to the short wave length. Multi-photon excitation generated by multi-pulse lasers allows then to pursue deep-tissue penetrance with little light-scattering and less phototoxicity. The principle of two photon microscopy is based on the pulsation of two photons of the same wavelength and doubled standard wavelength, in attosecond intervals, at the specimen and excite fluorophores in the tissue with half of the energy.[101] Thus three photon excitation is based on pulsation of three photons with threefold wavelength onto fluorophores (Figure 5). Light scattering in multiphoton microscopy (MPM) is diminished by focussing the laser beam in objective lenses with high numerical apertures. MPM further permits imaging via so called higher harmonic generation with doubled (second harmonic generation (SHG)) or triplicated (third harmonic generation (THG)) oscillation frequency. When photons pass through highly repetitive structures such as collagen in skin or bone or myosin in muscles second harmonic signals are generated and emit light of doubled frequency and half the wavelength.

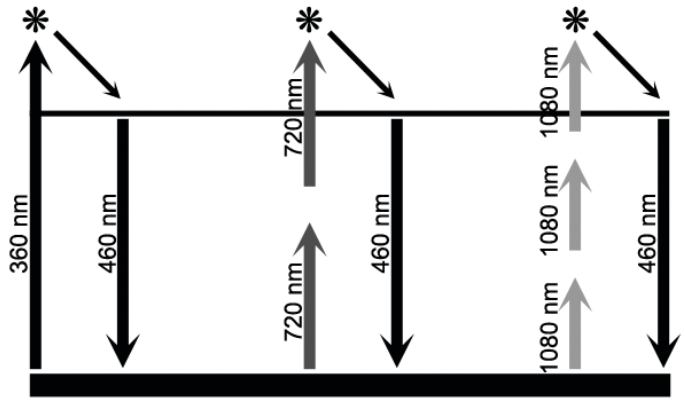

Figure 5 - Jablonski scheme. Depicting the excitation-principle of standard, two-photon and three-photon microscopy.

Standard confocal microscopy reaches a lateral resolution of 200 nm and an imaging depth of approximately 50 μm,[102] though electron microscopy resolution is less then 1 nm, only surface imaging is possible or permeablizing pretreatment is necessary.[103] In contrast, MPM enables imaging with a lateral resolution of 350 nm and a tissue penetrance of 500 μm up to 1 mm.[102] Therefore MPM has become a potent method to analyze dynamic deep tissue mechanisms in whole in situ tissue contexts. Particularly in immuno- and neuro sciences e.g. reviewed in Ref. 104,[104] MPM has become substantial to understand in vivo cell-cell communication and cell motility. MPM has been applied to answer substantial hematological issues, for instance thrombopoiesis in

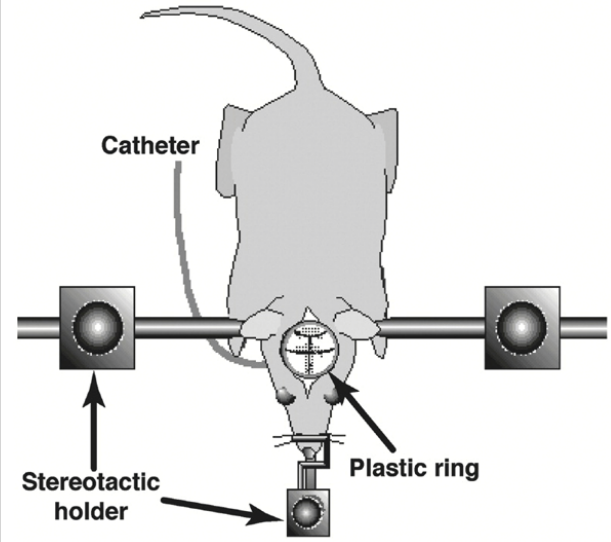

Figure 6 - Scheme of mouse skull preparation for MPM. The frontoparietal bone is dissected and the skin is spread by a plastic ring aimulatnously warming PBS avoiding tissue drying and providing solution for the water immersion lens.[105]

BM was visualized in vivo.[23] Therefore the frontoparietal skull bone of an anesthetized mouse was dissected, the area was spread and warmed by a plastic ring with a radial fixed hose, transporting 37°C warm water heating physiological buffered saline (PBS) in the center. During BM imaging the mouse head was fixed by stereotactic holders (Figure 6).[105]

To compare skull and long bone BM, methods to image tibia BM have been additionally established.[106] Both preparation methods have advantages and disadvantages. Preparation of skull BM is fast (approximately 30 min after anesthesia), less invasive and provides stable images. Preparation of tibia BM includes milling of the bone cortex. It is too thick for two photon penetration. The bone fixation at the *trochanter major* of the murine *os femoris* includes additional dissection of the area. The milling procedure often comes with bleedings from injured vessels, which have to be cauterized, and an uneven imaging area. However the long bone BM differs from the calvarian BM and additional analysis of long bone BM are indispensable regarding native BM analysis. Furthermore the area to image is bigger compared to the cranial method.

1.5. Specific aims

The generation of functional blood platelets underlies a complex variety of biochemical and cell biological mechanisms which support or antagonize development and functionality from in- and outside. In platelets and their precursor cells, the MKs, some of those mechanisms are very well analyzed and helped to develop and improve therapies of severe hemostatic diseases. Nevertheless the global understanding of how hundreds of virtually identical, functional platelets are generated out of one single MK and how these platelets are fully activated has so far remained poorly understood.

In this thesis three different aspects of platelet biogenesis and function are addressed:

1. As an object of relevant intrinsic mechanisms of functional blood platelets, a mouse model was used to analyze the knock out of RanBP10, a cytoplasmic GEF, harboring Ran and β1-tubulin binding capacity. These mice were reported to have severe bleeding phenotype by an otherwise normal platelet count, allowing to use intravital microscopy techniques to refine the defect in hemostasis. These data were supplemented with a series of functional experiments regarding granule centralization, content, and release and by biochemical analyses to understand the role of microtubule polymerization and dynamics in this process.

2. Besides the presence of functional platelets in the peripheral blood stream the biogenesis of platelets from MKs was to be addressed in order to analyze cell extrinsic mechanisms that influence MK dynamics in BM. In this thesis a simple mouse model for the autoimmune disease ITP was developed in order to mimick and manipulate the MK pool. MK differentiation and proliferation dynamics in situ were analyzed supported by intravital MPM data of platelet biogenesis.

3. The BM microenvironment of MKs is essential for MK development, proliferation, differentiation and finally for platelet biogenesis across the endothelial barrier. Although some components of this complex network have been identified, the three-dimensional topology is still unknown. In this thesis, a series of histological analyses supplemented by functional studies on adhesion and proplatelet formation were performed to gather data that could become the first draft of an MK-specific BM-atlas. This work is expected to contribute to characterize the three-dimensional BM niche.

2. Materials and Methods

2.1. The microtubule modulator RanBP10 plays a critical role in regulation of platelet discoid shape and degranulation

2.1.1. Mouse husbandry, MK culture, and 5-bromo-4-chloro-3-indolylbeta-D-galactopyranoside (X-Gal) staining

RanBP10-knockout mice were generated by a gene trap approach by use of the embryonic stem cell clone RRZ226 provided from BayGenomics. After germline transmission heterozygous mice were back-bred to either C57/BL6 or 129/Sv strains, respectively. Animal care and all experiments were performed according to institutional guidelines with the approval of the ethical review board at Charité-Universitätsmedizin. Fetal liver–derived MKs were isolated and cultured as described.10 To determine genotypes by expression of the transgenic fusion protein, fetuses were stained with X-Gal and were incubated for 30 minutes in fixation buffer (100mM phosphate buffer containing 5mM EGTA (ethyleneglycoltetraacetic acid), 0.2% glutaraldehyde, and 2mM MgCl2) and washed in 100mM phosphate buffer (pH 7.3) and 2mM MgCl2. Staining was performed for 6 hours (hrs) or overnight at 37°C in staining buffer (5mM K4[Fe(CN) 6]–3H2O, 5mM K3[Fe(CN)6]) containing 1 mg/mL X-Gal.

2.1.2. Reverse transcription–polymerase chain reaction, polymerase chain reaction, cloning, and sequencing

Total RNA from bone marrow or cultured MKs was isolated by the use of Trizol (Invitrogen) according to the manufacturer's instructions. mRNA was reverse-transcribed with oligo-(dT) primers and amplified by the use of a multiplex polymerase chain reaction (PCR): forward primer 5-GCTTGTACCCTGCGGTTAATC, reverse primer (RanBP10) 5-AAGCGCTGGGTTGTCTCAATG, and reverse primer (-geo cassette) 5-ATTCAGGCTGCGCAACTGTTGGG. Genomic DNA was isolated from tail or ear biopsies according to standard protocols. The supernatant is used for allele-specific PCR with 2 primer sets: wild-type forward 5-CAGAGCTATCACATTGATAGAAC, wild-type reverse 5-TAGTCCCAGCTGGCCTAAAC, mutant forward 5-TTATCGATGAGCGTGGTGGTTATG, mutant reverse 5-GCGCGTACATCGGGCAAATAATATC. Primers used for breakpoint analysis PCR were as follows: forward (common) 5-GACAAGAATTTCTCTGTGTAG, reverse (wild-type) 5-TAGTCCCAGCTGGCCTAAAC, and reverse (mutant) 5-

GTGTGGGAAAGCCTTCAAAG before cloning into the TOPO-TACloning-Kit (Invitrogen).

2.1.3. Antiserum, platelet activation, and immunoblot analysis

NHS-columns (GE Healthcare).Atotal of 10 to 30 g of protein lysates was applied per lane before standard sodium dodecyl sulfate–polyacrylamide gel electrophoresis (SDS-PAGE) was conducted and immunoblotted onto polyvinylidenefluoride membranes, incubated with primary antibodies as indicated, and detected by the use of horseradish peroxidase–conjugated secondary antibodies (Santa Cruz Biotechnology) before standard enhanced chemoluminescence detection (GE Healthcare). For activation studies, platelets were washed and resuspended in HEPES (N-2-hydroxyethylpiperazine-N-2-ethanesulfonic acid)-Tyrode buffer containing $CaCl_2$ (1mM). Thrombin or PAR-4 peptide was added with the indicated concentrations and stimulation stopped by centrifugation. Onethird volume of 4 sample buffer was added to the supernatant while the pellet was dissolved in one volume of 1 sample buffer and both fractions subjected to SDS-PAGE and blotted against platelet factor 4 (Peprotech). For granule protein studies, membranes were additionally probed against von Willebrand factor (clone H-300; Santa Cruz Biotechnology) and P-selectin (clone CTB; Santa Cruz Biotechnology).

For further materials and methods please cf. Kunert et al.[43]

2.2. Altered microtubule equilibrium and impaired thrombus stability in mice lacking RanBP10

2.2.1. Animal husbandry

RanBP10 deficient mice were generated as described recently.[43] Animal husbandry and all experiments were performed according to institutional guidelines with the approval of the local ethics authorities.

2.2.2. Megakaryocyte ploidy and immunohistochemistry

Bone marrow cells were extracted from femur bones by rinsing PBS through the cavity and washed in PBS prior to resuspension in citrate buffer supplemented with RNase K (10mg/µl) and propidium iodide (1 mg/mL). After 30 minutes megakaryocyte ploidy

profile was evaluated flow cytometrically. For immunofluorescence stainings washed platelets were stimulated with PAR4p as indicated and the reaction stopped by adding 8% formaldehyde with subsequent centrifugation on poly-L-lysine coated coverslips. Samples were permeabilized by incubation with 0.5% Triton-X 100. Free binding sites were then blocked with 3% goat-serum. β1-tubulin was stained with a generated antiserum. Cytospins were next mounted with Fluoromount-G (Southern Biotech via Biozol, Eching, Germany) and dried. Analysis was performed on a Nikon A1 confocal microscope using a CFI Plan Apo VC 100x oil lens with a numerical aperture of 1.4. Platelet perimeter was measured using Nikon NIS Elements software on 80-180 platelets of at least three independent fields per time point and concentration with a total of 1740 platelets.

2.2.3. Gene expression quantification via real-time PCR

Total RNA was extracted from cell suspension using TRIzol (Invitrogen, Darmstadt, Germany) according to the manufacturer‘s instructions. cDNA synthesis was performed via Superscript II First-Strand Synthesis System (Invitrogen). For amplicon quantification SYBR-Green (Applied Biosystems, Darmstadt, Germany) was used. ΔΔCT-analysis[107] was performed using 7500 Fast Real-Time software (Applied Biosystems). Quantitative real-time PCR analysis was executed with the following primer-pairs (Metabion, Munich, Germany). For β 1-tubulin forward 5‘-AGCCAAGTTCTGGGAGGTGATCGG and reverse 5‘-GGTCCACAAGGACGGCTCGC, for β 5-tubulin forward 5‘-CGACCTGCAGCTGGACCGAA and reverse 5‘-CCTGCCCCAGACTGACCGAA, for GAPDH forward 5‘-TTCACCACCATGGAGAAGG and reverse 5‘-CACACCCATCACAAACATGG and RanBP9 forward 5‘-GACTGTACCGGAGCTAAAC and reverse 5‘-AGTTTCTCCAACTCCATTG, RanBP10 forward 5'-AGGACTATATGCGGGAGTGG and reverse 5’ TGCACCAGGTAAGACGAGAC.

2.2.4. Platelet isolation and analysis

Platelet rich plasma (PRP) was isolated from citrated blood after differential centrifugation. For transmission electron microscopy (TEM) platelets were stimulated with 1 mM or 0.1 mM PAR4p respectively. Samples were fixed with 4% glutaraldehyde in 0.1 M cacodylate-buffer for 15 min. After pelleting (6 min, 400 g) samples were

resuspended in 0.1 M cacodylate-buffer containing 2% glutaraldehyde and stored at 4°C until analysis.[108] De- and repolymerization studies were performed as recently described.[109] Briefly, platelets were incubated at 4°C, 37°C or 4°C with subsequent rewarming to 37°C. Samples were fixed followed by centrifugation onto poly-lysin coated coverslips and immunostained using an anti-tubulin-antibody (Sigma-Aldrich). Platelet life-span was determined daily over a period of 5 days by the recovery rate of a 488-Dylight-coupled anti GPIX-IgG derivative (Emfret Analytics, Eibelstadt, Germany) injected retroorbitally into mice. For glycoprotein expression of resting and stimulated platelets, 50 µl heparinized blood was diluted in 2 mM Ca2+ containing HEPES-Tyrodes buffer and incubated with 1:5 antibody-solution at RT. Reaction was stopped by adding 500 µl PBS followed by flow-cytometric analysis. Glycoproteins with their corresponding antibody were named hereinafter and purchased from Emfret Analytics unless designated otherwise. Antibodies against GPVI (JAQ1), α2-integrin (Sam.G4), β1-integrin (Becton Dickinson, Heidelberg, Germany), CD9 (Nyn.H1), GPIb (Xia.G5), GPIX (Xia.B4), αIIbβ3 (14A3), CLEC-2 (INU1) and α-GPV (Gon.C6).

2.2.5. Flow-chamber, platelet spreading and in vivo thrombus formation

Coverslips were coated over night at 37°C with either HORM-collagen (Nycomed, Munich, Germany) or anti-human vWF-antibody (A0082; Dako, Hamburg, Germany) followed by blocking with 1% bovine serum albumin (BSA), 1 h at RT. For adhesion on vWF coverslips were subsequently incubated with murine plasma for vWF to adhere on immobilized antibody for 2 h at 37°C. Heparinized blood (20 U/mL) was diluted with ½ volume HEPES Tyrode‘s buffer with antibody (56F8 conjugated to Dylight 488) and incubated for 5 min at 37°C. Perfusion was performed as previously described.[110,111] For platelet spreading analysis coverslips were coated at 4°C over night with fibrinogen (100 µg/mL; Sigma-Aldrich), collagen (50 µg/mL; Stemcell Technologies, Grenoble, France), or BSA (1.5% in PBS) and excess matrix proteins washed away. Platelets were allowed to adhere for 45 minutes at 37°C before non-binding platelets were washed with PBS. Samples were fixed with 4% paraformaldehyde and mounted with Fluoromount-G (Southern Biotech, Echingen, Germany).[112] For intravital thrombus formation mice were anesthetized via intraperitoneal application of a ketamine/xylazine mix (100:5 mg/kg; Parke-Davis, Berlin, Germany and Bayer, Leverkusen, Germany) followed by retro-orbital injection of 2 µg 488-Dylight-coupled GPIX-IgG derivative

(X488, Emfret Analytics) in 150 µl PBS. Mesenteric tissue was exteriorized and arterioles injured by topic application of 20% ferric chloride solution. Thrombus formation of fluorescent platelets was visualized as previously described[111] during an overall observation period of 40 min or until complete arteriole occlusion occurred for a period longer than 1.5 min.

2.2.6. Mepacrine assay, Modified Tubulins, Aggregometry and dense granule release

Citrated blood was diluted in HEPES-Tyrodes-buffer. Platelet dense-granules were labeled in suspension with 390 µM mepacrine,[113] and incubated in the dark at 37°C for 30 min. Platelets were stimulated with thrombin concentrations and time points as indicated. Granule release was followed flow cytometrically and the residual platelet granule content calculated: Non-secreted δ-granules [%] = MFI (activated platelets) x 100 / MFI (resting platelets). For protein analysis platelets were incubated with agonists as indicated. Modified tubulins were analyzed in total platelet lysates with antibodies against tyrosinated and glutamylated tubulins over night. For microtubule stabilization platelets were preincubated 5 minutes with 50 µM paclitaxel in PHEM-buffer and subsequently ultracentrifuged at 150'000 g for 30 minutes. The pelleted fraction was dissolved at 37°C over night and immunoblotted against α-, pan-β-, and β1-tubulin. [25]Cell fractioning into pellet and supernatant was performed as described[43] recognizing pro- and antiangiogenic factors with antibodies against fibrinogen, VEGF, and thrombospondin 1.[114,115]

For aggregometry and ATP release platelets were washed as described[116] and resuspended in Tyrode's buffer containing 2 mM calcium and 100 *µ*g/mL human fibrinogen (Sigma) at a concentration of 50'000 per *µ*l. Shape change and aggregometry was induced by thromboxane A2 analogue U46619 (Merck, Darmstadt, Germany), ADP, or collagen (Probe & go, Osburg, Germany) at concentrations indicated. Microtubule stabilization was performed by preincubating platelets with 0.5 mM paclitaxel (Sigma) for 30 minutes at 37°C prior to adding the agonists. For ATP release blood was diluted 1:4.5 in prewarmed saline. Subsequently 50 *µ*l luciferase (Probe & go, Osburg Germany) was added for 2 minutes. Platelets were stimulated with indicated concentrations of thrombin and compared to an ATP standard by Chrono-Lume. Serotonin release was measured in the supernatant of resting and stimulated

platelets by ELISA (IBL, Hamburg, Germany) according to the manufacturer's instruction.

2.2.7. Statistical analysis

Data was analyzed by Student's t-tests where p-values <0.05 were defined as statistically significant.

2.3. Effect of an anti-GPIb-platelet antibody on bone marrow megakaryocytes in a mouse model of passive immune thrombocytopenia

2.3.1. Animal husbandry

All work was performed according to institutional guidelines and approved by the local government (G0010/10). Each mouse of appr. 30g was fed daily with 25mg EdU embedded in glucose-agarose cubes for at least 10 days.

2.3.2. Platelet depletion and hemograms

Mice were treated with 2μg/g body-weight depletion antibody or control antibody, #R300 or #C301 (Emfret Analytics, Eibelstadt, Germany), per intraperitoneal bolus injection. After single application mice were sacrificed on indicated days and whole blood, bones and spleens collected. Citrated whole blood was analyzed with settings for mouse blood parameters (Synlab, Berlin, Germany). One fraction of the antibody was conjugated to Atto590-fluorophore for intravital imaging. The vasculature was visualized by either applying high molecular rhodamine-dextran or quantum dots (Qtracker 655, Invitrogen - Life Technologies, Darmstadt, Germany).

2.3.3. Tissue preparation and staining

Femurs were prepared at the indicated time-points and fixed in 4% paraformaldehyde (Electron Microscopy Science, Hatfield, USA) for 4 hrs, followed by 24 hrs incubation in serial dilutions of 10%, 20%, and 30% sucrose. Tissues were embedded in SCEM medium (Section Lab Co. Ltd., Hiroshima, Japan) and cut into 7μm thick longitudal sections on adhesive foil C9 (Section Lab). Sections were rehydrated for 20 minutes in PBS, blocked in 10% goat serum for 20 minutes. Subsequent washing was followed by antibody incubation for 1 hour at RT. The platelet depletion antibody was detected by a secondary Alexa 647-conjugated goat anti rat IgG antibody (Invitrogen - Life

Technologies, Darmstadt, Germany). Click-it reactions were performed according the manufacturers protocol (Invitrogen Life Technologies, Darmstadt, Germany) MKs were stained by a FITC-labelled anti-CD41 (BD Biosciences, Heidelberg, Germany). Nuclei were visualized by DAPI containing Fluoromount G mounting medium (Southern Biotech, Eching, Germany). Slides were analyzed with a Nikon A1 (Eclipse) confocal laser scanning microscope with a 20x-lens and CFI Plan Apo VC with a numerical aperture of 1.4.using the NIS-Elements software (Nikon, Dresden, Germany).

2.3.4. Apoptosis detection assay

Apoptotic cells were detected by TdT-mediated dUTP-biotin nick end labeling (TUNEL)-assay which detects DNA single strand breaks, according to the manufacturer's instruction (In situ cell death detection kit, Roche, Mannheim, Germany). This assay will also detect endogenous terminal deoxynucleotide transferase (TdT) as expressed during T- and B-cell development.

2.3.5. Multiphoton Microscopy

Experiments were performed using a specialized two-photon laser scanning microscope based on a commercial scan head (TriMScope; LaVision BioTec, Bielefeld, Germany). The setup allows for dual NIR (700–1020 nm, 100fs, 80 MHz, MaiTai, Spectra Physics Darmstadt, Germany) and IR via optical parametric oscillator (OPO) (APE, Berlin, Germany) pumped at 850 nm and tuned at 1100 nm, excitation. A objective lens for deep-tissue imaging (20x dipping lens, NA 0.95, WD 2mm, Olympus, Hamburg, Germany) is used. The whole wavelength range of Ti:Sa dichroic mirror settings are used to detect with the following interference filters: 460 ± 30 nm (blue), 525 ± 25 nm (green), 593 ± 20 (red) and 655 ± 20 nm (far red).

2.4. Future directions: Development of a MK BM atlas

2.4.1. Preparation, staining and analysis of cryosections

Tissues were prepared and stained as described in 2.3.3 with the cryosection preparation kit (Section lab, Hiroshima, Japan) developed in cooperation with the group of Prof. Hauser, DRFZ Berlin. Primary antibodies for stainings were applied as listed in Table 1. For analysis of MK distribution and colocalization analysis complete femur sections (thickness 7 μm) of 5 animals were quantified with a Nikon A1 (Eclipse) confocal laser scanning microscope with a 20x-lens and CFI Plan Apo VC with a numerical aperture of 1.4.using the NIS-Elements software (Nikon, Dresden, Germany).

Table 1 - Utilized antibodies. Working-dilution and manufacturers.

Epitope	Dilution	Manufacturer
CD31 (PECAM-1)	1:50	eBioscience
CD41	1:100	Becton Dickinson GmbH
CD42	1:100	Becton Dickinson GmbH
CD61	1:100	Becton Dickinson GmbH
CD105 (Endoglin)	1:100	eBioscience
Collagen IV	1:50	Millipore
Fibronectin	1:50	Millipore
GPVI	1:100	emfret Analytics
Laminin	1:100	Sigma-Aldrich
vWF	1:50	Dako
α2-integrin	1:100	emfret Analytics

Secondary Antibodies were obtained from Invitrogen (Life Technologies, Darmstadt, Germany Life Technologies) as Alexa Fluor conjugates in 488, 594, 647.

2.4.2. Fetal liver cell culture

Timed pregnant mice are sacrificed on day 14.5 post coitum and the uterus is prepared and stored in DMEM-medium. Fetal livers are isolated and a single cell suspension prepared by shear forces in 18 gauge (G) and 21 G 1 1/2 needles. The quality of the single cell suspension was monitored by light microscopy and finally resuspended in DMEM-medium containing 10% FCS, 1% penicillin-streptomycin mixture and 1% L-

glutamine. After 5 min centrifugation at 130 *g* the cell pellet is resuspended in 10 mL additives containing Dulbecco's Modified Eagle Medium (DMEM) and the suspension is filtered through a cell strainer with a pore size of 70 *µ*m. The culture medium is subsequently conditioned with 0.5 - 1% TPO.[117]

2.4.3. BSA-gradient enriched MKs

Cultured cells are washed in PBS and transferred into a tube and centrifuged for 5 min. at 130 *g* at room temperature. A single step gradient is prepared by overlaying 3% (w/v) BSA solution in PBS with the same volume of 1.5% (w/v) BSA-solution. MKs are resuspended in 0.6-fold volume DMEM and carefully overlaid onto the top layer of the gradient. Via gravity, mature MKs are allowed to sediment in the gradient and separate into three fractions enriched for non-MKs (top fraction), proplatelet-forming MKs (intermediate fraction) and MKs (bottom fraction).

2.4.4. Flow cytometry

MKs are enriched by a single step BSA gradient (see 2.4.3.) on day 3 of culture. 1 - 1.5x10^5 cells were stained in 100 *µ*l FACS-buffer (PBS supplemented with 0.1% BSA) for 20 min. at room temperature with 1 *µ*l anti-CD61 FITC-conjugated antibody. A subsequent washing step removed excess antibody.

Cells were further costained with 2 *µ*l anti-GPVI or anti-α2-integrin antibodies, respectively, excess antibody again was removed by washing. 0.2 *µ*l Alexa-647-conjugated secondary antibody were used to detect primary reagents. Staining reactions were stopped by the addition of 250 *µ*l FACS-buffer. Analysis was performed on a Becton Dickinson (Heidelberg) FACS Canto II and data analyzed using FloJo software 7.6.3 (TriStar, Ashland, USA).

2.4.5. Adhesion experiments

Cover slips (1.2 cm in diameter) were coated over night at 4°C with ECMs as indicated in Table 2. After 2 washing steps with water, cover slips were allowed to dry under the clean bench for 30 minutes. Subsequently 2.8 x 10^5 MKs enriched by a BSA gradient of a day 5 culture (see 2.4.3) were applied onto the cover slips in DMEM supplemented with 300ng/mL CXCL12. After 4 hrs of incubation at 37°C and 5% CO_2, medium was aspirated. Cover slips were washed with PBS twice and cells fixed with 4% PFA for 30

min. After additional three washing steps (PBS) free binding sites were blocked with 3% BSA in PBS. MKs were identified by staining with an anti-CD41-FITC antibody and mounted in DAPI containing Fluoromount G medium (Southern Biotech, Eching, Germany). Surface coverage of coated cover slips was analyzed using Nikon NIS elements software (Nikon, Düsseldorf, Germany). For adhesion-blocking GPVI and α2-integrin-antibodies (cf. Table 1) were added to the cell suspension (1:100) and then applied on the coverslips.

Table 2 - Utilized ECM proteins. Final working-concentration, species origin and manufacturers.

Protein	Species origin	Concentration	Manufacturer
Collagen I	Murine	10μg/cm^2	Abd Serotec
Collagen I	Human	10μg/cm^2	Sigma
Collagen III	Human	10μg/cm^2	Beckton Dickinson GmbH
Collagen IV	Murine	10μg/cm^2	Beckton Dickinson GmbH
Fibronectin	Human	5μg/cm^2	Beckton Dickinson GmbH
Laminin	Murine	10μg/cm^2	Millipore
BSA	Bovine	3% BSA/PBS	Biochrom AG

2.4.6. Proplatelet formation assay

For the PPF assay, wells from 48-well cell culture dishes were coated with proteins listed above in Table 2. Day 3 MKs in suspension were applied into the wells, analyzed and quantified every 24 hrs for proplatelet-formation.

2.4.7. Zymography

Zymography is used as a functional in gel-assay to show enzymatic activity of collagenases and gelatinases. It was performed with cell lysates of day 3 MKs, derived out of fetal liver cell culture, which were additionally incubated for 24 hours on ECMs as described above in chapter 2.4.4. Cells were lysed in 10mM Tris-HCl pH7.4, 60mM EDTA, 1% IGEPAL, 0.4% sodium deoxycholate. 20μg total lysate was applied for one sample and proteins were first concentrated electrophoretically in a 7.5% plyacrylamide-gel and then were separated in a gel supplemented with 1% (w/v) gelatin under non reducing conditions. MMP-activation was controlled by application of 1μU MMP2-

standard and 0.05ng/μl MMP9 recombinant protein (both ProteaImmun, Berlin). After electrophoresis, the gelatin gel was washed at 4°C, 2x 1hr in washing buffer I (50 mM TrisHCl, 10 mM $CaCl_2$, 2.5% TritonX-100, 0.02% NaN_3,pH 7.5) and over night at 37°C in washing buffer II (50 mM TrisHCl, 150 mM NaCl, 10 mM $CaCl_2$, 0.02% NaN_3,pH 7.5).Subsequently the gel was Coomassie-stained (0.25g Coomassie, 50 mL ddH_2O, 10 mL glacial acetic acid, 40 mL methanol) and color stripped with destaining solution (80% ddH_2O, 10% glacial acetic acid, 10% methanol).

3. Results and Discussions

3.1. RanBP10

3.1.1. The microtubule modulator RanBP10 plays a critical role in regulation of platelet discoid shape and degranulation

3.1.1.1. In vivo disruption of RanBP10 by gene trap

Another β1-tubulin binding factor is Ran binding protein 10 (RanBP10), a novel protein that also binds Ran. RanBP10 localizes in the cytoplasm of mature MKs and platelets, where it concentrates on polymerized noncentrosomal MTs.[42] In addition, RanBP10 harbors guanine nucleotide exchange factor (GEF) activity toward Ran. Depletion of RanBP10 protein in MKs leads to the disruption of MT filaments.16 This result, together with its high GEF activity for Ran, indicates a potential role for RanBP10 as a regulator of MT organization and stabilization in mature MKs and prompted us to examine RanBP10-null platelets in a mouse model. Efficient knockdown of RanBP10 protein in primary MKs is technically difficult; low transduction rates and sustained protein stability result in the need to analyze single infected cells. We sought to study the consequences of complete RanBP10 ablation in vivo and took advantage of a gene-trap approach to generate RanBP10-deficient mice by using the embryonic stem cell clone RRZ 226. The gene trap lies within intron 2 of the RanBP10 gene, introducing a β-geo exon with a strong splice acceptor site. On the affected allele, mRNAis transcribed under the endogenous RanBP10

promoter, but exon 2 splices into the gene trap exon, which is followed by a strong termination signal. We intercrossed RanBP10 heterozygous mice to generate animals of all genotypes, isolated fetuses, and stained with X-Gal to visualize reporter gene activity (Figure 7A). Blue color was absent in wild-type controls (left panel) but clearly detectable in mice harboring the transgene, with increased intensity in nullizygous mice (middle and right panels). Nonuniform staining confirmed the restricted RanBP10 spatiotemporal expression observed by Northern blot.[42] Nullizygous mice showed no RanBP10 protein (Figure 7C) and no RanBP10 mRNA (for data cf. Kunert 2009, Figure 2D).[43] PCR-based genotyping of genomic DNA was successfully established and exclusively amplify wild-type or mutant alleles (Figure 7B). In summary, we generated mice lacking functional RanBP10. These mice were viable and showed no conspicuous phenotype, hence permitting analysis of the consequences of RanBP10 loss on MKs and platelet biogenesis.

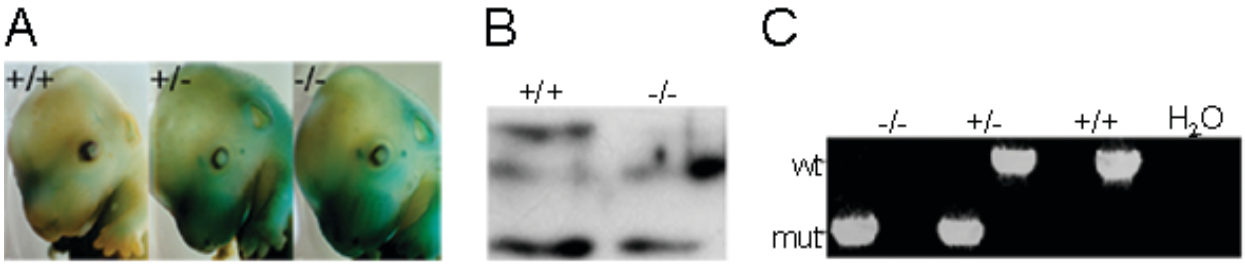

Figure 7 - Generation of RanBP10-deficient mice by a gene trap approach. RanBP10 deficiency in mice can be identified by (A) X-gal staining, (B) immunoblotting using a specific anti-RanBP10 rabbit antiserum and (C) genomic PCR . Subpanels (A) and (B) by Stefan Kunert, subpanel (C) Imke Meyer. Adopted from Kunert et al. Figure 2.[43]

3.1.1.2. MT filaments in MKs from RanBP10-null mice

We first compared tubulin expression in mature MKs forced to overexpress EGFP–RanBP10 and those depleted for RanBP10. Whereas MKs overexpressing RanBP10 showed increased MT filament bundling, shRNA-mediated depletion of endogenous protein resulted in many short MT filaments or an absence of tubulin staining, a phenotype not detected with any other manipulation. Cortical tubulin staining is only found in cells undergoing proplatelet formation, and quantitation of the staining pattern confirmed that increasing or reducing RanBP10 expression in primary MKs affects MT filaments in opposing directions (Figure 3A[43]). We next asked whether the tubulin staining pattern in RanBP10-null MKs would resemble our in vitro results and examined MT staining patterns in MKs from wild-type and knockout animals. Most MKs derived from control animals revealed the expected reticular staining pattern of MT filaments (Figure 3B[43]), whereas only half the mutant MKs showed such staining. In 46% of the RanBP10-null cells, MT filaments were shortened and showed discontinuous MT filaments indicated by a punctate MT network (Figure 3C[43]). Thick bundling of MTs, as observed in RanBP10-overexpressing MKs, was never seen in MKs of wild-type or RanBP10-null animals. Quantitation of the tubulin staining (Figure 3D[43]) indicated that RanBP10-deficient mice phenocopy the reduced tubulin staining found after RNA interference and confirmed that RanBP10 plays an important role in MT filament function in MKs.

3.1.1.3. RanBP10 ablation leads to reduced proplatelet-forming MKs

Proplatelet production is impaired in β1-tubulin–deficient mice.[39] Because RanBP10 was originally identified as a β1-tubulin binding protein,[42] we checked for a similar influence of RanBP10. Fetal liver cells were cultivated in the presence of thrombopoietin

and analyzed for occurrence and frequency of CD61 MKs. Wild-type cultures yielded 47% CD61 cells compared with 51% in RanBP10-knockout cultures, indicating that RanBP10 has no major influence on megakaryopoiesis per se. Cell death and proliferation rates were comparable, excluding the possibility of an indirect effect of RanBP10 on the fraction of CD61 MKs (data not shown). Analysis of proplatelet production in culture is a bona fide technique for examining platelet biogenesis, as shown for NF-E2, GATA1 β1-tubulin, and other mouse models.[39,118,119] We followed proplatelet formation by phase-contrast light microscopy. In wildtype cultures, 34% of MKs elaborated proplatelets on day 4 to 5 of culture in accordance with published data.

Table 3 - Blood cell counts of RanBP10-deficient mice. Ery indicates erythrocyte; Hb, hemoglobin; Hk, hematocrit; MCH, mean cellular hemoglobin; MCV, mean cellular volume and - not significant. Data were generated by Stefan Kunert and Imke Meyer. Table adopted from Kunert et al. Table 1.[43]

	+/+ (n=13)	+/- (n=16)	-/- (n=17)	*p*
Platelets, nL	857 ± 202	789 ± 217	832 ± 169	-
Leukocytes,	6.71 ± 2.53	8,32 ± 3.95	6.51 ± 2.20	-
Erythrocytes,	9.48 ± 0.47	9.58 ± 0.62	8.96 ± 0.35	< .05
MCV, fL	83 ± 2.52	83 ± 4.08	89 ± 2.62	< .05
MCH, fmol/Ery	1.01 ± 0.02	1.01 ± 0.05	1.07 ± 0.04	< .05
Hk, %	0.79 ± 0.04	0.80 ± 0.05	0.80 ± 0.03	-
Hb, mM	9.54 ± 0.56	9.68 ± 0.54	9.54 ± 0.46	-

In RanBP10-null cultures the fraction of proplatelet forming MKs was consistently less than 30% (cf. Kunert et al. Figure 3E[43]). This statistically significant reduction did not, however, influence peripheral platelet counts (832 nL in mutant animals compared with 857 nL in littermate controls; see Figure 3F[43] and Table 3); the slight reduction in proplatelet formation in vitro might be compensated in vivo. Values for hemoglobin, hematocrit, and leukocyte counts were virtually identical in the 2 groups (Table 3), but erythrocyte counts were reduced by 6% in RanBP10$^{-/-}$ mice and mean red cell volume was increased by 7% (Figure 8). In summary, RanBP10 is dispensable for MK formation and platelet biogenesis but affects red blood cell size and number slightly.

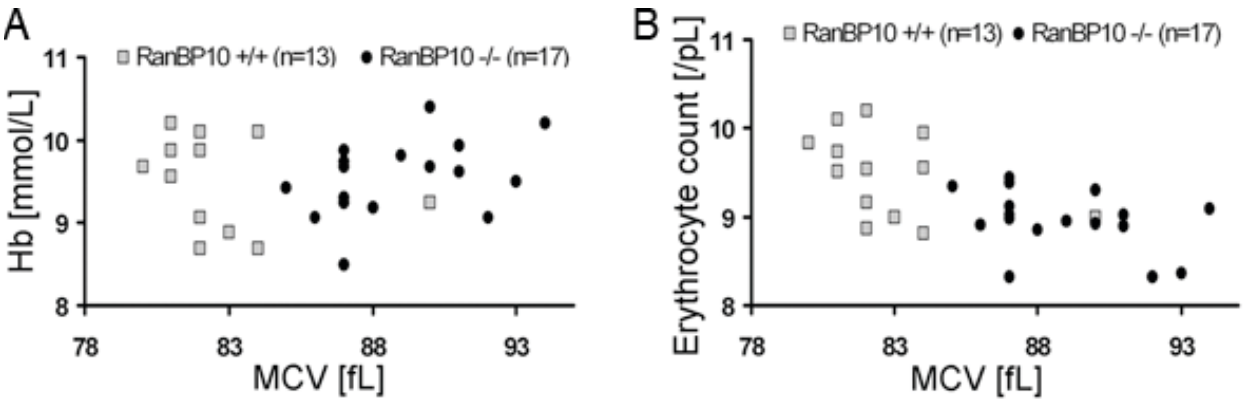

Figure 8 - Parameters of peripheral red blood cells in RanBP10-null and wildtype mice. (A) RanBP10-null mice have an increased mean cellular volume (MCV) without effecting the overall hemoglobin (Hb). (B) The erythrocyte count in RanBP10-null mice is slightly decreased. Data were generated by Stefan Kunert and Imke Meyer, Figure adopted from supplementary Figure 1 Kunert et al.[43]

3.1.1.4. Loss of RanBP10 results in a disordered platelet marginal band

Although RanBP10 seems dispensable for megakaryopoiesis and platelet biogenesis in vivo, MT filaments play additional roles in maintaining platelet shape and function, as shown in mice lacking β1-tubulin.[39] To determine whether platelet shape is affected in RanBP10-null mice, we studied their ultrastructure by using immunofluorescence and transmission electron microscopy. Those experiments confirmed that mutant platelets have a more spherical shape. There were no obvious differences in the appearance of RanBP10-null platelets with respect to distribution, size, shape, or number of granules.

Platelets from β1-tubulin mice are spherical and harbor only 2 to 3 MT filaments per coil in their marginal band.[39] Because RanBP10 is a β-tubulin binding protein, we asked whether lack of RanBP10 affects the composition of the marginal band. In agreement with the literature,[39,120] wild-type platelets exhibited 8 to 12 MT filaments (cf. Kunert et al. Figure 4D[43]). In RanBP10-null platelets we found a spectrum of reduced, normal, or highly increased filament numbers, ranging from 5 to 26 (4E,H[43]). In single cross-sections we even found MT bundles cut in both longitudinal and transverse sections (for data see Figure 4F[43].), and in some platelets, coils were not restricted to the platelet poles but also located internally (Figure 4G[43]). IF performed on platelets stained for β-tubulin verified the data. These results argue strongly that RanBP10 helps keep cortical MT filaments in structurally precise configuration to avoid platelet anisocytosis (Figure 4H[43]).

3.1.1.5. Defective hemostasis, platelet activation, and aggregation in RanBP10-deficient mice

Having demonstrated that the MT coil is impaired in many RanBP10-null platelets, we asked next whether RanBP10-deficient mice have a bleeding defect by using a standard assay where tail bleeding is followed during the course of 6 minutes.We found that 8 of 10 RanBP10$^{-/-}$ mice showed a markedly prolonged bleeding time compared with only 2 of 10 wild-type animals (cf. Kunert et al. Figure 5A). Blood flow decreased over time but soon resumed in mutants because there was no stable plug formation. To define whether the hemostatic defect is caused by impaired platelet activation, we investigated granule release by stimulating platelets with different concentrations of PAR4p for 5 minutes, followed by flow cytometric analysis of CD62P expression. RanBP10 $^{-/-}$ platelets showed reduced CD62P release in response to PAR4p (Figure 5B right panel[43]) and failed to release dense granules, even after exposure to 1mM PAR4p (Figure 5D[43]).

Because granule number was normal in mutant platelets (see Figure 4B,E[43]), we suspected that defective MT dynamics may prevent degranulation. To test this hypothesis, we studied release of the α-granule protein platelet factor 4 (PF4) in response to agonists. In resting platelets, PF4 was solely present in pellet fractions, whereas increasing concentrations of thrombin lead to its release into supernatant fractions. In RanBP10-deficient platelets, by contrast, 1mM PAR4p or 0.1 U/mL thrombin did not result in PF4 translocation, and protein remained in the pellet. Greater thrombin concentrations (1 U/mL) led to nearly complete release of PF4 from wild-type platelets, whereas in mutants, approximately one-half of PF4 remained within the pellet fraction (Figure 9A). To exclude a reduced granule cargo load in mutant platelets, we tested for

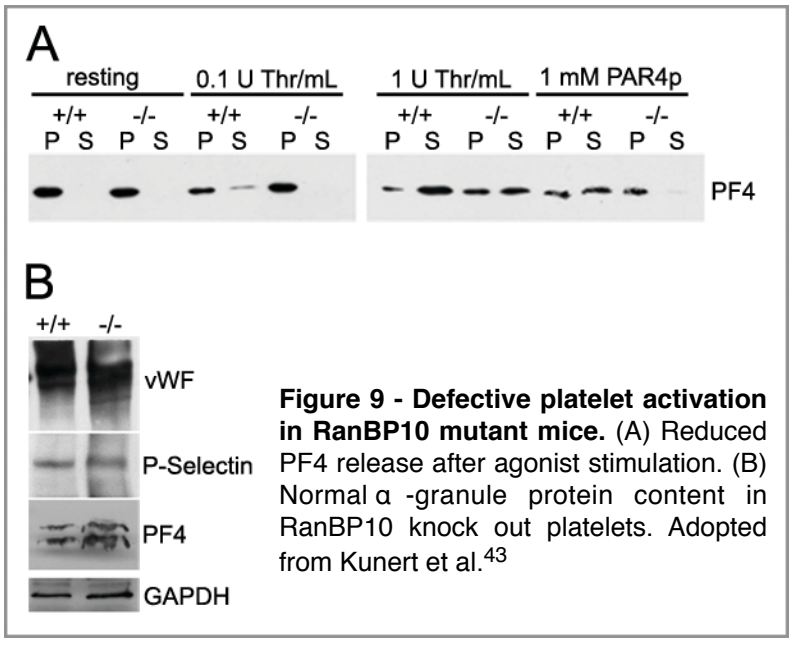

Figure 9 - Defective platelet activation in RanBP10 mutant mice. (A) Reduced PF4 release after agonist stimulation. (B) Normal α -granule protein content in RanBP10 knock out platelets. Adopted from Kunert et al.[43]

expression of von Willebrand factor, P-selectin, and PF4 by immunoblotting (Figure 9B). Glyceraldehyde-3-phosphate dehydrogenase loading control of both lanes was adjusted after densitometric analysis, showing that protein expression in RanBP10-null platelets was within 10% range of the expression found in wild-type controls (data not shown).

Taken together, these data support the hypothesis that the MT-binding factor RanBP10 is essential for platelet function in hemostasis, most likely by modulating MT dynamics and marginal band contraction during platelet activation. The main feature of platelet function is thrombus formation, mediated by both adhesion and aggregation. We therefore measured aggregation of wild-type and mutant platelets stimulated with collagen, thrombin, or adenosine diphosphate (ADP). As summarized in Figure 6, RanBP10$^{-/-}$ platelets showed reduced aggregation, especially with low concentrations of collagen or thrombin. These data strongly suggest the conclusion that the bleeding defects in RanBP10$^{-/-}$ mice result at least partly from diminished platelet function by reduced granule release.

3.1.2. Altered microtubule equilibrium and impaired thrombus stability in mice lacking RanBP10

3.1.2.1. RanBP10 depletion is partially compensated for by overexpression of RanBP9

Microtubules are polymerized filaments assembled from α- and β-tubulin dimers that harbor distinct functions during the cell cycle including the mitotic spindle or the aster-type fibers that emanate from the microtubule-organizing center present during interphase.[121,122] While most β-tubulin isotypes are broadly expressed and highly homologous, β1-tubulin is only expressed in MKs and platelets. TUBB1-deficient mice are thrombocytopenic and show platelet spherocytosis demonstrating the importance of β1-tubulin for platelet formation and function. [39] RanBP10 binds to the C-terminus of β1-tubulin, however, RanBP10 ablation in mice does not lead to a reduced peripheral platelet count.[43] As proplatelet formation was slightly reduced in MKs derived from nullizygous animals, we first asked whether compensatory mechanisms are responsible for the unaltered platelet count. RanBP10 shares a cellular homolog, designated RanBP9 which is ubiquitously expressed.[123] We isolated RNA from liver, spleen, bone marrow and purified CD61 cells and compared mRNA expression levels of RanBP9, TUBB1 and TUBB5 between RanBP10-deficient mice and wildtype controls. While expression levels were comparable in liver and bone marrow, we found marked upregulation of RanBP9 mRNA in $CD61^+$ MKs and in spleen, a tissue enriched for MKs. TUBB1 was also upregulated while TUBB5 expression was unaffected (Fig. 10A). Ploidy analysis of primary bone marrow MKs revealed that 2N/4N levels were normal, while the fraction of high ploidy (8N/16N/32N) was significantly increased in the absence of RanBP10 (Fig. 10B), suggesting that these MKs might produce more platelets. Next, we quantified bone marrow MKs in sectioned femur bones from transgenic and mutant mice. As shown in Fig. 10C the amount of $CD41^+$ MKs in mutant mice was slightly elevated. Finally, we analyzed platelet life span by labeling with a fluorophore-conjugated antibody against GPIX.[116] As expected the fraction of fluorescent platelets decreased during the next 5 days, but there was no difference between mutant and control animals (Fig. 10D). Taken together these results imply that the reduced proplatelet formation found in RanBP10-null mice is compensated for by several mechanisms including increased MK number, ploidy and upregulation of RanBP9 that finally result in an overall unaltered platelet count.

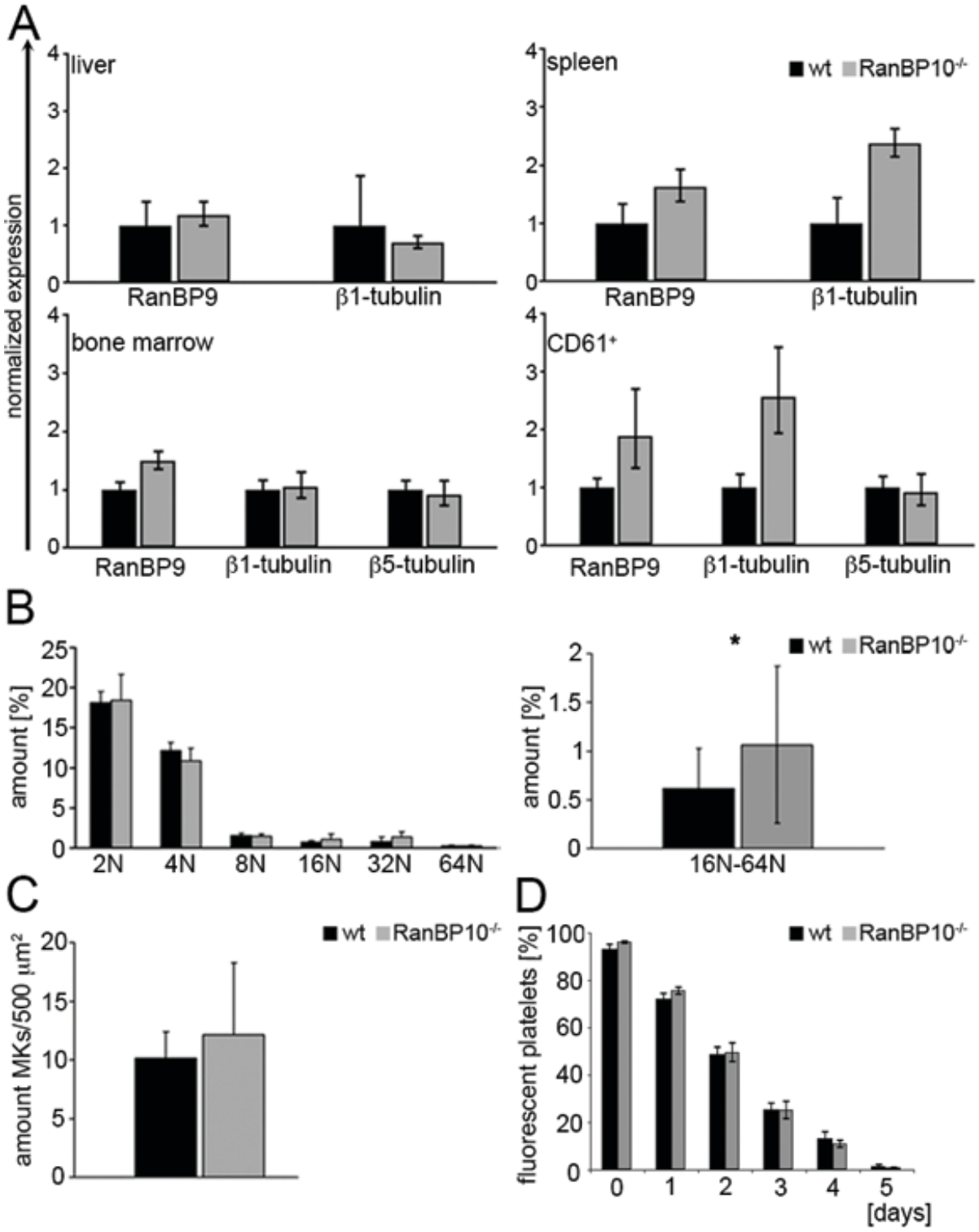

Figure 10 - RanBP10 depletion is partially compensated for by overexpression of RanBP9 but does not influence platelet turn-over, MK numbers or receptor expression. (A) RanBP9 mRNA expression is upregulated in spleen and CD61+ cells of RanBP10-null mice. Expression levels were analyzed by quantitative real-time PCR and were normalized to GAPDH. (B) Bone marrow MKs were stained with PI and ploidy evaluated by flow cytometry. The amount of 16N-64N MKs is significantly elevated in RanBP10$^{-/-}$-mice compared to controls. (C) The amount of bone marrow MKs is slightly elevated in mutant mice. (D) Platelet life span in vivo is unaltered in mice lacking RanBP10. * indicates $p<0.05$. (A) and (B) by Stefan Kunert, subpanel (C) by Stefan Kunert and Imke Meyer, subpanel (D) by Imke Meyer.

3.1.2.2. Slightly altered platelet adhesion under shear and normal spreading

To exclude the possibility that the platelets produced in the absence of RanBP10 have altered surface receptors we stained resting platelets with a series of specific fluorophore-labeled antibodies. Platelets lacking RanBP10 harbor the same density for fibrinogen receptor (αIIb/β3), von Willebrand receptor (GPIbβ, GPV, GPIX), collagen receptors (GPVI, α2β1) as well as CD9 and CLEC-2 on their surface as platelets of control mice (Fig. 11A). While the flow cytometric expression analysis provides important information on density and composition of platelet surface receptors, it does not address their binding properties to matrix proteins under more physiological conditions. Therefore, we analyzed spreading of platelets adhering to fibrinogen or collagen and found no alterations in RanBP10$^{-/-}$-mice (Fig. 11B). Adhesion of mutant platelets to collagen under flow tended to be slightly increased under high shear (7700 s^{-1}), but was rather normal under intermediate shear (1000 s^{-1}, Fig. 11C) or when the chamber was coated with vWF (data not shown). Additionally, we calculated the thrombus volume and could not observe any differences between wildtype and RanBP10-null platelets adhering to collagen under intermediate shear rates of 1000 s^{-1} and 1700 s^{-1} (Fig. 11D). These data together imply that binding mechanisms to matrix proteins under flow conditions are overall unaffected in the absence of RanBP10.

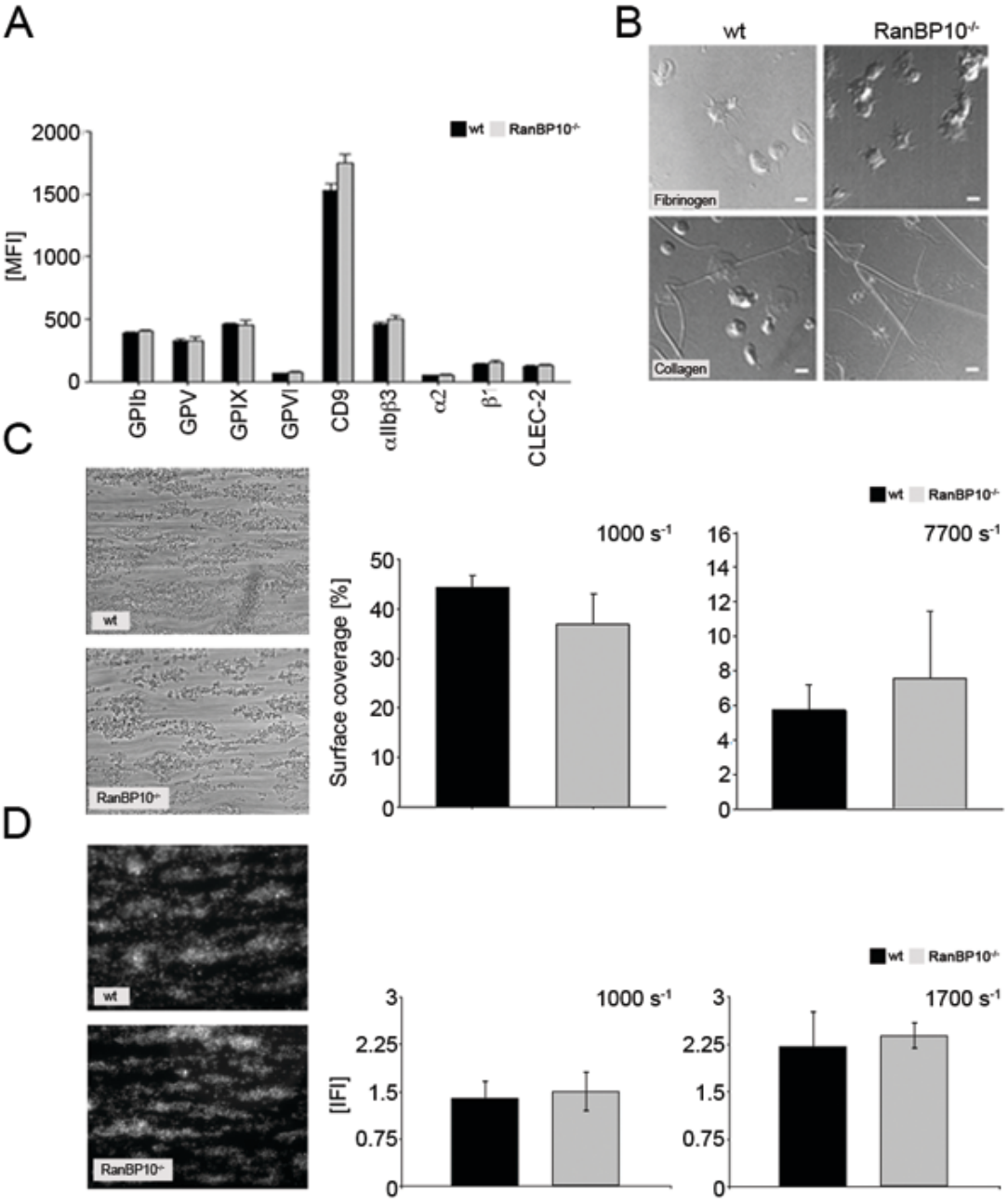

Figure 11 - RanBP10$^{-/-}$-platelets show modestly altered adhesion under shear but spread normally. (A) Regular receptor density of platelet surface markers in RanBP10-null and control mice. (B) Platelet spreading on fibrinogen (top row) and collagen (bottom row) is unaffected in RanBP10-null platelets, showing the typical flat "fried-egg" appearance.(C) Phase contrast microscopy and quantitative analysis of surface coverage of wildtype and RanBP10$^{-/-}$-platelets aggregating on collagen under intermediate flow (1000 s^{-1} left panel) and high flow (7700 s^{-1} right panel) show overall unaltered adhesion. (D) Analysis of thrombus volume in integrative fluorescence intensities (IFI) and quantification shows that wt and RanBP10$^{-/-}$-platelets form equal-sized thrombi at each shear rates as depicted for 1000 s^{-1} left panel and 1700 s^{-1} right panel Subpanels (A) and (D) by Imke Meyer, subpanel (B) by Stefan Kunert subpanel (C) by Stefan Kunert and Imke Meyer.

3.1.2.3. Thrombus formation is impaired in RanBP10$^{-/-}$ mice

As RanBP10-null mice display a severe bleeding phenotype in a tail bleeding assay,[43] we sought to determine whether thrombus formation is affected in vivo in mice lacking RanBP10. We used an intravital mouse thrombosis model where thrombus formation in mesenterial arterioles is initiated by ferric chloride and visualized by intravital fluorescence microscopy. In wildtype controls (n=9), initial thrombus formation at the vessel wall was first detectable 8 minutes after injury, followed by thrombus growth. Typically within 20 to 25 minutes the vessel was obstructed (Fig. 12A, top row and for Videos see Suppl. Video 1 on the website of BLOOD journal[43]). In RanBP10-null mice, platelet adhesion at the site of injury was normal and we could observe the beginning of thrombus formation after 7.5 minutes (n=13). Intriguingly, the growing thrombus was unstable and continued to disintegrate during the overall observation period of up to 40 minutes (Fig. 12A, lower row and Suppl. Video 2 on the website of BLOOD journal[43]). Quantification indicates that recanalization in arterioles was only found in RanBP10-null mice. Onset of thrombus formation was within the same time range as in wildtype controls (Fig. 12B, left panel), but 8/13 arterioles failed to occlude within the overall observation time of 40 minutes in mutant mice compared to 1/9 wildtype arterioles (Fig. 12B, right panel). These findings together imply that RanBP10 plays an essential role to ensure thrombus stability in vivo which may also provide an explanation for the severe bleeding phenotype found in the tail-bleeding assay in the mutant mice.[43]

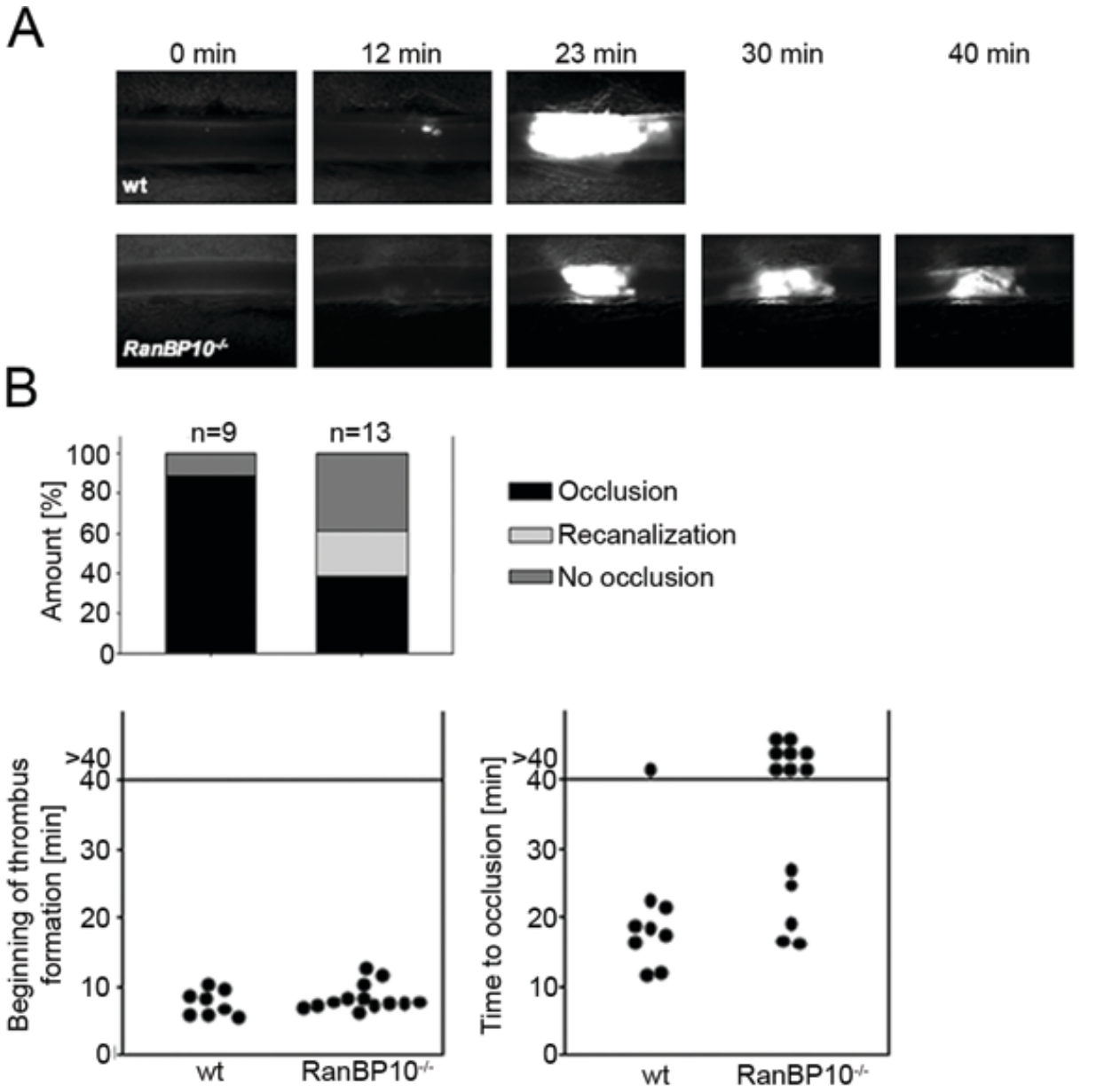

Figure 12 - RanBP10$^{-/-}$-mice show impaired thrombus formation in an arterial thrombosis model. (A) The onset of thrombus formation after $FeCl_3$-induced injury is unaffected (upper panel). In wildtype mice vessels are occluded within 20 minutes whereas in mutant animals no stable clot is formed within 40 minutes observation time (lower panel). (B) Quantification reveals that in wildtype mice 8/9 injured arterioles show normal occlusion, while this was only present in 5/13 arterioles of RanBP10$^{-/-}$-mice. In 8/13 arterioles we found no occlusion or recanalization within the observation time.Those experiments were performed by Stefan Kunert.

3.1.2.4. RanBP10 is not essential for δ-granule number, composition or release but for platelet shape change

We recently showed reduced release of α- and lysosomal granules in RanBP10$^{-/-}$ platelets in response to suboptimal agonist concentrations by impaired expression of P-selectin (CD62P), or CD63 by flow cytometry. Furthermore, exocytosis of antiangiogenic factor PF4 was diminished in response to PAR4p in mutant platelets.[43] As α-granules harbor either pro- or antiangiogenic proteins that can be released differentially,[114,124] we analyzed whether there is any bias in release between both genotypes. Platelets were stimulated with ADP for release of proangiogenic factors VEGF and fibrinogen and with thromboxane A2 mimetic U46619 for antiangiogenic factor thrombospondin. Overall, we found less granule factors of either type in the supernatant of mutant platelets, indicating that there is no difference between pro- or antiangiogenic factors (data not shown), which implies that RanBP10 causes a general defect in granule release. However, we found that α-granules in mutant platelets harbor slightly less VEGF and fibrinogen than in wildtype controls (data not shown).

Dense granule release can be monitored by different methods: the most convenient way is to stain resting platelets with the fluorescent dye mepacrine and document the decline of fluorescence after agonist treatment. The extent of fluorescence retained after stimulation is a measure of dense granules that failed to be released. Platelets from either strain labeled equally well for mepacrine (Fig. 13A, left panel). When suboptimal concentrations of thrombin (0.1 to 0.2 U/mL) were applied, slightly more fluorescence was retained in mutant platelets compared to wildtype controls after 1 minute. This was normalized after 5 minutes. After stimulation with 1 U/mL thrombin, dense granule release was identical in both strains (Fig. 13A, right panel). As mepacrin release is an indirect marker for dense granule release, we next determined the ATP release in response to suboptimal thrombin and collagen by aggregoluminometry. Using this technique in whole blood we encountered some variability between different samples of either genotype but did not find any significant difference in maximal (Fig. 13B) or cumulative (data not shown) ATP release between transgenic animals and wildtype controls. Additionally, we determined the release of the dense granule constituent serotonin. Washed platelets were stimulated with PAR4p and pelleted and serotonin concentrations measured after 1, 3 and 5 minutes in the supernatant. We found no difference between wildtype and mutant platelets indicating that serotonin

release is overall unaltered (Fig. 13C). The small discrepancy between mepacrine assay, maximal ATP release and serotonin release is most likely due to the different methods in platelet preparations and readouts and also found in other studies.[116] Therefore, we refined our analysis on numbers and size of α- and dense-granules. On electromicrographs of wildtype and mutant platelets there was no significant difference between granule numbers (Fig. 13D) or diameter (Fig. 13E), although in mutant platelets dense granule number was slightly increased by 18%, most likely due to the increased size. It is worth mentioning that platelet fragments after complete granule release are underrepresented in the ultramicrographs due to their markedly reduced density compared to intact platelets. We thus cannot determine the amount of granules in completely degranulated platelets. Next, we asked whether exogenous ADP can at least partially rescue the aggregation phenotype in RanBP10-null platelets. We added 0.25 μM ADP to platelets from either genotype prior to stimulation with 5 μg/mL collagen. This threshold of ADP concentration alone had no impact on aggregation. When added to collagen in wildtype platelets, shape change and maximal aggregation were not significantly altered. In contrast, ADP preincubation of RanBP10-null platelets normalized the shape change and - in part - the maximal aggregation (Fig. 13F, left panel). We measured the duration of shape change in response to collagen and found a statistically significant attenuation in mutant platelets. In the presence of ADP this attenuation was restored to normal levels (Fig. 13F, right panel). These findings together imply that lack of RanBP10 does not affect dense granule number, composition or release, although the release is attenuated somewhat in response to low agonist concentrations, but that RanBP10 is important for optimal platelet shape change when suboptimal or threshold concentrations are used.

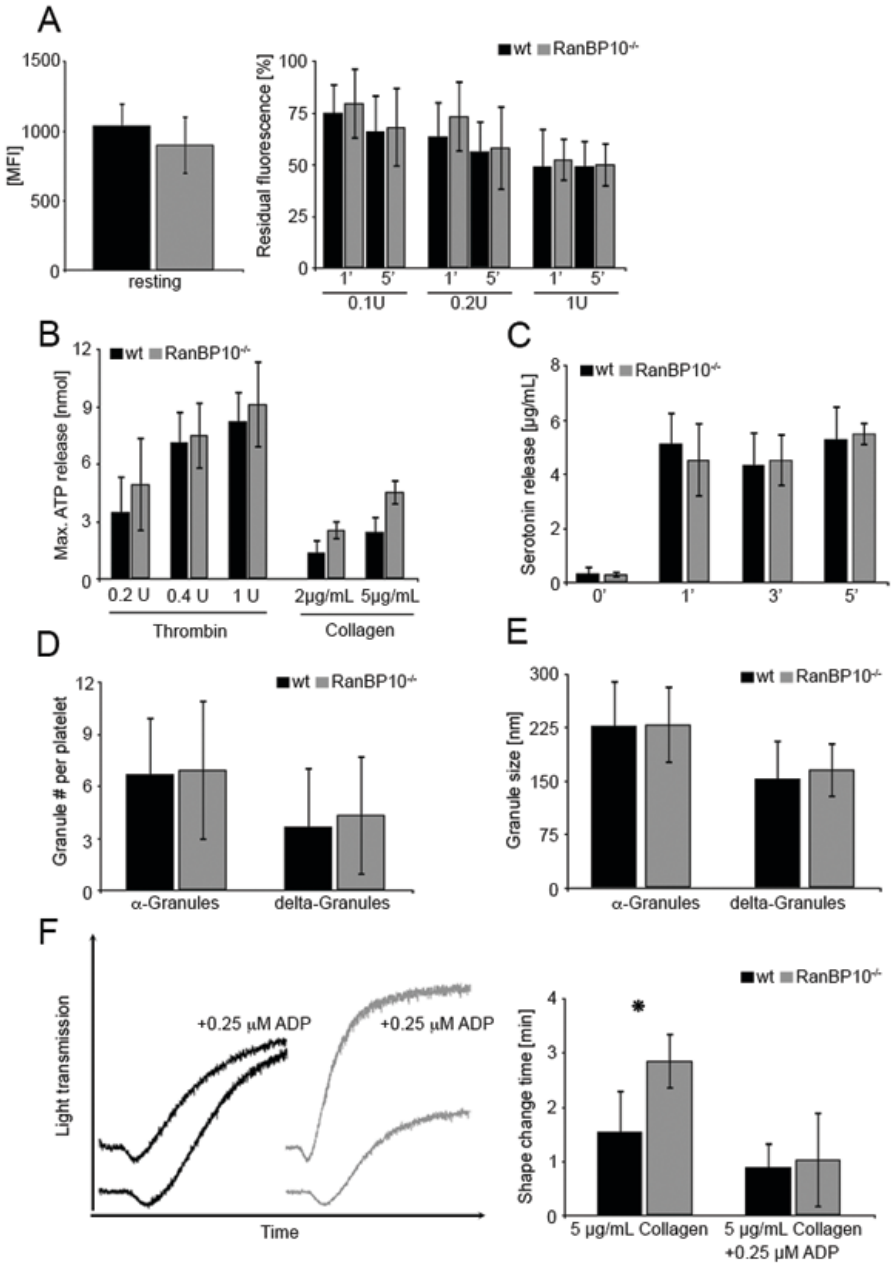

Figure 13 - Release of α- and delta-granule contents of platelets in RanBP10$^{-/-}$ mice. (A) Similar mepacrine uptake in platelets of either genotype (MFI = Mean Fluorescence Intensity (left panel). Mepacrine release after 5 minutes is overall unaltered between wildtype and RanBP10-null platelets, whereas it is slightly slower in mutant platelets after 1 minute when suboptimal thrombin concentrations (0.1 or 0.2 U/mL) are used. Data show an average of six independent experiments. Error bars depict the standard deviation. (B) Maximal ATP release in whole blood of RanBP10-null animals and controls was determined by aggregoluminometry revealing a slightly increased ATP release after treatment with 0.2, 0.4 or 1 U/mL thrombin or with 2 or 5 μg/mL collagen. (C) Serotonin release in response to 0.5 μM PAR4p treatment showed no difference after 1, 3 or 5 minutes between wildtype and mutant platelets. (D) α- and dense granules were counted on electron micrographs showing no difference in intact platelets. (E) Measurements of the diameter of α- and dense-granules show that there is no difference between wildtype and RanBP10-null platelets. (F) Wildtype and RanBP10-null platelets were activated with 5 μg/mL collagen in the presence or absence of 0.25 μM ADP. This concentration had little impact on collagen-induced aggregation in wildtype platelets (black), but restored attenuated shape change and aggregation in knockout platelets (grey curves) almost to wildtype levels (left panel). Time of shape change is significantly prolonged in mutant animals, but can be restored in the presence of threshold ADP concentrations (right panel). Mean of 5 experiments is shown, error bars indicate standard deviation (* indicates $p<0.05$).

3.1.2.5. RanBP10 is crucial for marginal band contraction after platelet activation

RanBP10 binds to both Ran and β1-tubulin. The distribution of these proteins offers mechanistic insight into how RanBP10 might modulate noncentrosomal microtubules: De novo nucleation of microtubule filaments can be induced by cooling and rewarming of platelets and cold-induced depolymerization is reversed when platelets are rewarmed again.[108] We stained wildtype and RanBP10$^{-/-}$ platelets after cooling (4°C) and after rewarming (4°C --> 37°C) for β-tubulin and did not detect any differences in the staining pattern between the two genotypes, demonstrating that RanBP10 is not required for de novo nucleation of microtubule filaments from dimeric tubulins. Ran, co-localizing with tubulin in resting platelets, is also found throughout the cell in cooled platelets and redistributes with newly polymerized cortical microtubules after rewarming, indicating that the binding properties of RanBP10 are unaffected (Fig. 14A). We recently found that in many activated RanBP10-null platelets the microtubule coil remained larger in size.[43] We thus asked whether RanBP10 affects the centralization of granules by impaired microtubule ring contraction by performing TEM on stimulated platelets. In most wildtype platelets treated with 1 or 0.1 mM PAR4p, granules were found in the platelet center, whereas they were scattered throughout the complete cytoplasm in RanBP10$^{-/-}$ platelets (Fig. 14B). Contracted microtubule filaments were visible in wildtype platelets stimulated with either concentration (Fig. 14B i and ii arrow), whereas in many RanBP10$^{-/-}$ platelets the marginal band was still detected in the periphery. It showed an irregular distribution pattern forming longitudinal and cross-sectioned coils or had spiral instead of circular coils (Fig. 14B iii and iv) giving independent evidence that microtubule ring contraction is impaired in the absence of RanBP10. In platelets of either genotype agonist treatment led to formation of pseudopodia, indicating that redistribution of actin filaments occurs independently of tubulin dynamics. Staining of platelets with fluorophore-labeled phalloidin also showed no difference in actin filament morphology (data not shown). To gain better insight into the kinetics of marginal band contraction we performed β1-tubulin immunostainings. In resting platelets the marginal band size was comparable between the genotypes. However, already 1 minute after stimulation with PAR4p, we found contraction in wildtype, but not in knockout platelets (Fig. 14C). After 5 minutes the average diameter converged toward the wildtype. Thus, in RanBP10-null platelets the attenuated or incomplete marginal band contraction occurs shortly after stimulation.

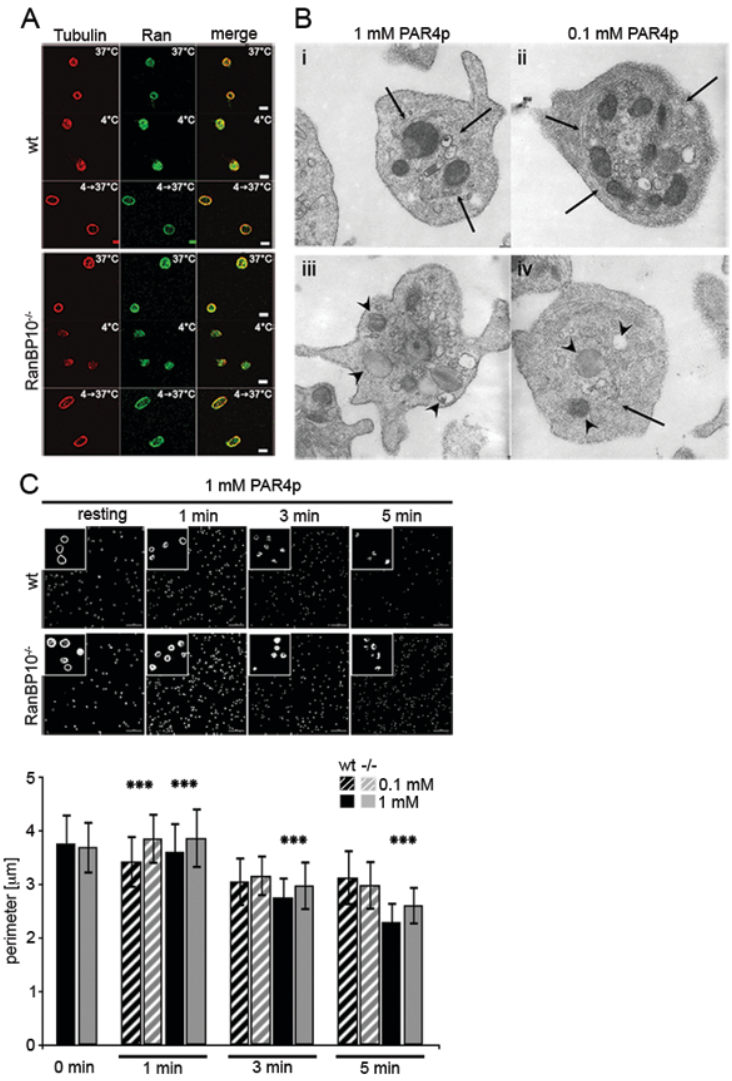

Figure 14 - RanBP10 is dispensable for spontaneous microtubule polymerization but is essential for marginal band contraction after platelet activation. (A) Microtubule de- and repolymerization was normal after platelet cooling and rewarming. Tubulin is stained in red (Alexa647) and Ran in green (Alexa488). (B) TEM ultragraphs of platelets treated with 1 mM or 0.1 mM PAR4p show that in wildtype platelets the microtuble coil contracts (arrows in i and ii) and granules become centralized. In RanBP10$^{-/-}$-platelets (iii and iv) the marginal microtubule band fails to contract and granules are no longer centralized (arrowheads). Normal platelet activation is shown by protrusions in either strain. Subpanel iv shows an example of dysorganized microtubule filaments (arrow). (C) Immunofluorescence stainings with anti-β1-tubulin antibody and quantification of fixed platelets at time-points indicated after stimulation with PAR4p (top panel). Quantification of wildtype (black) and RanBP10$^{-/-}$ platelets (grey) after stimulation with 0.1 mM PARp (hatched bars) and 1 mM PAR4p (filled bars). *** indicates $p<0.001$ with a double-sided Student's t-test with independent variances. Subpanels (A) by Stefan Kunert, subpanel (B) by Stefan Kunert and Imke Meyer, subpanel (C) by Imke Meyer.

3.1.2.6. RanBP10 modulates the tubulin-equilibrium

If RanBP10 alters the dynamic of the microtubule ring contraction in low agonist concentrations, lack of RanBP10 might best be detected using the initial shape change in Born aggregometry. The murine thromboxan A2 (TxA2) receptor couples to the more sensitive Gα12/13 subunits and at higher agonist concentrations additionally to the Gαq subunit, leading to RhoA activation upstream of platelet shape change, granule centralization and release.[58] At high concentrations of TxA2 mimetic U46619 (0.5 µM) mutant and wildtype platelets showed the same shape change and aggregation as expected. Intermediate agonist concentrations (0.1 µM) caused shape change without aggregation in either strain, while threshold concentrations (0.04 µM) led to shape

change only in wildtype animals, while it was abrogated in RanBP10$^{-/-}$ platelets (Fig. 15A). Lower concentrations did not induce any shape change (data not shown). Posttranslational tubulin modifications are indicators of microtubule filament stability and turn-over.[125] Antibodies recognizing glutamylated or tyrosinated tubulin showed normal expression in resting platelets of both strains or when platelets of either strain were stimulated with ADP or PAR4p (Fig. 15B). Platelets also contain EB1, an end binding protein that binds selectively to the plus-end of filaments.[126] Again, there was no difference between wildtype and knockout platelets, indicating that these properties are not affected by RanBP10. Finally, we sought to analyze the effect of RanBP10 ablation on tubulin polymerization biochemically. Polymerized microtubules were isolated from fetal liver-derived MKs after ultracentrifugation and the pelleted fraction compared with the soluble supernatant. Total β1-tubulin protein was upregulated in RanBP10-null MKs and a substantial part found in the pellet fraction enriched for polymerized microtubules (Fig. 15C). α-tubulin was shifted in a comparable amount into the polymerized form. To our surprise, β2- and β5-tubulin that are ubiquitously expressed, are not affected by RanBP10 ablation, as the commerical β-tubulin antibody has a low affinity for the β1-tubulin isotype. When taxol was added prior to ultracentrifugation, the majority of all tubulin isotypes was found in the polymerized fraction as described,[39] while GAPDH remained in the soluble fraction (data not shown). These data imply that RanBP10 might prevent α/β1-tubulin dimers from premature polymerization. As this interaction is specific for β1-tubulin, RanBP10 function might be more profound in MKs and platelets where β1-tubulin is highly expressed.[34] In order to test whether this altered microtubule equilibrium causes a delayed shape change, we preincubated wildtype platelets with taxol prior to activation with collagen. As shown in Fig. 15D taxol-stabilized platelets had a delayed shape change and showed less aggregation, partially phenocopying the RanBP10-phenotype. Taken together, our data suggest that RanBP10 acts more on the β1-tubulin monomer-polymer equilibrium than on a direct bundling of MT filaments.

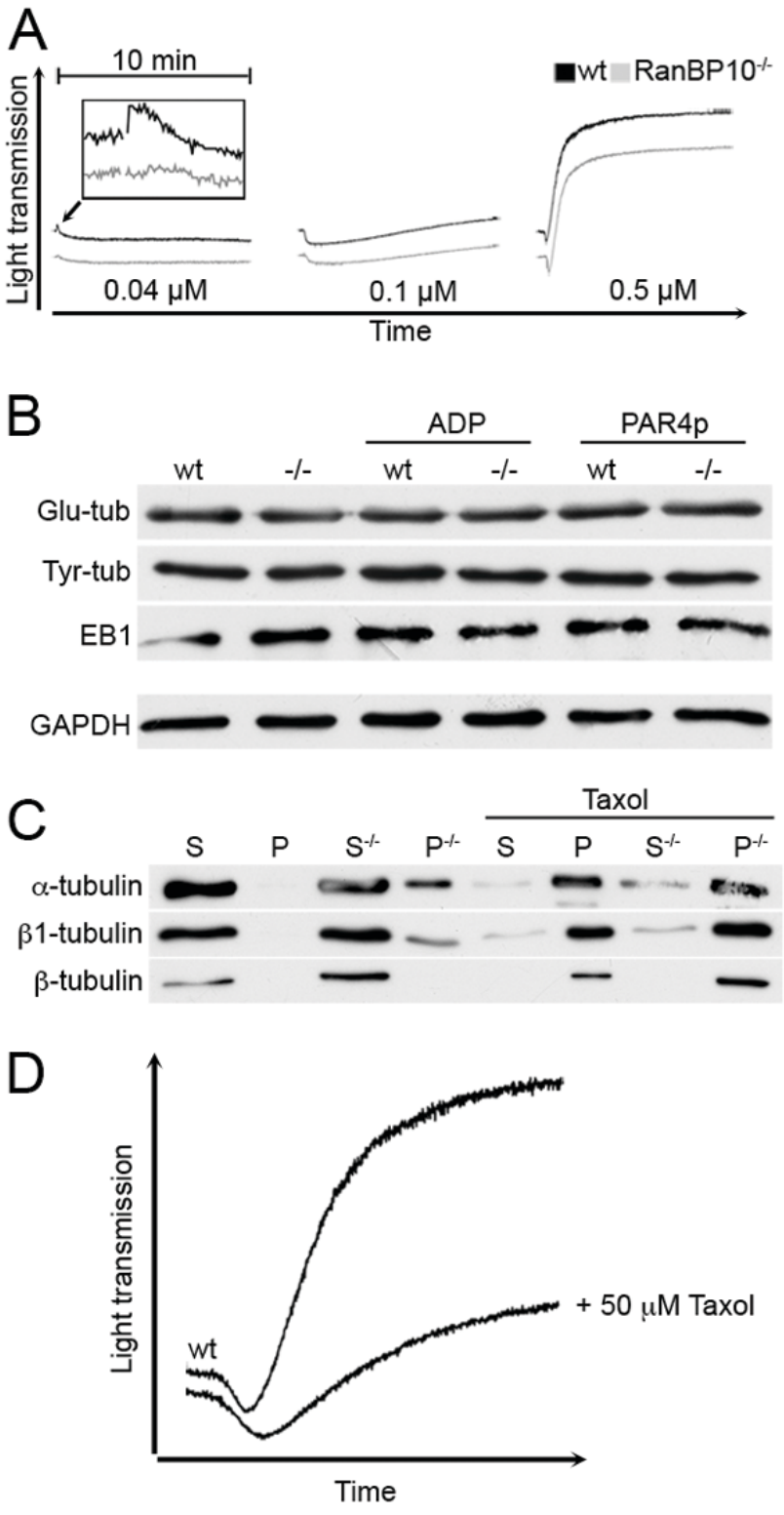

Figure 15 - RanBP10 modulates the tubulin-microtubule equilibrium and is essential for the platelet shape change. (A) Platelet activation with 0.04 *µ*M U46619 (left panel) still caused a shape change in wildtype (black curve), but not in RanBP10$^{-/-}$ platelets (grey curve). Intermediate concentrations (0.1 µM, middle panel) induced shape change without aggregation in both strains, while high concentrations led to similar shape changes in platelets of wildtype and mutant platelets with full aggregation (right panel). (B) The amount of glutamylated (Glu-tub) or tyrosinated tubulin (Tyr-Tub) as well as EB1 proteins were unaffected in resting, ADP or PAR4p-stimulated knockout platelets (-/-) compared to wildtype (wt) controls. (C) RanBP10 prevents premature polymerization of α/β 1-tubulin dimers. Megakaryocytes lacking RanBP10 (-/-) show an increased fraction of β1-and alpha-tubulin in the pelleted fraction (P) representing polymerized microtubules compared to the soluble (S) fraction isolated from the supernatant. Other β-tubulins recognized by a commerical β-tubulin antibody remain unaffected. In the presence of taxol filaments polymerize independent of RanBP10. (D) Platelets were incubated with either 0.5 mM taxol or PBS prior to aggregometry with 5 *µ*g/mL collagen. When microtubules were stabilized with taxol, the shape change is delayed and aggregation diminished, mimicking the RanBP10-null phenotype.

3.1.3. Discussion

The transition from hemostatic thrombocytes in other vertrebrates to anucleate blood platelets in mammals and humans has come with a specialized set of proteins like β1-tubulin. In the absence of this most diverse β -tubulin isotype, mice are thrombocytopenic and the platelets formed are spheric with reduced reactivity toward thrombin. Although other tubulins including β2- and β5-tubulin are upregulated, the equilibrium of tubulin monomers and polymerized microtubules is shifted toward the monomeric state.[39] Schwer and coworkers concluded that β1-tubulin helps to polymerize microtubules in MKs and platelets. The divergent C-terminus of β1-tubulin including the helices α10 and α11 that protrude from the globular core of tubulin and are known to bind microtubule-associated proteins. This domain has been used as bait in a yeast two-hybrid screen and we identified RanBP10, a novel protein whose expression is restricted to bone marrow and spleen and enriched in MKs.[42] Several compensatory mechanisms might contribute to compensate for slighty impaired proplatelet formation seen in MKs that lack RanBP10: an overall increase in bone marrow MKs, higher ploidy, and the upregulation of RanBP9, its only known paralog. While both proteins have 68% sequence homology on the amino acid level[127] and share a SPRY, LisH and CTLH domains, the RhoGEF-consensus domain has not been identified in RanBP9. While both proteins bind to Ran, it is unclear whether RanBP9 binds to β1-tubulin. None of the original clones in the two-hybrid screen encoded for RanBP9, although it is expressed in MKs and has been found in many screens using different baits.[128]

The severe bleeding phenotype in RanBP10-null mice has originally been attributed to impaired granule release in response to sub-optimal concentrations of agonists[43] rather than to platelet spherocytosis, which has a weaker impact on platelet function.[109] Our data presented in this study rather suggest that lack of RanBP10 leads to a delayed contraction of the circumferential microtubule coil in reponse to threshold concentrations of platelet agonists that attenuates granule centralization and release (Fig. 14B and 14C). In RanBP10$^{-/-}$ animals the average microtubule coil consists of 12 filaments compared to 10 in wildtype mice.[43] This is independently reflected by upregulation of β1-tubulin mRNA and protein found in this study (Fig. 10A and 15C). Although contraction of the peripheral microtubule coil precedes granule centralization and release, microtubule stabilizing agents do not prevent the release of granules,[129] suggesting that parallel pathways become activated in response to strong agonists.

The actin cytoskeleton seems to remain unaffected during activation of RanBP10-mutant platelets, as shown by pseudopodia formation (Fig. 14B) and phalloidin staining. Actin-fibers prevent premature granule release and differentially regulate α- and dense-granule secretion in response to agonists.[130]

Early secretion analysis revealed that dense granules are released first, 10 sec after agonist supplementation,[131] followed by α-granules and lysosomes.[52] The release of dense granules is MT-independent. In contrast, several reports describe that although MT interfering agents do not completely abrogate granule centralization, they clearly can inhibit secretion (reviewed in Ref.132).[132] Most likely, the marginal band contraction supports granule centralization by organizing the contractile microfilaments.[133] In mice lacking RanBP10 the release defect is more affecting α- then dense granule exocytosis, which is in concordance with the kinetics observed for the attenuated MT coil contraction. This defect, however, is indeed rather subtle, suggesting that the attenuated shape change seen in aggregometry (Fig. 13F) occurs in a small time window. This slow agonist response reaction present for multiple agonists in threshold concentrations might reflect best the in vivo situation. It is striking that most assays, in which platelet function was addressed under flow conditions, were completely normal and even the intravital thrombosis model revealed an effect only in the late phase of thrombus stabilization (Fig. 12), affecting the outer thrombus shell while platelet adhesion and the inner center remained stable.

Mouse RanBP10 is mainly expressed in liver and spleen, an organ in which MKs are enriched. In contrast, protein levels were virtually absent in neutrophils compared to MKs,[43] excluding a role of RanBP10 in leukocytes for defective thrombus formation. Although our data on aggregometry and flow cytometry has been performed with isolated platelets, indicating the defect to be intrinsic to platelets, we cannot completely rule out the possibility that RanBP10 expression in endothelial cells contributes to the defective thrombus formation. RanBP10 mRNA expression levels in endothelial cells were as low as in 3T3-fibroblasts, compared to 3-fold higher expression in primary MKs (data not shown), thus making it highly unlikely that RanBP10 in the endothelial tissue contributes significantly to the impaired thrombus formation. Interestingly, the pattern of reduced platelet reactivity, bleeding phenotype and impaired thrombus formation is partially phenocopied in transgenic mouse models lacking the G-protein receptor-

associated subunits Gα11/q and Gα12/13, which transduce their signals to the small GTPase RhoA. Several models imply that Gα11/q is essential for granule release and aggregation, but dispensable for shape change.[134] In contrast, both Gα13 and RhoA are essential for proper platelet shape change preceding granule concentration and release after activation.[58,135,136] Mice lacking RanBP10 show normal reactivity to thrombin or high concentrations of U46619 or ADP, suggesting that the Gq pathway is unaffected in these mice, whereas shape change and MT ring contraction in RanBP10$^{-/-}$-platelets is attenuated when lower agonist concentrations are used[43], Fig. 13F, 14C and 15A) similar to mice lacking Gα13[58] and platelets of RhoA$^{-/-}$-mice that are also more spherical and increased in size.[58,135,136] RanBP10 harbors a RhoGEF consensus domain which might have a so far uncharacterized enzymatic or binding activity to RhoA. Although the non-mammalian homolog Rho1 was not a substrate for the GEF-activity of RanBP10, we cannot exclude that this domain might modulate RhoA function. The attenuated marginal band contraction identified in RanBP10$^{-/-}$-platelets could thus be a mechanistic link between impaired cellular signaling and the microtubule dynamics underlying granule centralization and release. Several G-protein coupled receptors have been considered targets for influencing platelet activity,[137] however, more downstream targets are an alternate strategy, especially when their expression is overall restricted to the megakaryocytic lineage. RanBP10 might become one of these targets in the future.

3.2. Effect of an anti-GPIb-platelet antibody on bone marrow megakaryocytes in a mouse model of passive immune thrombocytopenia

Antibodies that recognize auto-antigens cause a variety of severe auto-immune disorders. Several triggers including infections and vaccinations have been described that generate antibodies cross-reacting to surface receptors on platelets and their immediate precursor cells in the bone marrow, the MKs. Typically, antibodies recognize either of the highly expressed fibrinogen receptor GPIIb/IIIa (CD41/61) or von Willebrand factor receptor GPIb/V/IX (CD42a-d) subunits, but other platelet receptors are also targeted.

Since MKs express the same surface receptors as platelets they can be targeted by auto-antibodies their fate in this regard is controversially discussed. To obtain insight in severity and impact of anti-platelet antibodies on MKs an anti GPIb antibody was applied to mice once or multiple times and particularly MKs were analyzed in situ.

3.2.1. Diametral affect of platelet depletion on MK homeostasis

Application of an antibody directed against platelet surface receptor GPIbβ (CD42b) into mice leads to an immediate clearance of peripheral platelets due to binding on the cell surface and subsequent degradation by the reticuloendothelial system. This strategy has been used by many groups as a simple animal model for passive immune thrombocytopenia.[138,139] In order to analyze the effect of the anti-GPIb antibody on bone marrow megakaryocytes (MK) we injected C57/BL6 mice once, twice or three-times intraperitoneally with the depletion or a control isotype antibody. Platelet depletion could be observed as quickly as 4 hrs after injection.[139] Mice were sacrificed on day 3, 5 or 7 after single application and on day 5, 8, 10, 12, and 14 after start of the multiple injection series (Figure 16A). Femur bones and spleen were removed and for each mouse platelet counts were determined in blood withdrawn by cardiac puncture . Our data clearly show the expected pattern of platelet depletion and recovery in single-depleted mice: Platelet counts recovered to normal within 5 - 7 days (Figure 16B). One additional application of antibody on day 4 kept platelet counts low on day 5. In contrast, when mice were treated a third time on day 7, platelet counts were doubled on day 10 (black squares in Figure 16B), only three days after the last injection, suggesting that platelet biogenesis is fully active. Spleen size and weights in animals of either group were normal and we found no signs of splenomegaly (data not shown).

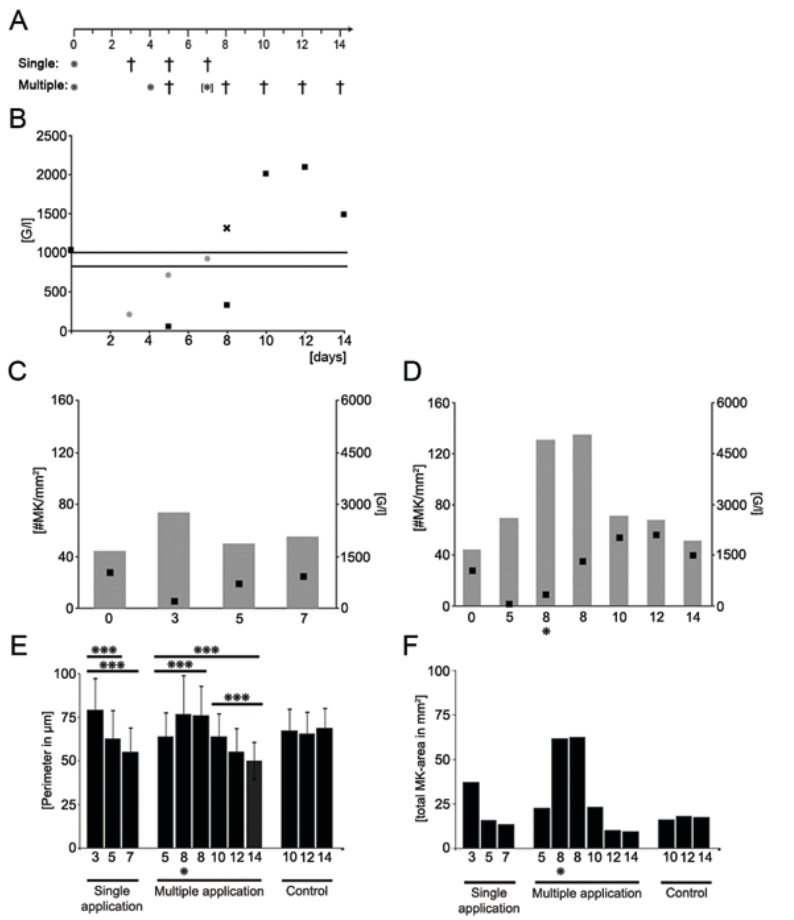

Figure 16 - Injection of depletion antibody leads to dynamic changes in BM. (A) Scheme of antibody application, time-points by asterisks. Mice were sacrificed on days indicated by †. (B) Platelet counts of mice in response to the antibody. Platelet counts recover within 7 days after a single antibody injection, as indicated by grey circles. Black squares: three-fold injections, the x indicates a mouse were the third injections was omitted. C) Correlation of platelet counts (black dots) and grey bars after a single antibody injection show that MK numbers increase in compensation for depletion of peripheral platelets. (D) After multiple injections platelet counts remain suppressed on day 5 and 8 and become overshooting on day 10 and 12. (E) Mean MK perimeter after single application decrease significantly. After multiple application perimeter increase and then decrease substantially. Control antibody application has no impact on MK perimeters. (F) BM area covered by MKs is markedly increased and subsequently reduced after a single antibody injection. Multiple injections lead to an increase of BM area covered by MKs which is followed by a substantial decrease in comparison to (C) control animals.

We next asked how platelet depletion does affect MK homeostasis within bone marrow. Mice were sacrificed and femurs sectioned on days indicated. As expected, we found a diametral correlation between platelet counts and MK number. After a single antibody application MK number almost doubled on day 3, but went down to normal on day 5 and 7 when platelet counts also restored (Figure 16C). In contrast, after multiple injections, MK numbers per area tripled on day 8 and were still elevated on day 10 and 12 when platelet counts from overshooting thrombopoiesis were above average (Figure 16D). In a refined analysis we determined MK perimeter and found that the mean MK size is significantly reduced after a single injection. In contrast, in mice who received multiple injections MK perimeter increases up to normal levels on day 8 and then declines after the last injection substantially (day 10-12) (Figure 16E and 18A). As platelet biogenesis correlates with MK size,[140] we estimated the potential thrombopoiesis rate by the product of MK number and area per bone area. These data clearly show that total MK

area within bone marrow is dramatically up-regulated on day 8. It is of interest that this is independent of whether a third injection on day 7 has taken place which further decreases the peripheral platelet count (see asterisk in Figure 16F).

Taken together our data show that MKs have a smaller perimeter in response to an increased demand caused by a single antibody injection. In contrast, multiple application of this antibody leads to a substantial compensatory increase in both MK number and size while after the last injection MK size shrinks when platelet counts normalize.

3.2.2. The depletion antibody decorates MKs in BM and does not lead to apoptosis

The dynamic changes in MK number and size in response to the depletion antibody raises the question how this anti-platelet antibody directly affects the megakaryocytic progenitor cells situated in bone marrow. We therefore stained bone sections of mice with both, a directly FITC-conjugated anti-CD41 antibody and an Alexa-647-fluorophore-conjugated antibody against rat-IgG which recognizes the depletion antibody. As shown in Figure 17A on day 3 all MKs were positive for the depletion antibody, whereas about 5% of MKs were negative on day 5. On day 7, virtually all MKs were negative for the depletion antibody. As expected, platelets were cleared in the spleen and we found many platelet-sized fragments in antibody-treated animals that stained positive for CD41 and rat IgG. In contrast, mice treated with a control isotype antibody showed no fragments in spleen sections and $CD41^+$ MKs are negative for the secondary antibody (Figure 17B). It has been reported that MKs from patients with ITP show features of apoptosis or para-apoptosis.[93] We next asked whether binding of the depletion antibody leads to any signs of apoptosis. To address this question we performed a TUNEL assay in situ on bone sections to label nuclei of cells that have single strand breaks. Analysis of stained sections clearly indicates that MKs of mice treated with an anti-platelet antibody are not TUNEL-positive (Figure 17C). In addition, MK morphology based on the overall appearance, CD41 staining pattern and the shape of the nucleus after DAPI counterstaining was inconspicuous. In contrast, MKs in control bone sections treated with DNase were clearly positive (data not shown). We also detected some background staining of small cells as expected, indicating - as expected - that the assay is able to

sensitive enough to detect apoptotic cells or lymphoid cells expressing TdT during development on our bone sections.

In summary, our data show in situ that the anti-GPIb platelet depletion antibody is detectable on bone marrow MKs until at least day 5 post application. Despite the presence of the depletion antibody on the MK surface, these cells do not show any features of apoptosis. CD41- and depletion-antibody positive covered cellular fragments are present in the spleen where they are cleared by the reticuloendothelial system.

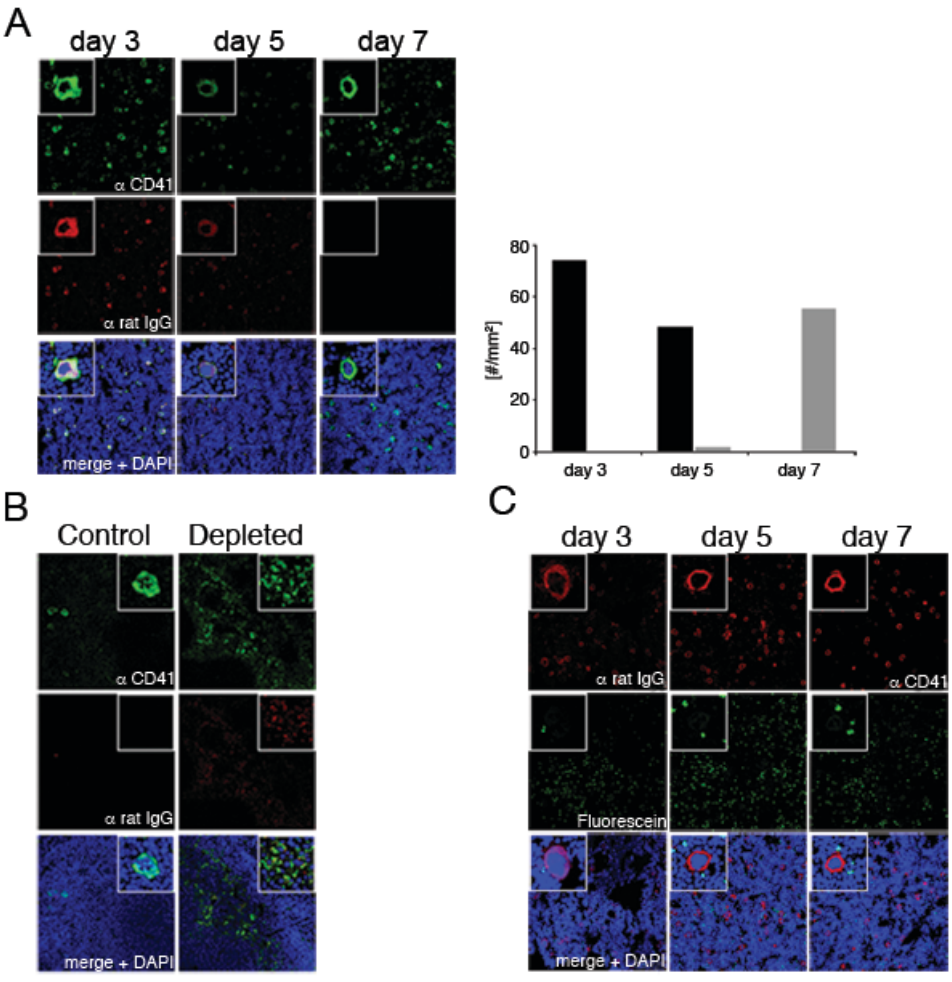

Figure 17 - Effect of anti-platelet antibody on bone marrow MKs in situ. (A) IF on bone marrow MKs. Cells were stained with a FITC-conjugated anti-CD41 antibody and an Alexa-647-conjugated anti-rat IgG antibody for detection of the depletion antibody. This antibody is detectable until day 5 and not present on day 7. Insets show magnification of a representative MK indicating an overall inconspicuous morphology (left panel). Fractions of antibody-decorated (black columns) and antibody-free (grey columns) MKs on day 3, 5, and 7 after antibody application (right panel). (B) Spleen sections indicate that antibody-positive platelet fractions are found on day 5 after application. (C) TUNEL assay on whole bone sections indicates that antibody-decorated MKs are not apoptotic. Sections are stained with an Alexa-647-conjugated anti-rat IgG antibody or anti-CD41 antibody counterstained with an Alexa-647-conjugated anti-rat IgG antibody (red cell upper row). Single strand breaks are visible by incorporation of Fluorescein labelled nucleotides (green color, middle row). DNA in nuclei is stained by DAPI inclusion (lower panel).

3.2.3. Studies on MK proliferation after platelet depletion

The increased demand of platelets in mice with sustained thrombocytopenia as well as the compensatory increase in MK numbers and area on day 8 in animals treated three times with the depletion antibody (Figure 16E) prompted us to analyze MKs morphology in these animals. As shown in Figure 18A MKs harbored an overall inconspicuous morphology, but showed a substantial decrease in cell size. The MK population was positive for antibody decoration until day 5 post first injection (Fig. 18A). Interestingly, all MKs were negative on day 10, 12 and 14, indicating that the antibody is not present on MKs 3, 5, or 7 days after the last antibody application. This is in contrast to the kinetic found for mice treated only once (Fig. 2A). We further showed that MK size further shrinks from day 10 - 14 (Fig. 3A and data not shown), in contrast to mice only treated once (Fig. 1E and data not shown).

This finding prompted us to ask where the increased MK population is derived from, whether they are generated de novo from the HSC pool or derived from a pre-existing immature MK pool. The complex biology of MK proliferation and endomitosis makes it difficult to perform simple proliferation assays, particularly when addressed in vivo. We therefore took advantage of the nucleotide derivative 5-ethynyl-2'deoxyuridine (EdU) that can be fed to animals and becomes incorporated into DNA in S-Phase of proliferating cells during mitosis[141]. De novo MK synthesis should be accompanied by highly EdU-positive cells and differentiation from an existing immature pool should come along with cells only mediocre positive for EdU. In situ visualization of EdU is accomplished on BM sections by a copper-catalyzed azide addition, a so called Click-it reaction. For proliferation analyses mice were fed with EdU daily, starting from the first day of antibody application (day 0). First signals could not be seen in bone sections before day 10. As expected we readily detected strong signals in small cells that have undergone DNA synthesis in the presence of sufficient bio-availability of EdU. In contrast, MKs and megakaryocytic progenitor cells are present in distinct ploidy grades of 2N, 4N, 8N, 16N and 32N. MKs of any stage can undergo further rounds of endomitosis and thus have a mixed composition of modified nucleotides in respect to their DNA content. Indeed, we found MKs labeled to different extent and we decided to classify the staining intensity into the following 4 categories: no stain, weak stain, moderate stain, and strong stain (Figure 18B, lower row).

By concept, our approach is a continuous labeling experiment rather than a classical pulse-chase experiment where a marked metabolite is followed over time. Our first question was to identify how continuous feeding of mice with EdU affects the staining of MKs with the Click-it reaction. We have treated mice with control isotype antibody on day 0, 4, and 7 and analyzed bone sections on day 10, 12, and 14 for staining intensity. We found that most MKs had a weak staining on day 10 which increases to day 14 as does the strongly positive cell population (Figure 18, on graph left panel).

Next, we looked at mice treated with the platelet-depleting antibody on the same days. On day 10 MKs classified to the 4 categories showed a similar distribution pattern as those from the control animals. Interestingly, we found that many more MKs were strong positive for EdU on day 12, indicating that these MKs have undergone many rounds of endomitosis in the presence of EdU and might have derived from de novo differentiation together with further maturation of a pre-existing precursor pool. On day 14 the amount of highly positive has declined in comparison to control animals, indicating a high MK turn-over in treated animals. These data are verified by the weakly stained population which is substantially higher than on day 12 and compared to control animals on day 14.

Taken together, these data show for the first time, that MKs forced to compensate for the elevated platelet-demand seem to be generated from an existing cell pool, as categorization shows no markedly differences between treated and control animals. However, the existing pool of MKs is not uniformly active in proliferation, as there were strong positive MKs on day 10 and negative ones on day 14. In response to triple platelet depletion, on day 12 a MK pool fraction becomes highly positive implying high MK proliferation rates compensating for the lack of peripheral platelets by increased thrombopoiesis.

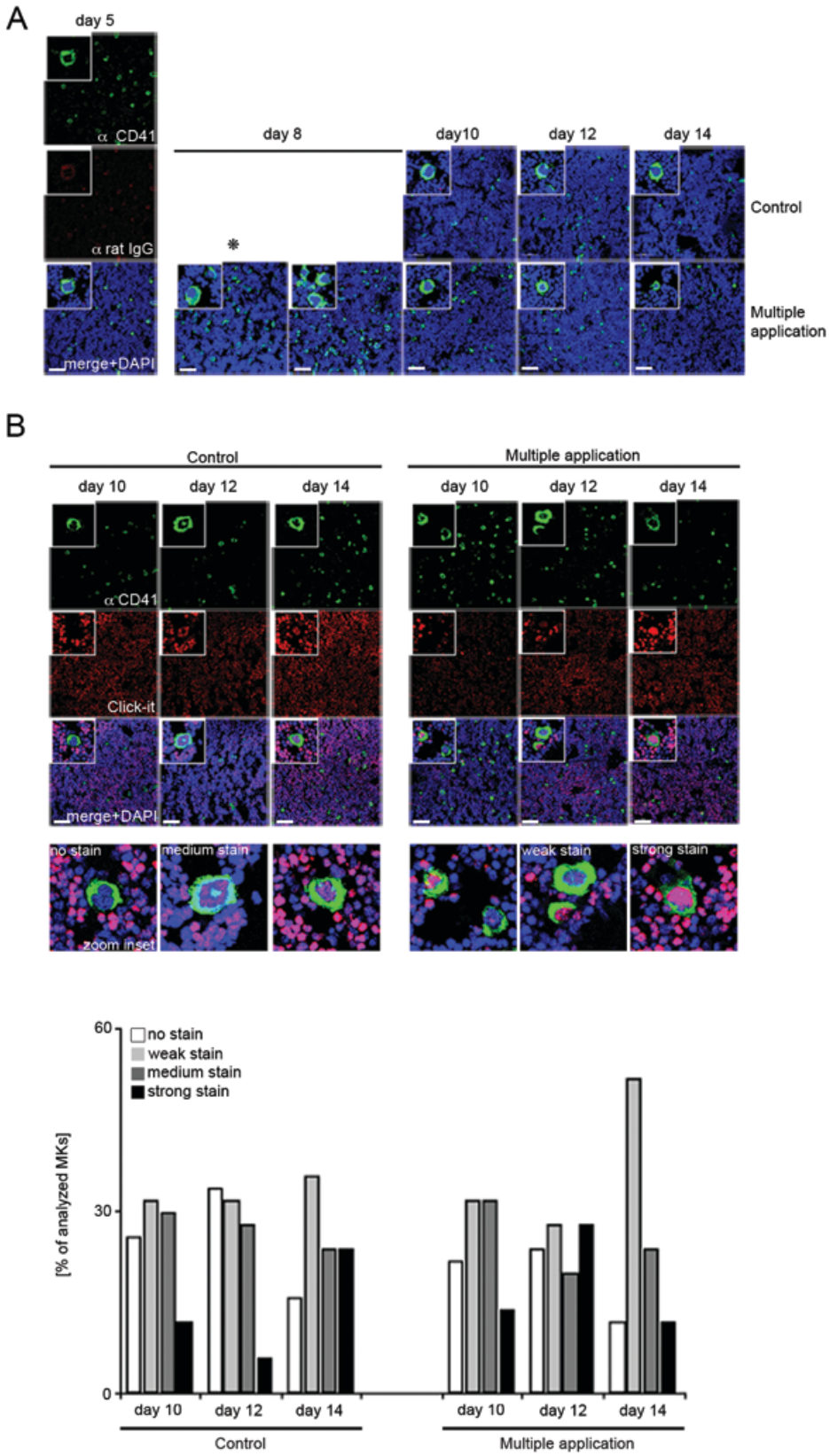

Figure 18 - MK morphology and proliferation rate after multiple antibody injection . (A) MKs in situ are decorated with depletion-antibody until day 5 post first antibody application. The cell morphology is overall inconspicuous but cell count (day 8) is dramatically increased and cell size substantially decreases within overall observation period. (B) Mice were fed with EdU and proliferation rate was determined on time-points as indicated. Control animals show an increase in strongly positive stained MKs during the overall observation period. In treated animals MK this increase seems to be faster and the strongly stained MK-population decreases within the observation period.

3.2.4. Antibody decorated MKs give birth to pro- and pre-platelets

ITP has been considered an autoimmune disorder with accelerated platelet turnover in response to peripheral destruction associated with an increased turnover of MKs that cannot fully compensate for the immense demand. Recent data suggest that low platelet counts in ITP might - at least in some patients - also be attributed to impaired platelet production.[142] Incubation of CD34-positive hematopoietic stem cells in the presence of sera from some ITP patients led to impaired MK growth and reduced MK ploidy in vitro.[95,143] Thrombopoiesis in vivo takes place across the endothelial barrier where megakaryocytic protrusions penetrate the fenestrated tissue and proplatelets or larger preplatelets are shed into the blood stream.[23,24,144] In order to address whether MKs decorated with anti-platelet antibody still undergo pre- and proplatelet formation in vivo, we used a transgenic mouse model in which a modified cDNA encoding eYFP is expressed under the control of the GPIIb (CD41) promoter. Mice heterozygous for the knock-in (GPIIb$^{wt/eYFP-ki}$) still express the GPIIb/IIIa heterodimeric complex on the surface of MKs and platelets, but the demarcation membrane system of the MK becomes positive for eYFP which harbors a myristyl acceptor site. This allows the lipid moiety to become anchored into the internal membrane system. Thrombopoiesis of the cranial bone marrow in these mice can be visualized by intravital two-photon microscopy (Figure 19 and Supplementary Video 1).[23] First, we applied filter settings that eYFP is excited by the two photon-laser with a wavelength of 880 nm. The fluorescence derived from eYFP is displayed in green (Figure

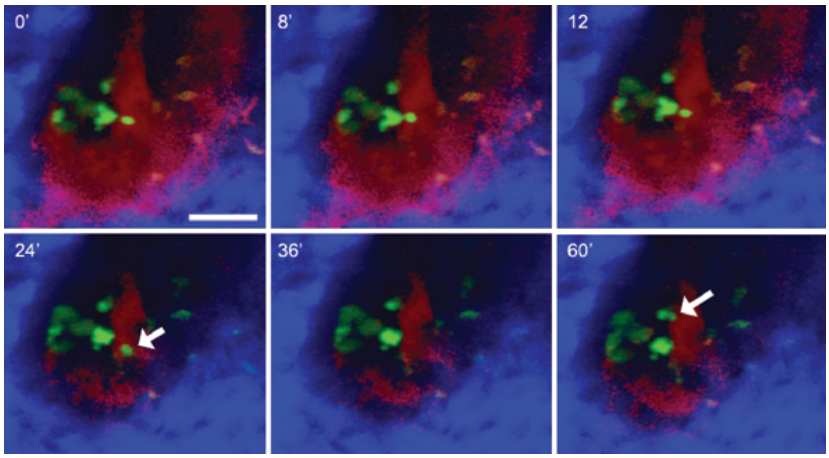

Figure 19 - Still images from Supplementary Video 1. One MK (green) situated within the bone marrow releases a large cytoplasmic fraction into the blood (counterstained with rhodamin-conjugated high moelcular dextran in red). Observation time is indicated. At 24' the piece is torn of into the blood stream (arrow). Bone emerges in blue. At 60' a new (smaller) fragment is penetrating across the endothelial barrier (arrow). Bar = 50 µm. The red color in the lower row is underestimated due a technical problem with the laser stability. For Supplementary Video 1 scan with QR-code reader or see provided data disc.

20A). The depletion antibody was conjugated to an Atto-590 fluorophore and applied to mice either directly before the imaging process (Supplementary Video 2) or 3 days before imaging (Supplementary Videos 3-6 and Figure 20C). This antibody can detected simultaneously with different filter settings and fluorescence is false-coloured depicted in blue. As shown in Figure 20A (middle panel), the MK residing juxtaposed to a vessel within the bone marrow cavity is clearly positive for the anti-GPIb-antibody. In order to separate the bone marrow cavity from the vascularity, we injected Quantum-dots with a fluorescence of 655 nm. Staining of sinusoids and larger vessels was readily visualized (Figure 20A). We performed a series of z-stacks to follow the dynamics of the megakaryocytic cytoplasm. over time As seen in the femur sections, many mature MKs with intense fluorescence staining were juxtaposed to the vasculature. We identified MKs shedding protrusions into the sinusoids either 1 hour after antibody injection (Supplementary Video 2 and Figure 20B) and 3 day post antibody application (Supplementary Videos 3-6 and Figure 20C). These pre- or proplatelets were shed into the bloodstream (Figure 20, arrows). The in Supplementary Videos 4-6 and Figure 20C observed megakaryocyte formes two protrusions. Interestingly, one of these preplatelets started to form long shafts extending a size of over 200 μm, mimicking the extended shafts of a proplatelet found in the in vitro culture system. Over the next hour we observed a continuous release of MK cytoplasm into the blood stream, clearly indicating that the depletion antibody, albeit binding to the bone marrow MKs, does not per se inhibit thrombopoiesis in vivo.

Taken together our results show for the first time that low platelet counts in a simple passive mouse model of immune thrombocytopenia is not solely due to abrogated platelet release across the endothelial barrier, but that MKs, even though decorated with the depletion-antibody, are not apoptotic and can release preplatelets and proplatelets into the blood stream.

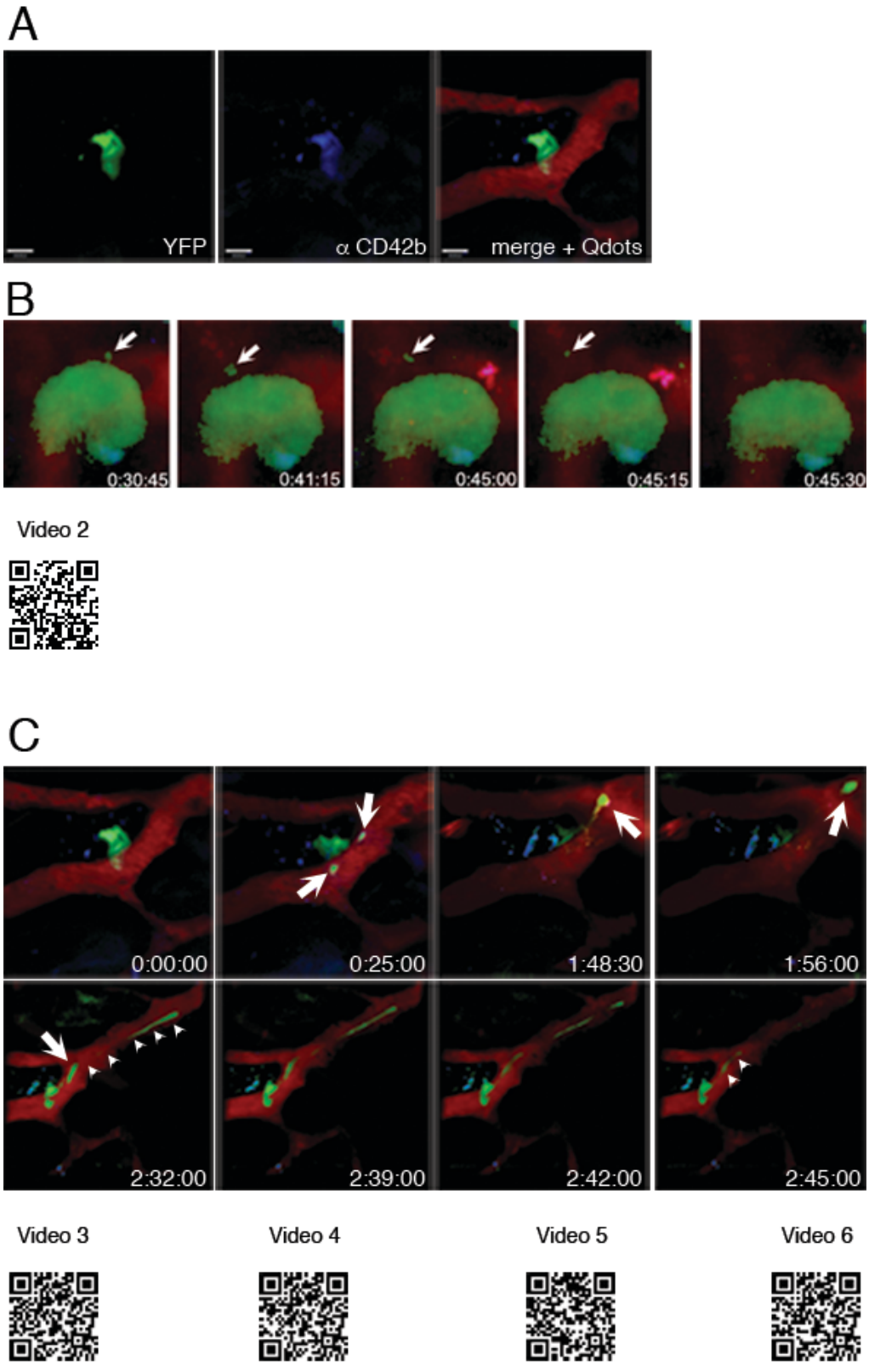

Figure 20 - Antibody decorated MKs can form pre- and pro-platelets in vivo (Still images from Supplementary Videos 2 and 4-6). (A) YFP^{+}-MKs are visible in MPM (left panel) and are antibody-decorated (middle panel). Vascularity is visualized by intravenous injection of Qdots-655. Scale bars indicate 100 μm. (B) Time-lapse microscopy 1 hour after antibody injection. Antibody decorated MKs are able to form proplatelets (arrows). (C) Time-lapse microscopy revealed that the antibody-decorated MK is able to form protrusions (arrows) which grow substantially within the overall observation period (arrowheads, lower panel) and seem to be shed after 2 hrs and 45 min. For Supplementary Videos scan with QR-code reader or see provided. data disc.

3.2.5. Discussion

ITP is an autoimmune disease that affects both children and adults. Thrombocytopenia is always mediated by the presence of antibodies that cross react to platelet surface molecules causing opsonization. Although many features of ITP are shared between children and adults, there are some major differences in the pathophysiology.[145] For most children, ITP is an acute, self-limiting disorder, platelet counts normalize within 3 months and patients get into remission. Only in less than one third of patients thrombocytopenia becomes chronic and often refractory to standard therapy. In contrast, adult ITP patients often has a chronic course of disease and it remains unclear which mechanisms will direct whether platelet counts normalize or not. It is well accepted that the initial trigger for the generation of autoantibodies is an immunization event, often mediated by infection, drug application or a vaccination.[146] Thrombocytopenia in ITP is mediated by a complex interaction of cellular and humoral immunity.[92] Antibody production can be suppressed by anti-CD20 therapy and rituximab treatment is second line therapy for adult patients. The role of T-cells is - despite being present in the literature for decades - still more elusive and mostly based on indirect evidence including elevated cytokine levels or presence of altered populations of Th1, Th2, Th22 or regulatory T-cells.[147] As a consequence of the complex pathomechanism underlying ITP, animal models are rare and typically only mimick a certain aspect. The development and characterization of anti-murine platelet antibodies that induce immediate peripheral platelet destruction[138,139] has led to a simple and robust mouse model that has been exploited extensively. The depletion antibody has been raised in rats and is therefore not a genuine auto-antibody. Nevertheless, application of this antibody leads to immediate depletion of virtually all platelets in the peripheral circulation and can be used to mimick severe platelet loss and is a model for increased platelet demand. It has been shown that continuous daily application of this antibody leads to a refractory state and is thus not a good model for extended thrombocytopenia in ITP.[148] In order to avoid an additional immunization event directed against the rat antibody, we restrained the application of the antibody to three times within one week. Platelet counts clearly show that during this time frame the antibody has still the potential to deplete platelets. Moreover, threefold injection of an antigen within one week is typically not enough to cause an immune response of germinal B-cell mediated maturation toward high-affinity antibodies. In agreement with this finding, it was found

that the platelet kinetics in response to multiple antibody injections were similar when NOD-SCID mice were used as recipients in which no lymphocytes can contribute to the immune response.[148]

Our data show that multiple platelet depletions lead to highly dynamic changes in the bone marrow MK population, by number and by size and by proliferation activity (Figures 16 and 18). It is obvious that changes in MK size and morphology found in bone marrow smears of patients with ITP might reflect those changes[93,149] without being pathological. We have carefully looked for signs of apoptosis but could not detect nuclear condensation, DNA blebbing or single strand breaks, suggesting that these MKs do not become apoptotic (Figure 17C).

Finally, our intravital data clearly demonstrate that MKs decorated with the depletion antibody form cellular protrusions into the bone marrow sinusoids and are able to form both smaller proplatelet-like structures (Supplementary Videos 2 and 3 and Figure 20B) and larger preplateles (Supplementary Videos 4-6 and Figure 20C). Whether the extremely long and extended structures within the vessel lumen, seen in Supplementary Videos 4-6 is due to the presence of the antibody requires analysis of more animals. However, it is long known that the few platelets circulating in ITP-patients are much larger in size and have reticulated appearance due to the presence of residual RNA derived from the MK. Both features have been used to set the diagnose of ITP, either by determining the fraction of large, reticulated platelets after thaizol-orange staining flow cytometrically[150] or by standard automated blood counters that use fluorescent dyes to stain for RNA and determine the Immature Platelet Fraction.[151,152] These larger platelets are typically considered as "young" platelets and the term "immature" is a misnomer, especially as these platelets are thought to be more hemostatically active[153] and children with very low platelet counts (less than 20/nL) have overall less severe episodes of bleeding compared to patients in which a comparable platelet count is due to congenital platelet production defects or in iatrogenic thrombocytopenia due to chemotherapy-induced bone marrow suppression. [154,155]

In this study we were primarily interested to better understand the responses of bone marrow MKs to an increased platelet demand after auto-antibody induced platelet destruction. We have used a well-characterized antibody directed against GPIbα (CD42b), one subunit of the multimeric vWF receptor complex which is expressed in high copy number on the platelet surface. In addition, both subunits of the fibrinogen

receptor GPIIb/IIIa (CD41/CD61) have been the target of autoantibody causing ITP. This has also been found for mice, in which antibodies recognizing the GPIIb/IIIa receptor lead to transient thrombocytopenia.[139] However the mechanism of platelet depletion is different between both target epitopes: injection of $F(ab)_2$ fragments still caused platelet depletion for GPIIb/IIIa, but not for GPIbα-directed antibodies, suggesting that Fc-receptor-mediated phagocytosis might not account for all antibodies causing ITP. This might also explain why some patients with ITP are refractory to IvIG therapy while it is beneficiary for most. In addition, it reflects different outcomes in ITP-mouse models of IvIG treatment.[156]

In this study we provide for the first time direct in vivo evidence that thrombocytopenia due to immune-mediated platelet depletion is reflected by a dynamic change of MK number and size and that the depletion antibody quickly binds to its antigen present on MKs in the bone marrow. MKs decorated with the anti-GPIbα-antibody do not per se cause apoptosis, but are found to continue with proplatelet shedding across the endothelial barrier into bone marrow sinusoids. In addition, we found the release of larger, extended fragments with a length of over 200 μm which we have not observed earlier in untreated $GPIIb^{wt/eYFP\text{-}ki}$ mice.[23] Our mouse model provides a basis for further systematic analyses to better understand the pathomechanism of platelet depletion and MK reactivity in ITP and might help to find the best treatment options for patients that have become chronic and refractory to standard therapy regimens.

3.3. Future directions: Development of a MK BM atlas

Only efficient MK proliferation and differentiation ensures a stable platelet population. For MK proliferation and differentiation the micro-architecture of their BM niche is crucial. However, precise cellular, structural and humoral composition, cellular turnover and signaling pathways of the MK BM niches are still ill-defined. Knowledge about distribution patterns and the influence on cell differentiation and proliferation will help to better understand the BM environment and will build the basis for further studies, especially regarding BM and HSC transplantation. The mobilization and the connected engraftment of HSC after BM transfusion still carries problems especially regarding the megakaryocytic lineage. After transplantation platelets repopulate rather slow in comparison to other myeloid cell lineages. This leads to sustained thrombocytopenia increasing the risk of bleedings, including intracerebral hemorrhage. Precise in situ niche characterization was so far limited by crude decalcification of bone sections which destroyed epitopes for antibody binding. To get insight into BM tissue architecture influencing MK differentiation and proliferation analyses of the MK BM niche using a new technique that does not require bone decalcification. This technique allows to sustain the whole tissue composition and enables whole femur sections with maintaining most of the cells. Parallel immunostaining of various epitopes and multicolor confocal laser scanning microscopy analysis and additional functional assays facilitated the development of a MK specific BM-atlas.

3.3.1. Identification and distribution of BM MKs in situ

For MK detection in situ, a series of specific surface markers representing different MK maturation stages was used (cf. chapter 1.1.2. and Tomer et al.[7]). Cells recognized by FITC-conjugated anti-CD41, anti-CD61 or anti-CD42 antibodies are considerable large in cell size (Figure 21, 20 μm - max. 50 μm in diameter) and show big multi lobed nuclei identified by DAPI staining.

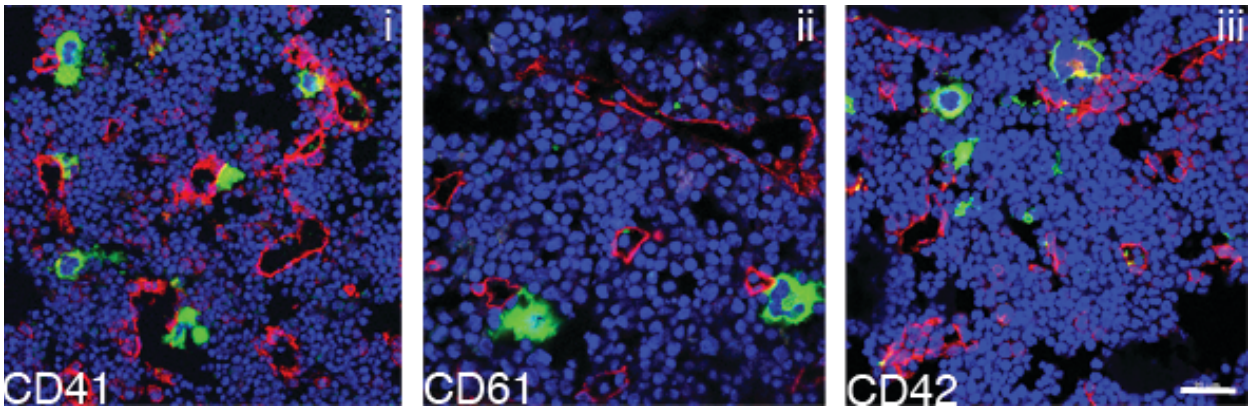

Figure 21 - MKs can be identified in femur BM by specific surface markers. Overview over intact BM. MKs stained by anti-CD41 FITC-conjugated antibody (green) (i). Magnifications: MKs stained by anti-CD61-FITC (green) (ii) and CD42 (green) (iii). Sinusoids are stained by CD105-antibody detected by anti-rat Alexa-647-fluorophore (red). Nuclei were DAPI-stained (blue). The scale bar indicates 20 μm.

To get a first overview of where MKs are located within BM a general analysis of cell distribution in long bone regarding their maturation stage was performed. Vascularity was identified by the endothelial marker CD105, and bone anatomy discriminating the two epiphysis and the diaphysis (Figure 22A) conduced as orientation of MK-localization. CD41, as an early lineage-marker, served as identification for the whole megakaryocytic population and stains small young MKs and bigger multilobed fully maturated MKs. As a marker of late maturation stages CD42 positive cells were determined and assigned to their localization in the bone.

CD41-positive cells were evenly scattered all over the BM, in correlation to BM area 25% of the cells can be found in the trabecular BM within the distal epiphysis. For mature CD42 positive cells this is true for approximately 20%. In contrast, only 12 - 15% of CD41 and CD42 positive cells are located in the proximal epiphysis, around 60% of MKs are present in the BM cavity (Figure 22B). No clear difference in cell size is observable between CD41 and mature CD42 positive cells. In total only 60% of all MKs colocalize to BM sinusoids (Figure 22C). This colocalization pattern might be underrepresented as interactions in z-dimension between MKs and sinusoids cannot be

considered in two dimensional images. Taken together, MKs are evenly distributed all over the BM in long bones. The trabecular BM in the distal epiphysis is somewhat enriched for MKs and might be of function for MK maturation.

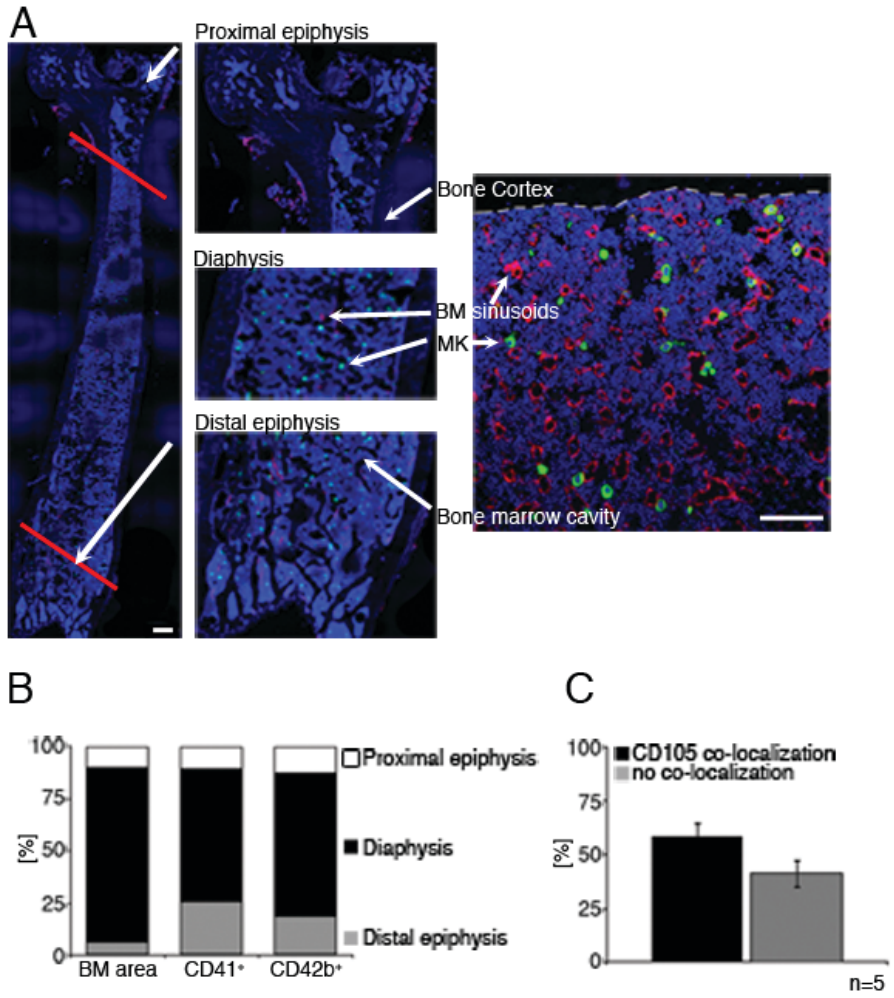

Figure 22 - MK localization and distribution in BM. (A) Immunohistograph of an intact femur section (left panel), magnifications show proximal & distal epiphysis with trabecular bone and BM-cavity. CD41-positive cells emerge in green, sinusoids are stained by anti-CD105-Alexa647 antibodies (red). DAPI stains nuclear DNA (blue). The right panel shows a typical BM field of view 20x magnification. (B) Quantification of MK distribution in 5 animals. 20-25 % of MKs are located in the distal epiphysis. (C) Around 60% of all CD41-positive cells colocalize with CD105-positive BM sinusoids in 5 animals. Scale bars indicate 100 μm.

3.3.2. In situ distribution of BM ECMs and factors of the vascular BM niche

The influence of different niche factors on MK differentiation has been subject of several studies, whereas the components of the MK BM niches have been analyzed regarding their stimulatory or antagonistic effects on PPF or platelet function. However, their distribution pattern and localization regarding MK haunt are poorly characterized. Therefore, we started to analyze in situ distribution of vascular niche components. CD31 also referred to as PECAM-1 as cellular component and vascular marker molecule, collagen IV, fibronectin and laminin as structural elements and the cellular and connective tissue bound glycoprotein vWF. Whole femur sections were stained with antibodies against the molecules mentioned above and additionally against CD105 as vascular marker.

Analysis revealed that expression patterns are not restricted to the vascularity, here defined as CD105 positive cells.

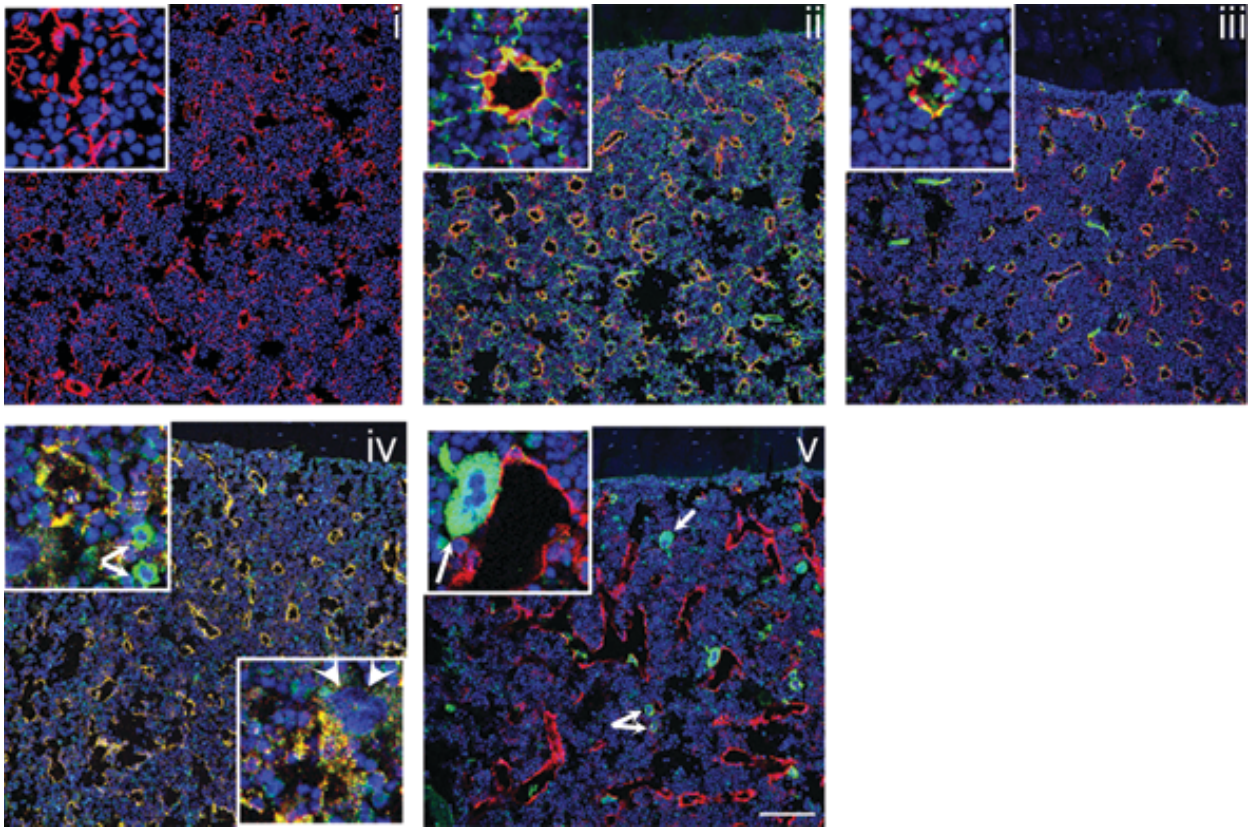

Figure 23 - Distribution of vascular niche factors. Collagen IV, stained by Alexa-647 in red (i) and fibronectin stained by Alexa-488 in green (ii) form a BM-wide fibrillar network. Laminin (green) (iii) and CD31 (green)-expression (iv) are restricted to the BM vessels. CD31 stains small cells (arrows) and only slightly stains MKs (arrow heads). vWF (green) (v) is not detectable in CD105-positive BM-sinusoids (red) (ii-v) but on MKs. Scale bar indicates 100 μm.

Especially structural elements as collagen IV and fibronectin are distributed throughout the BM cavity and form a mesh, with fibers emerging radiantly from sinusoids (Figure 23 i and ii). In contrast, laminin and CD31 are more restricted to BM-sinusoids. While laminin shows an alternating distribution with CD105 positive cells when cross sectioned, it encloses vessels seen by longitudinal sectioned sinusoids. CD31 is highly expressed on endothelial cells and therefore often used as vascular marker. Consistent with those data, CD31 colocalizes with CD105 positive endothelial cells depicted by the yellow color in Figure 23 iii and iv and its distinct expression pattern on hematopoietic cells should be of interest in further biochemical analysis. Additionally cells of approx. 15 μm size are CD31-positive (arrows, iv). In contrast, big (approx. 30 μm in diameter) multilobed MKs show only weak CD31 expression (arrowheads, iv). CD31 is known to be expressed on most hematopoietic cells[157] and can support integrin activation on T-cells[158] or effects negatively collagen platelet activation.[159] One cardinal component for platelet activation, vWF, is part of the subendothelial matrix but cannot be detected in BM sinusoids (Figure 23, v). This might be due to the heterogenic vWF-expression in endothelial cells.[160,161] But vWF-expression is found in MKs (arrows, v). Collagen IV and fibronectin as structural elements of the BM vascular niche form a fibrillar network all over the BM and around BM-cells. Laminin expression, in contrast, is restricted to the vascularity itself. Taken together components of the vascular niche do not clearly demarcate a specific anatomic location.

3.3.3. MKs are embraced by collagen IV and fibronectin fibers in situ

The structure giving proteins collagen IV and fibronectin form a fibrillar network through out the BM. Fibers of either protein are known to stimulate MK maturation and PPF to a similar extend.[87] Therefore histological analysis regarding MKs in collagen IV or fibronectin vicinity were performed to determine whether those stimulating proteins can be found in direct cell contact. Frozen femur sections were stained with an anti-CD41 FITC-conjugated antibody to determine the MK population and anti-collagen IV or anti-fibronectin antibodies. Either collagen IV or fibronectin fibers embrace MKs and can be found in direct cell contact (Figure 24). However, as potent platelet agonists, here they do not lead to premature platelet release or proplatelet activation within BM or during endothelial penetration.

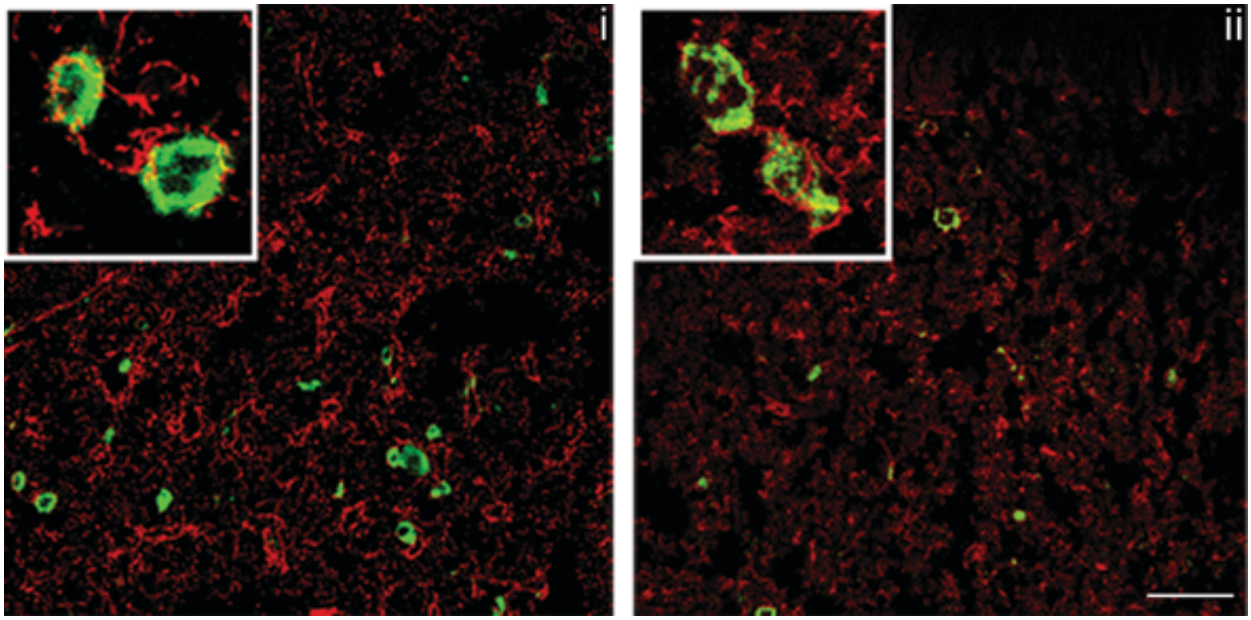

Figure 24 - Colocalization of collagen IV and fibronectin with MKs. Collagen IV (red) (i) and fibronectin (red) (ii) fibers embrace MKs stained by CD41-FITC (green). Scale bar indicates 100 μm.

3.3.4. MKs in direct agonist contact express both collagen receptors

The close vicinity of collagen IV fibers and MKs in BM does not lead to premature platelet release or activation during PPF. This might be due to a lack in collagen receptor expression. The interaction of either MKs or platelets with collagen can occur indirectly via immobilized vWF or directly through receptors. GPVI is known to be the most potent collagen receptor on MK and platelet surface, which is needed to trigger conformational changes and thus activation of the second collagen receptor α2β1-integrin. Immunohistological expression analysis of both MK collagen receptors was

performed by single and costaining of either GPVI or the α2-subunit with the MK-marker CD41 on femur sections.

Either GPVI and α2-integrin were detectable by specific antibodies on cell surface in BM (Figure 26 i and ii). Costaining with the megakaryocytic marker CD41 revealed that every CD41-positive cell was additionally positive for α2-integrin and GPVI (Figure 26 iii and iv). Further stainings revealed that collagen IV fibers embrace MKs which express the corresponding collagen receptor (Figure 26, v). Additional flow cytometrical analysis of day 3 fetal liver cell derived MKs verified, that approx. 95% of gated cells are CD61 and collagen receptor GPVI positive. For α2-integrin this was true for approx. 93% (Figure 25). The CD41/CD61 receptor complex is known to be first expressed during megakaryopoiesis.[7] Studies revealed that in early MK maturation stages, GPVI is expressed only at low levels and receptor expression level rise with MK-maturation and then show full functional activity.[162] The in situ data here show that the expression of either GPVI and α2-integrin on CD41-positive cells is remarkable high. Receptor functionality should be examined next.

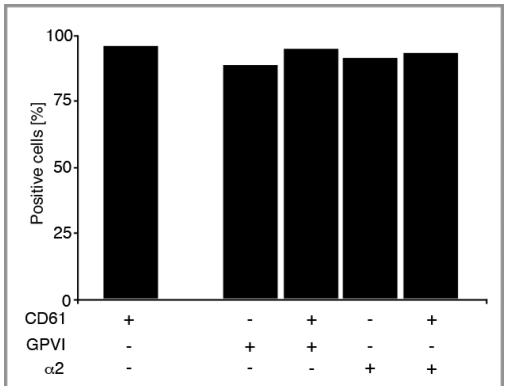

Figure 25 - Flow cytometrically analysis of collagen receptor expression on MKs. 95.9% of gated cells are MK-marker CD61 positive. 88.7% and 91.4% of cells are positive for GPVI and α2-integrin, respectively. GPVI/CD61 double-positive are 94.8% and 77.5% are double-positive for α2-integrin and CD61.

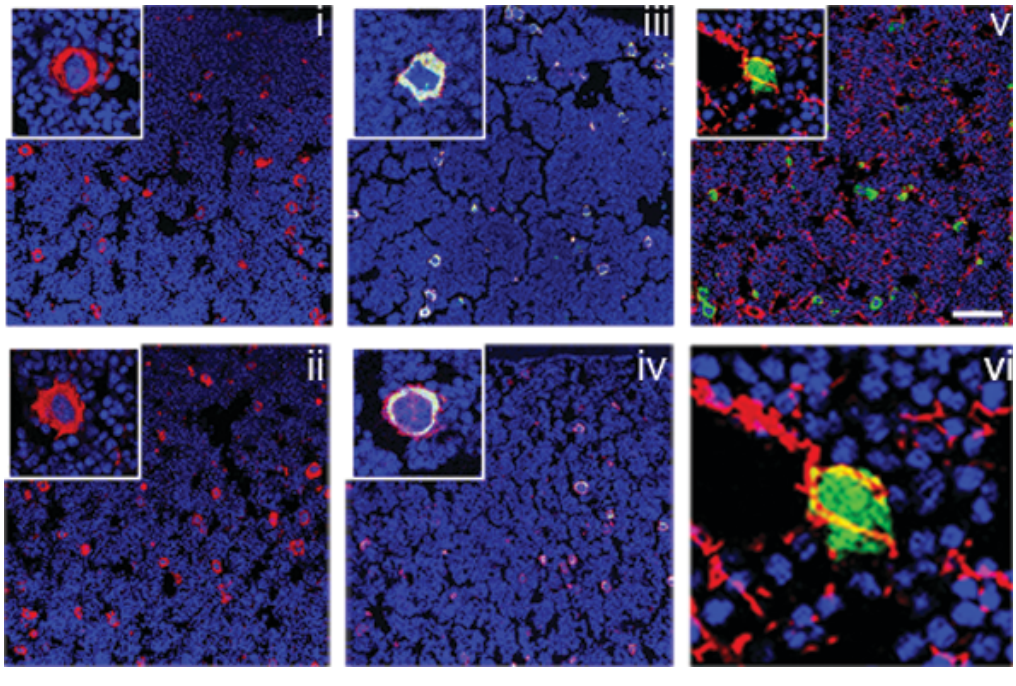

Figure 26 - Collagen receptor expression in BM. α2-integrin (red) (i) and GPVI (red) (ii) are expressed in BM on CD41-positive cells stained by FITC in green (iii & iv). These cells are encoiled by collagen (red) IV fibers. Inset-magnification from subpanel (v) in (vi) The scale bar in V exemplifies 100 μm in overviews.

3.3.5. MKs adhere best in vitro onto ECMs of the vascular niche

The relevance of ECMs for platelet hemostasis has been analyzed under resting and flow conditions i.e in Savage et al.[163] Those studies unfortunately substantially lack a precise species-specific experimental setting and collagen types of different species are used merely to their availability. This explains why results of different groups might be distinct or even contradictory.

In contrast, the significance of ECMs for BM homeostasis, in particular for MK biology, is less well characterized. Studies in 1992 revealed that guinea pig MKs are able to form proplatelets on type I collagen, which can be blocked by RGDS peptide but not by specified antibodies against integrin receptors for fibronectin (α5β1), laminin (α6β1) and fibrinogen (αIIbβ3). However, anti vitronectin-receptor (αvβ3) antibodies did inhibit PPF on collagen I.[164] These data were later challenged by studies in $CD34^+$ derived MKs, which might be due to species differences.[165] The influence of extracellular signals in BM niches on MK development is indisputable, despite the paucity in topical analyses.

Using ECMs designated as components of the osteoblastic (collagen type I and III)[77,166] or vascular niche (collagen IV, fibronectin and laminin) for in vitro MK-adhesion analysis[167], fetal liver cell derived MKs were allowed to sediment and adhere to ECMs coated cover slips for 4 hrs at 37°C and 5% CO_2. On fibronectin-coated cover slips MK surface coverage was the highest (11% in Figure 27). Interestingly, adhesion potential toward collagens of type III, which is often associated with collagen I and implied as part of the osteoblastic niche and collagen IV known to be expressed in the vessel basal lamina together with laminin, prompted MK adhesion to approx. 5% and 3%, respectively (Figure 27A). Whereas their association partners collagen I and laminin showed no or only very low adhesion potential, respectively (Figure 27A). In summary, molecules from either osteoblasic or vascular BM niche allow MKs to adhere. The fibrillar-network building molecule fibronectin, highly associated to MKs in situ (Figure 24), revealed to be the most effective surface for MK adhesion. However, those data should be discussed with precaution due to the human origin of the proteins. ECMs of other than human origin are often not commercially available which makes experiments of this type even more ambitious. Specificity of those simple adhesion experiments was obtained by independent experiments with additional pre-incubation of antibodies directed against either of the two mammalian collagen-receptors: GPVI or against the α2-chain of the α2β1-integrin.

Vascular niche molecules collagen IV, fibronectin and laminin were examined. As expected we found that anti-α2-integrin-antibodies and especially anti-GPVI-antibodies inhibit cell adherence on collagen IV-coated cover slips (Figure 27B). Further inhibition was observed on laminin and especially fibronectin-coated cover slips (Figure 27B). This can be explained by the fact that fibronectin has binding properties towards 20 distinct receptors.[168] Collagen receptors on MK surface are cardinal for activation of signal transduction and once hampered might influence MK binding ability. Thus, α2-integrin and GPVI seem to have an impact not only on signal transduction, but also on ECM-adherence.

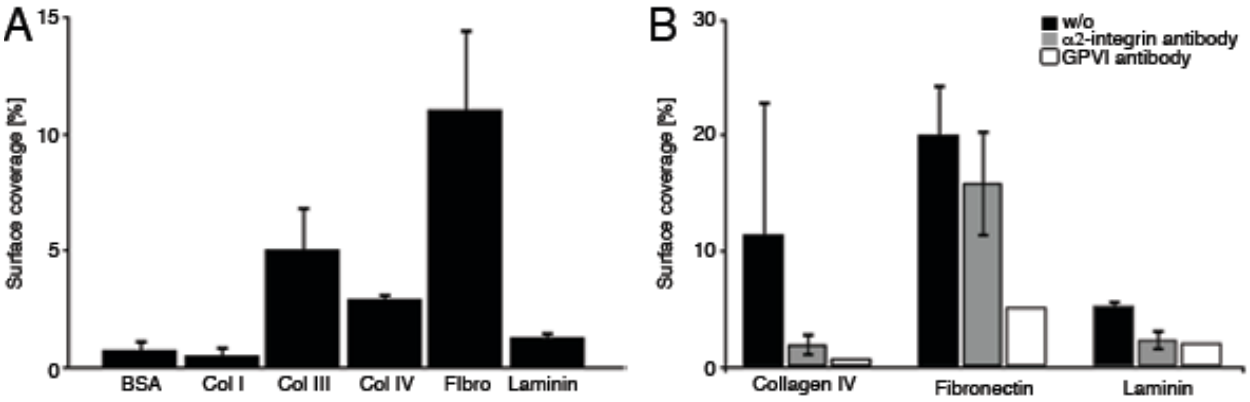

Figure 27 - Adhesion potential of MKs on different ECM proteins. (A) MK-adhesion on ECM in vitro. MKs adhere best on fibronectin coated surfaces. No adhesion can be observed on surfaces coated with murine collagen I. (B) MK adhesion-blocking by α2-integrin- and GPVI-antibodies. MK adhesion can best be blocked by GPVI-antibodies. Adhesion is completely abolished on collagen IV-coated surfaces and reduced on fibronectin and laminin coated cover-slips. α2-integrin antibody reduces adhesion.

3.3.6. MK adhesion on ECMs supports PPF

MK maturation and finally PPF are know to rely on different humoral factors as TPO and SCF for differentiation and CXCL12 for migration and PPF.[12,19] The influence of other, structural factors in the BM environment is less well characterized. Even though MKs do not show premature PPF in BM or activation of proplatelets, as a direct response to agonistic factors in the extracellular matrix, the influence of ECMs on murine MK maturation is still ill-defined. For human MKs it has been proposed that collagen I in vitro inhibits PPF whereas collagens of the vascular niche and fibronectin have a conducive influence on PPF.[87]

Here, a set of similar experiments was performed with murine MKs on ECMs of different species origin. Fetal liver cells were differentiated to MKs and subsequently seeded onto uncoated or coated culture dishes. On uncoated dishes an overall rate of 9% PPF

was observable after 3 days. In contrast, cells seeded onto coated cultures dishes had an overall attenuated PPF. Only cultures on fibronectin showed similar PPF with approximately 8%. Analysis of the same cultures one day later revealed a different pattern of PPF (Figure 28). Cultures on ECMs known to be components of the vascular niche (collagen IV, fibronectin and laminin) showed an accelerated PPF (around 18%, Figure 28F-H) in comparison to uncoated dishes. Interestingly, cultures coated with murine collagen I demonstrated a similar acceleration in PPF as cultures coated with human collagen III. Human collagen I coated cultures show an inhibited progress with only 9% PPF (Figure 28C and D). On the last day of the observation period cultures coated with murine collagen I and collagen III reach a plateau-phase (Figure 28C and D), whereas cultures from collagen IV and fibronectin coated dishes already show reduced PPF (under 18%, Figure 28F and G). Cultures from uncoated dishes, laminin and human collagen-coated dishes still show an increase in PPF, as do control cultures from BSA coated dishes (Figure 28A, B, E, H). All 28 known collagen subtypes are characterized by their triple-helical structure with a highly repetitive amino acid sequence. In most subtypes every third amino acid is a G-residue. Due to its structure difference collagen IV fibers, in contrast to collagen I fibers, do not assemble in parallel, thus a network forming arrangement is achieved. Those structural differences in collagen subtypes might influence MK adhesion and PPF substantially.

Taken together we observed an overall positive effect of distinct matrix molecules on PPF in MK cultures compared to BSA (control) coating and dishes coated with human collagen I. Thus all kind of ECMs found in murine BM favor at least in vitro MK maturation and platelet generation and no discrimination can be made regarding this component of the vascular or osteoblastic niche, respectively. It should be considered for future analysis that species origin of molecules tested in such assays must not be underestimated in respect to the impact on result and thus their interpretation.

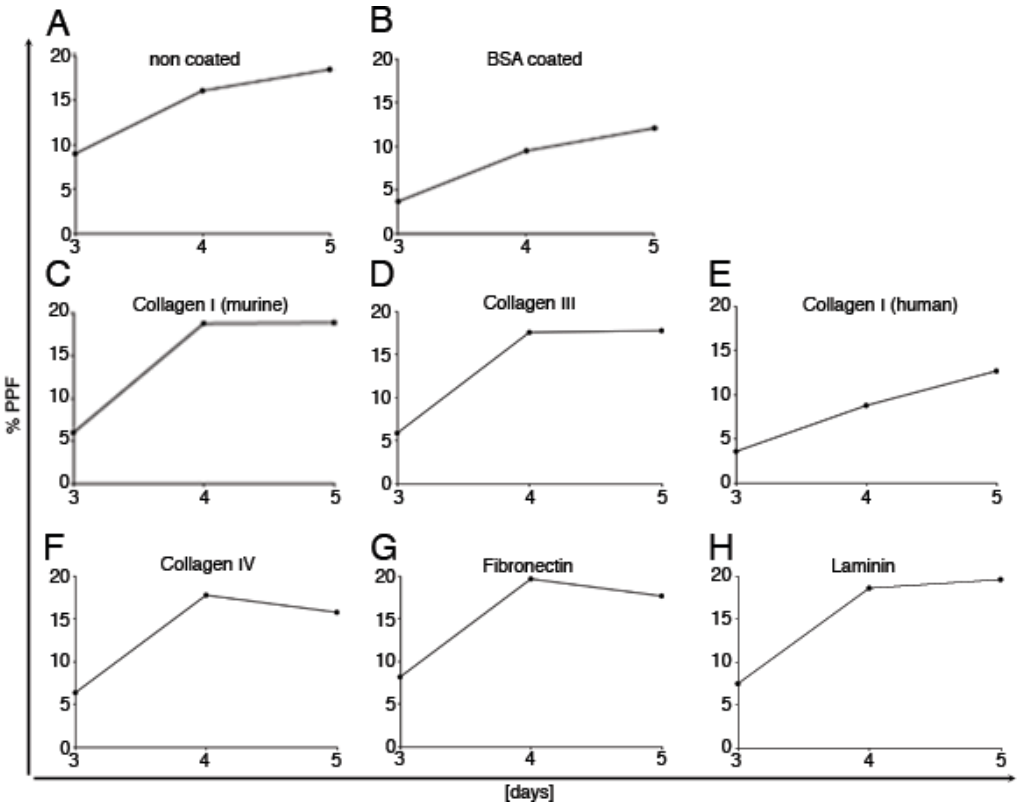

Figure 28 - MK Adhesion on ECM favors PPF. (A) PPF on uncoated dishes, (B) BSA coated culture conditions (C) murine collagen I, (D) human collagen III, (E) human Collagen I, (F) murine collagen IV, (G) fibronectin and (H) laminin. MKs seeded onto fibronectin showed fastest maturation with around 8% PPF after 3 days in culture. After 4 days most cultures showed similar PPF percentages except cultures on human collagen I and BSA.

3.3.7. MMP2 and MMP9 are not active in MKs when seeded on ECM coated dishes

Scanning electron microscopy of BM revealed that the dynamic network of ECMs can be divided into two major compartments, the basal lamina building a barrier between tissue compartments as vascularity and BM and the interstitial matrix formed out of filaments assembling to a network. ECM-rich environments as BM underlie mechanisms of constant protein secretion and self-association and degradation. ECM degradation is mainly catalyzed by the family of matrix metalloproteinases (MMPs).[169] The gelatinases MMP2 (degrading collagens of type I, II and III) and MMP9 (degrading laminin and collagens of type IV, V and XI) are known to play a substantial role in HSC mobilization. Both endopeptidases additionally cleave non-ECM molecules that are important for HSC migration including the chemokine CXCL12, or the cytokines tumor necrosis factor (TNF)-α, members of the transforming growth factor (TGF)-β family and others.[170,171] MMP9 levels are known to be elevated in BM after neutrophil activation which leads to HSC mobilization. $CD34^+$ cells express both gelatinases which leads to elevated basal transmigration. Migration capacity is relies on cytokine- and growth factor dependent gelatinase expression[172] Migration of differentiating and maturating MKs to BM vascularity and their localization encoiled in ECM fibers presumes that MMP2 and/or MMP9 could be involved in that process. Therefore, a series of zymography tests were performed in order to test expression and activation of MMP2 and MMP9 for MK migration. MKs were seeded on ECMs and harvested on day 3, lysed and subsequently loaded onto a gelatine-rich zymography gel. The assay is based on the enzymatic activity of gelatinases which digest their substrate gelatin, co-polymerized in to the gel. Enzymatic activity can be detected by negative bands after Coomassie-staining, where the substrate has been

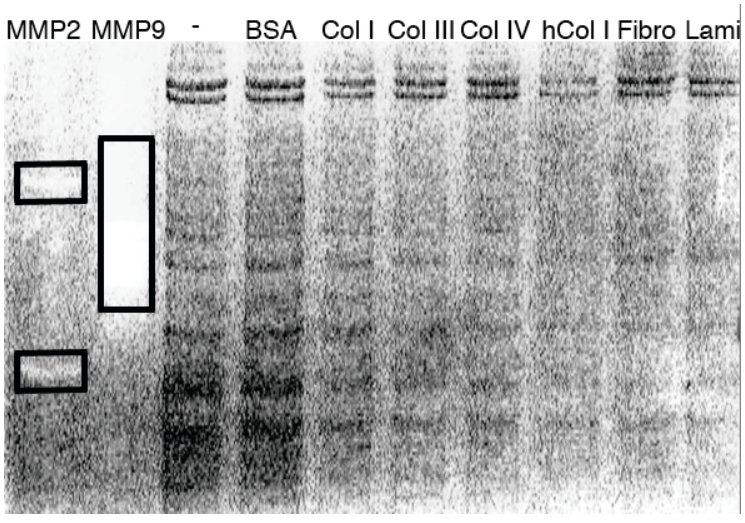

Figure 29 - Zymographic gelantine-riche gel. Enzyme activity is visible by negative staining (black boxes) in control lanes. MK-lysates from different cultures show no MMP-activity.

degraded. Here, zymography revealed that MMP2 and MMP9 are not active on MKs when exposed to ECMs (Figure 29) and seem not to play a key role for MKs when exposed to ECMs in vitro.

3.3.8. Summary

Taken together the following six points contribute to a first draft of a BM atlas regarding MK environment (Figure 30):

1. MKs are evenly distributed in the BM cavity and trabecular bone.
2. The distal epiphysis is enriched in CD41-positive cells.
3. 60% of CD41-positive cells are localized at the vascularity.
4. The laminin- and CD31-expression is restricted to BM sinusoids.
5. The vascular niche factors collagen IV and fibronectin form a fibrillar mesh throughout the BM.
6. MKs are encoiled by collagen IV- and fibronectin-fibers and do express the collagen receptors GPVI and α2-integrin.

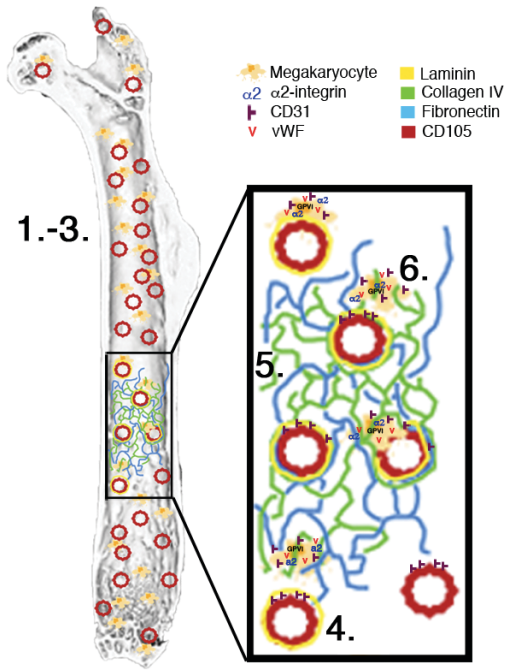

Figure 30 - Model of a megakaryocytic BM-Atlas. Bone scheme adopted from Jepsen et al..[173]

3.3.9. Future perspectives: Do different ECMs influence MK migration in vitro

During normal hematopoiesis HSCs migrate out of their stem cell niche into the vascular niche and/or peripheral blood. A mobilization process known to be dependent on multiple humoral, cellular and structural and other microenvironmental factors A normal BM characteristic is its hypoxia. The lowest tissue oxygen tension can be found in the endosteal stem cell region due to the distant to the O_2 transporting sinusoids. Hypoxia is discussed to be relevant for HSC quiescence via hypoxia inducible factors (HIFs) which might infuence cell motility. However, this oxygen gradient is hard to mimick in vitro. Therefore we like to confine our experimental settings to the most important chemokine ligand/receptor axis the for MK migration and transendothelial passage crucial CXCL12/CXCR4 interplay. To investigate whether MKs show discriminable migration in different ECM-environments we like to seed YFP-expressing purified MKs in a three dimensional matrix supplemented with different matrix molecules in a transwell. We aim to follow cell migration towards a CXCL12-gradient through the transwell membrane via MPM and hope to distinguish migration from non-supplemented matrix and matrices supplemented with ECMs from the stem cell niche or vascular niche respectively.

Thus characterization of the MK ECM-environment can be expanded by uncovering the significance of the direct cell-fibre contacts seen in the static in situ analysis.

4. Abstract

Blood platelets are essential in primary hemostasis preventing the body from blood loss by sealing injured vessels. During thrombopoiesis the platelet precursors, the MKs in BM form protrusions, designated as pro- and preplatelets, which penetrate vascularity and shed platelets into the peripheral blood stream. This process is dependent on a variety of cell-intrinsic and -extrinsic factors. The formation of proplatelets is the last step in the life of each MK and this differentiation step is highly dependent on the assembly of novel MT-filaments. MKs and platelets express the tissue-restricted β1-tubulin isoform. During activation the cortical MT coil contracts and therefore supports granule centralization prior to release. In a yeast-two-hybrid assay RanBP10 was identified as a new β1-tubulin interacting protein. Platelets from RanBP10 knock out mice show disordered MT bundling and reduced platelet reactivity. Mice harbor a severe bleeding phenotype despite normal platelet counts. In this context, three aspects have been analyzed:

1. The impact of RanBP10 depletion *in vivo* was examined regarding MT-equilibrium, platelet function and hemostasis. RanBP10-null platelets have a normal life time, are fully equipped with receptors and surface molecules and are not altered in adhesion potential under shear. In contrast, the thrombus stability in mutant mice is markedly impaired and shape change and the marginal band contraction are attenuated. However, dense granule secretion is not affected. In RanBP10 knock out mice more polymerized β1-tubulin is detected, thus it can be concluded that RanBP10 prevents premature MT polymerization in the presence of the MK/platelet-specific β1-tubulin isoform.

2. A mouse model for the autoimmune disease immun Thrombocytopenia (ITP) was exploited to analyze and characterize the dynamic extrinsic processes of platelet biogenesis. A platelet depleting antibody was injected into mice to disrupt the homeostasis between MKs and platelets. The MK-population showed a dynamic reaction on platelet depletion. *In vivo* proliferation studies revealed, that newly formed MKs were generated from a pre-existing cell pool and were overall significantly smaller in size after depletion. The depletion antibody was still present on BM MKs for at least 5 days after application but antibody binding did not lead to apoptosis. For the first time *in*

vivo, it has been shown by MPM that antibody decorated MKs are still able to form proplatelets.

3. The in situ-characterization of the megakaryocytic BM niche was so far limited, due to harsh epitope-destroying decalcification steps on bone sections destroing epitopes for antibody staining. With the establishment of new histology methods an initial BM atlas regarding MK environment was developed. For the first time, in vitro generated data of putative niche-factors were revised in situ in complete murine femur sections. With further functional analyses, it is now possible to map the three-dimensional topology not only of the megakaryocytic BM-niche environment.

In total this work summarizes in vitro, in situ and in vivo analyses on cell-intrinsic and cell-extrinsic factors affecting platelet biogenesis.

5. Zusammenfassung

Ein Gefäßverschluss zur Minimierung des Blutverlusts bei Verletzungen wird auf zellulärer Ebene von Blutplättchen (Thrombozyten) gewährleistet. Während der Thrombopoese schnüren sich neue Thrombozyten aus Megakaryozyten, den Vorläuferzellen im Knochenmark, in den peripheren Blutstrom ab. Für diesen Prozess müssen sowohl zell-intrinsische wie -extrinsische zellbiologische und biochemische Faktoren, ineinander greifen. Die Abschnürung von „Proplättchen“ aus Megakaryozyten während ihrer terminalen Differenzierungsphase ist ein von Mikrotubuli getriebener Prozess, wobei die heteropolymeren Mikrotubuli hier die β1-Tubulin-Isoform aufweisen, die spezifisch für Megakaryozyten ist. Der kortikal Mikrotubuli-Ring unterstützt nach Aktivierung die Granula Zentralisierung und verstärkt damit die Plättchen Aktivierung. In einem Hefe-2-Hybrid-Experiment wurde RanBP10 als ein neuer β 1-Tubulin-Bindungspartner identifiziert. Plättchen aus RanBP10 knock-out Mäusen zeigen eine ungeordnete Mikrotubulibündelung und einen Blutungsdefekt. Außerdem ist ein deutlicher Defekt in der Hämostase trotz normaler Thrombozytenzahlen beobachtbar.
In der vorliegenden Arbeit wurden drei Aspekte der Biogenese funktionaler Thombozyten untersucht:
1. Die RanBP10-Protein Depletion wurde hinsichtlich ihrer Auswirkungen auf Mikrotubuli-Gleichgewicht, Plättchenfunktion und Hämostase untersucht. Es wurde

gezeigt, dass Thrombozyten, trotz RanBP10-Depletion, die volle Rezeptorvielfalt exprimieren und nicht in ihrer Lebensdauer und nur wenig in ihrer Fähigkeit unter Scherkräften zu adhärieren beeinträchtigt sind. Es konnte *in vivo* gezeigt werden, dass die Thrombusstabilität in RanBP10-null Mäusen stark gestört ist. Trotz einer verzögerten Kontraktion des Mikrotubuli-Rings und der damit verlangsamten Zentralisierung der Granula ist deren Sekretion in den transgenen Tieren nur wenig beeinträchtig. In RanBP10-knock out Tieren liegt im Vergleich zum Wildtyp mehr β1-Tubulin in polymerisierter Form vor und RanBP10 verhindert ein verfrühtes polymerisieren von Mikrotubuli.

2. Es wurde ein Mausmodell der Autoimmunerkrankung Immunthrombozytopenie (ITP) verwendet, um zell-extrinsische Faktoren, die die Biogenese von Thrombozyten beeinflussen, weiter zu charakterisieren. Es wurde ein Plättchen-depletierender Antikörper in Mäuse injiziert und somit Megakaryopoese stimuliert. *In vivo* Proliferations-Untersuchungen ergaben, dass die neugeblideten Zellen aus einem schon vorhandenen Zellpool generiert werden und signifikant kleiner sind. Des Weiteren kann der injizierte Antikörper noch fünf Tage nach Injektion auf Megakaryozyten nachgewiesen werden, ohne zur Apoptose führt. Es wurde mittels 2-Photonen-Mikroskopie zum ersten mal *in vivo* gezeigt, dass Antikörper-dekorierte Megakaryozyten weiterhin zu Proplättchenbildung in der Lage sind.

3. Die *in situ* Charakterisierung der megakaryozytären Knochenmarknische mittels spezifischer Antikörper konnte in Vergangenheit auf Grund harscher Epitop-zerstörender Decalzifizierungsschritte nur unzureichend durchgeführt werden. Mit der Etablierung neuer histologischer Methoden konnte begonnen werden, einen Atlas der megakaryozytären Knochenmarksnische zu erstellen. Dies ermöglicht zum ersten mal, die in vitro generierten Daten von potentiellen Nischenfaktoren, in situ in komplett erhaltendem Knochenschnitten, zu überprüfen. Mittels weiterführender funktionaler Studien ist es dann möglich, die dreidimensionale Topologie nicht nur der megakaryozytären Knochenmarksumgebung zu entschlüsseln.

Diese Arbeit umfasst in vitro, in situ und in vivo Analysen zell-intrinsischer und cell-extrinsischer Faktoren die maßgeblich an der Plättchenbiogenese beteiligt sind.

6. References

1. Akashi K, Traver D, Miyamoto T, Weissman IL. A clonogenic common myeloid progenitor that gives rise to all myeloid lineages. *Nature*. 2000;404(6774):193-197.
2. Galloway JL, Zon LI. Ontogeny of hematopoiesis: examining the emergence of hematopoietic cells in the vertebrate embryo. *Curr Top Dev Biol*. 2003;53:139-158.
3. Mikkola HK, Gekas C, Orkin SH, Dieterlen-Lievre F. Placenta as a site for hematopoietic stem cell development. *Exp Hematol*. 2005;33(9):1048-1054.
4. Vainchenker W, Bouguet J, Guichard J, Breton-Gorius J. Megakaryocyte colony formation from human bone marrow precursors. *Blood*. 1979;54(4):940-945.
5. Gordon MY, Blackett NM, Douglas ID. Colony formation by human haemopoietic precursor cells cultured in semi-solid agar in diffusion chambers. *Br J Haematol*. 1975;31(1):103-110.
6. Levine RF. Isolation and characterization of normal human megakaryocytes. *Br J Haematol*. 1980;45(3):487-497.
7. Tomer A. Human marrow megakaryocyte differentiation: multiparameter correlative analysis identifies von Willebrand factor as a sensitive and distinctive marker for early (2N and 4N) megakaryocytes. *Blood*. 2004;104(9):2722-2727.
8. Debili N, Wendling F, Cosman D, et al. The Mpl receptor is expressed in the megakaryocytic lineage from late progenitors to platelets. *Blood*. 1995;85(2):391-401.
9. Nagata Y, Muro Y, Todokoro K. Thrombopoietin-induced polyploidization of bone marrow megakaryocytes is due to a unique regulatory mechanism in late mitosis. *J Cell Biol*. 1997;139(2): 449-457.
10. Vitrat N, Cohen-Solal K, Pique C, et al. Endomitosis of human megakaryocytes are due to abortive mitosis. *Blood*. 1998;91(10):3711-3723.
11. Kaushansky K. Thrombopoietin: the primary regulator of megakaryocyte and platelet production. *Thromb Haemost*. 1995;74(1):521-525.
12. de Sauvage FJ, Carver-Moore K, Luoh SM, et al. Physiological regulation of early and late stages of megakaryocytopoiesis by thrombopoietin. *J Exp Med*. 1996;183(2):651-656.
13. Bunting S, Widmer R, Lipari T, et al. Normal platelets and megakaryocytes are produced in vivo in the absence of thrombopoietin. *Blood*. 1997;90(9):3423-3429.
14. Choi ES, Nichol JL, Hokom MM, Hornkohl AC, Hunt P. Platelets generated in vitro from proplatelet-displaying human megakaryocytes are functional. *Blood*. 1995;85(2):402-413.
15. Alexander WS, Roberts AW, Nicola NA, Li R, Metcalf D. Deficiencies in progenitor cells of multiple hematopoietic lineages and defective megakaryocytopoiesis in mice lacking the thrombopoietic receptor c-Mpl. *Blood*. 1996;87(6):2162-2170.
16. Gurney AL, Carver-Moore K, de Sauvage FJ, Moore MW. Thrombocytopenia in c-mpl-deficient mice. *Science*. 1994;265(5177):1445-1447.
17. Avecilla ST, Hattori K, Heissig B, et al. Chemokine-mediated interaction of hematopoietic progenitors with the bone marrow vascular niche is required for thrombopoiesis. *Nat Med*. 2004;10(1): 64-71.
18. Levin J, Cocault L, Demerens C, et al. Thrombocytopenic c-mpl(-/-) mice can produce a normal level of platelets after administration of 5-fluorouracil: the effect of age on the response. *Blood*. 2001;98 (4):1019-1027.
19. Hamada T, Mohle R, Hesselgesser J, et al. Transendothelial migration of megakaryocytes in response to stromal cell-derived factor 1 (SDF-1) enhances platelet formation. *J Exp Med*. 1998;188(3): 539-548.
20. Stenberg PE, McEver RP, Shuman MA, Jacques YV, Bainton DF. A platelet alpha-granule membrane protein (GMP-140) is expressed on the plasma membrane after activation. *J Cell Biol*. 1985;101(3):880-886.
21. Italiano JE, Jr., Lecine P, Shivdasani RA, Hartwig JH. Blood platelets are assembled principally at the ends of proplatelet processes produced by differentiated megakaryocytes. *J Cell Biol*. 1999;147(6): 1299-1312.
22. Patel SR, Richardson JL, Schulze H, et al. Differential roles of microtubule assembly and sliding in proplatelet formation by megakaryocytes. *Blood*. 2005;106(13):4076-4085.
23. Junt T, Schulze H, Chen Z, et al. Dynamic visualization of thrombopoiesis within bone marrow. *Science*. 2007;317(5845):1767-1770.
24. Behnke O, Forer A. From megakaryocytes to platelets: platelet morphogenesis takes place in the bloodstream. *Eur J Haematol Suppl*. 1998;61:3-23.

25. Thon JN, Montalvo A, Patel-Hett S, et al. Cytoskeletal mechanics of proplatelet maturation and platelet release. *J Cell Biol*. 2010;191(4):861-874.
26. Howell WH, Donahue DD. The Production of Blood Platelets in the Lungs. *J Exp Med*. 1937;65 (2):177-203.
27. Clarke MC, Savill J, Jones DB, Noble BS, Brown SB. Compartmentalized megakaryocyte death generates functional platelets committed to caspase-independent death. *J Cell Biol*. 2003;160(4): 577-587.
28. De Botton S, Sabri S, Daugas E, et al. Platelet formation is the consequence of caspase activation within megakaryocytes. *Blood*. 2002;100(4):1310-1317.
29. Josefsson EC, James C, Henley KJ, et al. Megakaryocytes possess a functional intrinsic apoptosis pathway that must be restrained to survive and produce platelets. *Journal of Experimental Medicine*. 2011;208(10):2017-2031.
30. White MJ, Schoenwaelder SM, Josefsson EC, et al. Caspase-9 mediates the apoptotic death of megakaryocytes and platelets, but is dispensable for their generation and function. *Blood*. 2012;119(18): 4283-4290.
31. Tablin F, Castro M, Leven RM. Blood platelet formation in vitro. The role of the cytoskeleton in megakaryocyte fragmentation. *J Cell Sci*. 1990;97 (Pt 1):59-70.
32. Sullivan KF. Structure and utilization of tubulin isotypes. *Annu Rev Cell Biol*. 1988;4:687-716.
33. Downing KH, Nogales E. Tubulin structure: insights into microtubule properties and functions. *Curr Opin Struct Biol*. 1998;8(6):785-791.
34. Lewis SA, Gu W, Cowan NJ. Free intermingling of mammalian beta-tubulin isotypes among functionally distinct microtubules. *Cell*. 1987;49(4):539-548.
35. Wang D, Villasante A, Lewis SA, Cowan NJ. The mammalian beta-tubulin repertoire: hematopoietic expression of a novel, heterologous beta-tubulin isotype. *J Cell Biol*. 1986;103(5): 1903-1910.
36. Lecine P, Italiano JE, Jr., Kim SW, Villeval JL, Shivdasani RA. Hematopoietic-specific beta 1 tubulin participates in a pathway of platelet biogenesis dependent on the transcription factor NF-E2. *Blood*. 2000;96(4):1366-1373.
37. White JG. Influence of microtubule stabilization on platelet physiology. *Trans Assoc Am Physicians*. 1982;95:264-271.
38. White JG, Rao GH. Microtubule coils versus the surface membrane cytoskeleton in maintenance and restoration of platelet discoid shape. *Am J Pathol*. 1998;152(2):597-609.
39. Schwer HD, Lecine P, Tiwari S, Italiano JE, Jr., Hartwig JH, Shivdasani RA. A lineage-restricted and divergent beta-tubulin isoform is essential for the biogenesis, structure and function of blood platelets. *Curr Biol*. 2001;11(8):579-586.
40. Nogales E. Structural insight into microtubule function. *Annu Rev Biophys Biomol Struct*. 2001;30:397-420.
41. Schulze H, Korpal M, Bergmeier W, Italiano JE, Jr., Wahl SM, Shivdasani RA. Interactions between the megakaryocyte/platelet-specific beta1 tubulin and the secretory leukocyte protease inhibitor SLPI suggest a role for regulated proteolysis in platelet functions. *Blood*. 2004;104(13):3949-3957.
42. Schulze H, Dose M, Korpal M, Meyer I, Italiano JE, Jr., Shivdasani RA. RanBP10 is a cytoplasmic guanine nucleotide exchange factor that modulates noncentrosomal microtubules. *J Biol Chem*. 2008;283 (20):14109-14119.
43. Kunert S, Meyer I, Fleischhauer S, et al. The microtubule modulator RanBP10 plays a critical role in regulation of platelet discoid shape and degranulation. *Blood*. 2009;114(27):5532-5540.
44. Nieswandt B, Offermanns S. Pharmacology of platelet adhesion and aggregation. *Handb Exp Pharmacol*. 2004(165):437-471.
45. Varga-Szabo D, Braun A, Nieswandt B. Calcium signaling in platelets. *J Thromb Haemost*. 2009;7 (7):1057-1066.
46. Wurzinger LJ. Histophysiology of the circulating platelet. *Adv Anat Embryol Cell Biol*. 1990;120:1-96.
47. Hartwig JH. Mechanisms of actin rearrangements mediating platelet activation. *J Cell Biol*. 1992;118(6):1421-1442.
48. White JG. Platelets and atherosclerosis. *Eur J Clin Invest*. 1994;24 Suppl 1:25-29.
49. Handagama PJ, Bainton DF. Incorporation of a circulating protein into alpha granules of megakaryocytes. *Blood Cells*. 1989;15(1):59-72.
50. Harrison P, Wilbourn B, Debili N, et al. Uptake of plasma fibrinogen into the alpha granules of human megakaryocytes and platelets. *J Clin Invest*. 1989;84(4):1320-1324.

51. King SM, Reed GL. Development of platelet secretory granules. *Semin Cell Dev Biol*. 2002;13(4): 293-302.
52. Rendu F, Brohard-Bohn B. The platelet release reaction: granules' constituents, secretion and functions. *Platelets*. 2001;12(5):261-273.
53. Israels SJ, Gerrard JM, Jacques YV, et al. Platelet dense granule membranes contain both granulophysin and P-selectin (GMP-140). *Blood*. 1992;80(1):143-152.
54. Metzelaar MJ, Wijngaard PL, Peters PJ, Sixma JJ, Nieuwenhuis HK, Clevers HC. CD63 antigen. A novel lysosomal membrane glycoprotein, cloned by a screening procedure for intracellular antigens in eukaryotic cells. *J Biol Chem*. 1991;266(5):3239-3245.
55. Nieuwenhuis HK, van Oosterhout JJ, Rozemuller E, van Iwaarden F, Sixma JJ. Studies with a monoclonal antibody against activated platelets: evidence that a secreted 53,000-molecular weight lysosome-like granule protein is exposed on the surface of activated platelets in the circulation. *Blood*. 1987;70(3):838-845.
56. Offermanns S. Activation of platelet function through G protein-coupled receptors. *Circ Res*. 2006;99(12):1293-1304.
57. Hamm HE. How activated receptors couple to G proteins. *Proc Natl Acad Sci U S A*. 2001;98(9): 4819-4821.
58. Moers A, Nieswandt B, Massberg S, et al. G13 is an essential mediator of platelet activation in hemostasis and thrombosis. *Nat Med*. 2003;9(11):1418-1422.
59. Offermanns S, Toombs CF, Hu YH, Simon MI. Defective platelet activation in G alpha(q)-deficient mice. *Nature*. 1997;389(6647):183-186.
60. Wei AH, Schoenwaelder SM, Andrews RK, Jackson SP. New insights into the haemostatic function of platelets. *Br J Haematol*. 2009;147(4):415-430.
61. Shattil SJ, Brass LF. Induction of the fibrinogen receptor on human platelets by intracellular mediators. *J Biol Chem*. 1987;262(3):992-1000.
62. Ma YQ, Qin J, Plow EF. Platelet integrin alpha(IIb)beta(3): activation mechanisms. *J Thromb Haemost*. 2007;5(7):1345-1352.
63. Woods VL, Jr., Wolff LE, Keller DM. Resting platelets contain a substantial centrally located pool of glycoprotein IIb-IIIa complex which may be accessible to some but not other extracellular proteins. *J Biol Chem*. 1986;261(32):15242-15251.
64. Jenkins AL, Nannizzi-Alaimo L, Silver D, et al. Tyrosine phosphorylation of the beta3 cytoplasmic domain mediates integrin-cytoskeletal interactions. *J Biol Chem*. 1998;273(22):13878-13885.
65. Arthur WT, Petch LA, Burridge K. Integrin engagement suppresses RhoA activity via a c-Src-dependent mechanism. *Curr Biol*. 2000;10(12):719-722.
66. Flevaris P, Stojanovic A, Gong H, Chishti A, Welch E, Du X. A molecular switch that controls cell spreading and retraction. *J Cell Biol*. 2007;179(3):553-565.
67. Shattil SJ, Newman PJ. Integrins: dynamic scaffolds for adhesion and signaling in platelets. *Blood*. 2004;104(6):1606-1615.
68. Humbert M, Nurden P, Bihour C, et al. Ultrastructural studies of platelet aggregates from human subjects receiving clopidogrel and from a patient with an inherited defect of an ADP-dependent pathway of platelet activation. *Arterioscler Thromb Vasc Biol*. 1996;16(12):1532-1543.
69. Kuijpers MJ, Munnix IC, Cosemans JM, et al. Key role of platelet procoagulant activity in tissue factor-and collagen-dependent thrombus formation in arterioles and venules in vivo differential sensitivity to thrombin inhibition. *Microcirculation*. 2008;15(4):269-282.
70. Born GV. Aggregation of blood platelets by adenosine diphosphate and its reversal. *Nature*. 1962;194:927-929.
71. Ingerman-Wojenski C, Smith JB, Silver MJ. Evaluation of electrical aggregometry: comparison with optical aggregometry, secretion of ATP, and accumulation of radiolabeled platelets. *J Lab Clin Med*. 1983;101(1):44-52.
72. Holmsen H, Holmsen I, Bernhardsen A. Microdetermination of adenosine diphosphate and adenosine triphosphate in plasma with firefly luciferase system. *Anal Biochem*. 1966;17(3):456-473.
73. Scadden DT. The stem-cell niche as an entity of action. *Nature*. 2006;441(7097):1075-1079.
74. Schofield R. The relationship between the spleen colony-forming cell and the haemopoietic stem cell. *Blood Cells*. 1978;4(1-2):7-25.
75. Boskey AL, Posner AS. Bone structure, composition, and mineralization. *Orthop Clin North Am*. 1984;15(4):597-612.
76. Meghji S. Bone remodelling. *Br Dent J*. 1992;172(6):235-242.

77. Nilsson SK, Johnston HM, Coverdale JA. Spatial localization of transplanted hemopoietic stem cells: inferences for the localization of stem cell niches. *Blood*. 2001;97(8):2293-2299.
78. Zhang J, Niu C, Ye L, et al. Identification of the haematopoietic stem cell niche and control of the niche size. *Nature*. 2003;425(6960):836-841.
79. Bromberg O, Frisch BJ, Weber JM, Porter RL, Civitelli R, Calvi LM. Osteoblastic N-Cadherin is not required for microenvironmental support and regulation of hematopoietic stem and progenitor cells. *Blood*. 2012.
80. Calvi LM, Adams GB, Weibrecht KW, et al. Osteoblastic cells regulate the haematopoietic stem cell niche. *Nature*. 2003;425(6960):841-846.
81. Reya T, Duncan AW, Ailles L, et al. A role for Wnt signalling in self-renewal of haematopoietic stem cells. *Nature*. 2003;423(6938):409-414.
82. Muguruma Y, Yahata T, Miyatake H, et al. Reconstitution of the functional human hematopoietic microenvironment derived from human mesenchymal stem cells in the murine bone marrow compartment. *Blood*. 2006;107(5):1878-1887.
83. Shackney SE, Ford SS, Wittig AB. Kinetic-microarchitectural correlations in the bone marrow of the mouse. *Cell Tissue Kinet*. 1975;8(6):505-516.
84. Ara T, Tokoyoda K, Sugiyama T, Egawa T, Kawabata K, Nagasawa T. Long-term hematopoietic stem cells require stromal cell-derived factor-1 for colonizing bone marrow during ontogeny. *Immunity*. 2003;19(2):257-267.
85. Rafii S, Shapiro F, Pettengell R, et al. Human bone marrow microvascular endothelial cells support long-term proliferation and differentiation of myeloid and megakaryocytic progenitors. *Blood*. 1995;86(9):3353-3363.
86. Rafii S, Mohle R, Shapiro F, Frey BM, Moore MA. Regulation of hematopoiesis by microvascular endothelium. *Leuk Lymphoma*. 1997;27(5-6):375-386.
87. Balduini A, Pallotta I, Malara A, et al. Adhesive receptors, extracellular proteins and myosin IIA orchestrate proplatelet formation by human megakaryocytes. *J Thromb Haemost*. 2008;6(11):1900-1907.
88. Lapidot T, Kollet O. The essential roles of the chemokine SDF-1 and its receptor CXCR4 in human stem cell homing and repopulation of transplanted immune-deficient NOD/SCID and NOD/SCID/B2m(null) mice. *Leukemia*. 2002;16(10):1992-2003.
89. Mohle R, Green D, Moore MA, Nachman RL, Rafii S. Constitutive production and thrombin-induced release of vascular endothelial growth factor by human megakaryocytes and platelets. *Proc Natl Acad Sci U S A*. 1997;94(2):663-668.
90. Harrington WJ, Minnich V, Hollingsworth JW, Moore CV. Demonstration of a thrombocytopenic factor in the blood of patients with thrombocytopenic purpura. *J Lab Clin Med*. 1951;38(1):1-10.
91. McMillan R. Chronic idiopathic thrombocytopenic purpura. *N Engl J Med*. 1981;304(19):1135-1147.
92. Cines DB, Blanchette VS. Immune thrombocytopenic purpura. *N Engl J Med*. 2002;346(13):995-1008.
93. Houwerzijl EJ, Blom NR, van der Want JJ, et al. Ultrastructural study shows morphologic features of apoptosis and para-apoptosis in megakaryocytes from patients with idiopathic thrombocytopenic purpura. *Blood*. 2004;103(2):500-506.
94. Chang M, Nakagawa PA, Williams SA, et al. Immune thrombocytopenic purpura (ITP) plasma and purified ITP monoclonal autoantibodies inhibit megakaryocytopoiesis in vitro. *Blood*. 2003;102(3):887-895.
95. McMillan R, Wang L, Tomer A, Nichol J, Pistillo J. Suppression of in vitro megakaryocyte production by antiplatelet autoantibodies from adult patients with chronic ITP. *Blood*. 2004;103(4):1364-1369.
96. Branehog I, Kutti J, Weinfeld A. Platelet survival and platelet production in idiopathic thrombocytopenic purpura (ITP). *Br J Haematol*. 1974;27(1):127-143.
97. Harker LA. Thrombokinetics in idiopathic thrombocytopenic purpura. *Br J Haematol*. 1970;19(1):95-104.
98. Emmons RV, Reid DM, Cohen RL, et al. Human thrombopoietin levels are high when thrombocytopenia is due to megakaryocyte deficiency and low when due to increased platelet destruction. *Blood*. 1996;87(10):4068-4071.
99. Kappers-Klunne MC, de Haan M, Struijk PC, van Vliet HH. Serum thrombopoietin levels in relation to disease status in patients with immune thrombocytopenic purpura. *Br J Haematol*. 2001;115(4):1004-1006.

100. Chow L, Aslam R, Speck ER, et al. A murine model of severe immune thrombocytopenia is induced by antibody- and CD8+ T cell-mediated responses that are differentially sensitive to therapy. *Blood*. 2010;115(6):1247-1253.
101. Denk W, Strickler JH, Webb WW. Two-photon laser scanning fluorescence microscopy. *Science*. 1990;248(4951):73-76.
102. Zipfel WR, Williams RM, Webb WW. Nonlinear magic: multiphoton microscopy in the biosciences. *Nat Biotechnol*. 2003;21(11):1369-1377.
103. Keller PJ, Schmidt AD, Santella A, et al. Fast, high-contrast imaging of animal development with scanned light sheet-based structured-illumination microscopy. *Nat Methods*. 2010;7(8):637-642.
104. Reichardt P, Gunzer M. The biophysics of T lymphocyte activation in vitro and in vivo. *Results Probl Cell Differ*. 2006;43:199-218.
105. Sumen C, Mempel TR, Mazo IB, von Andrian UH. Intravital microscopy: visualizing immunity in context. *Immunity*. 2004;21(3):315-329.
106. Kohler A, Schmithorst V, Filippi MD, et al. Altered cellular dynamics and endosteal location of aged early hematopoietic progenitor cells revealed by time-lapse intravital imaging in long bones. *Blood*. 2009;114(2):290-298.
107. Kubista M, Andrade JM, Bengtsson M, et al. The real-time polymerase chain reaction. *Mol Aspects Med*. 2006;27(2-3):95-125.
108. White JG, Krivit W. An ultrastructural basis for the shape changes induced in platelets by chilling. *Blood*. 1967;30(5):625-635.
109. Italiano JE, Jr., Bergmeier W, Tiwari S, et al. Mechanisms and implications of platelet discoid shape. *Blood*. 2003;101(12):4789-4796.
110. Braun A, Varga-Szabo D, Kleinschnitz C, et al. Orai1 (CRACM1) is the platelet SOC channel and essential for pathological thrombus formation. *Blood*. 2009;113(9):2056-2063.
111. Elvers M, Stegner D, Hagedorn I, et al. Impaired alpha(IIb)beta(3) integrin activation and shear-dependent thrombus formation in mice lacking phospholipase D1. *Sci Signal*. 2010;3(103):ra1.
112. Calaminus SD, Thomas S, McCarty OJ, Machesky LM, Watson SP. Identification of a novel, actin-rich structure, the actin nodule, in the early stages of platelet spreading. *J Thromb Haemost*. 2008;6 (11):1944-1952.
113. Wall JE, Buijs-Wilts M, Arnold JT, et al. A flow cytometric assay using mepacrine for study of uptake and release of platelet dense granule contents. *Br J Haematol*. 1995;89(2):380-385.
114. Italiano JE, Jr., Richardson JL, Patel-Hett S, et al. Angiogenesis is regulated by a novel mechanism: pro- and antiangiogenic proteins are organized into separate platelet alpha granules and differentially released. *Blood*. 2008;111(3):1227-1233.
115. Battinelli EM, Markens BA, Italiano JE, Jr. Release of angiogenesis regulatory proteins from platelet alpha granules: modulation of physiologic and pathologic angiogenesis. *Blood*. 2011;118(5): 1359-1369.
116. Pleines I, Eckly A, Elvers M, et al. Multiple alterations of platelet functions dominated by increased secretion in mice lacking Cdc42 in platelets. *Blood*. 2010;115(16):3364-3373.
117. Shivdasani RA, Schulze H. Culture, expansion, and differentiation of murine megakaryocytes. *Curr Protoc Immunol*. 2005;Chapter 22:Unit 22F 26.
118. Shivdasani RA, Rosenblatt MF, Zucker-Franklin D, et al. Transcription factor NF-E2 is required for platelet formation independent of the actions of thrombopoietin/MGDF in megakaryocyte development. *Cell*. 1995;81(5):695-704.
119. Vyas P, Ault K, Jackson CW, Orkin SH, Shivdasani RA. Consequences of GATA-1 deficiency in megakaryocytes and platelets. *Blood*. 1999;93(9):2867-2875.
120. Kenney DM, Linck RW. The cystoskeleton of unstimulated blood platelets: structure and composition of the isolated marginal microtubular band. *J Cell Sci*. 1985;78:1-22.
121. Sazer S, Dasso M. The ran decathlon: multiple roles of Ran. *J Cell Sci*. 2000;113 (Pt 7): 1111-1118.
122. Dasso M. The Ran GTPase: theme and variations. *Curr Biol*. 2002;12(14):R502-508.
123. Denti S, Sirri A, Cheli A, et al. RanBPM is a phosphoprotein that associates with the plasma membrane and interacts with the integrin LFA-1. *J Biol Chem*. 2004;279(13):13027-13034.
124. Sehgal S, Storrie B. Evidence that differential packaging of the major platelet granule proteins von Willebrand factor and fibrinogen can support their differential release. *J Thromb Haemost*. 2007;5 (10):2009-2016.
125. Patel-Hett S, Richardson JL, Schulze H, et al. Visualization of microtubule growth in living platelets reveals a dynamic marginal band with multiple microtubules. *Blood*. 2008;111(9):4605-4616.

126. Lansbergen G, Akhmanova A. Microtubule plus end: a hub of cellular activities. *Traffic*. 2006;7(5): 499-507.
127. Wang D, Li Z, Schoen SR, Messing EM, Wu G. A novel MET-interacting protein shares high sequence similarity with RanBPM, but fails to stimulate MET-induced Ras/Erk signaling. *Biochem Biophys Res Commun*. 2004;313(2):320-326.
128. Suresh B, Ramakrishna S, Baek KH. Diverse roles of the scaffolding protein RanBPM. *Drug Discov Today*. 2012;17(7-8):379-387.
129. White JG, Rao GH. Influence of a microtubule stabilizing agent on platelet structural physiology. *Am J Pathol*. 1983;112(2):207-217.
130. Flaumenhaft R, Dilks JR, Rozenvayn N, Monahan-Earley RA, Feng D, Dvorak AM. The actin cytoskeleton differentially regulates platelet alpha-granule and dense-granule secretion. *Blood*. 2005;105 (10):3879-3887.
131. Rendu F, Marche P, Viret J, et al. Signal transduction in normal and pathological thrombin-stimulated human platelets. *Biochimie*. 1987;69(4):305-313.
132. Reed GL. Platelet secretory mechanisms. *Semin Thromb Hemost*. 2004;30(4):441-450.
133. Stark F, Golla R, Nachmias VT. Formation and contraction of a microfilamentous shell in saponin-permeabilized platelets. *J Cell Biol*. 1991;112(5):903-913.
134. Klages B, Brandt U, Simon MI, Schultz G, Offermanns S. Activation of G12/G13 results in shape change and Rho/Rho-kinase-mediated myosin light chain phosphorylation in mouse platelets. *J Cell Biol*. 1999;144(4):745-754.
135. Vogt S, Grosse R, Schultz G, Offermanns S. Receptor-dependent RhoA activation in G12/G13-deficient cells: genetic evidence for an involvement of Gq/G11. *J Biol Chem*. 2003;278(31):28743-28749.
136. Pleines I, Hagedorn I, Gupta S, et al. Megakaryocyte-specific RhoA deficiency causes macrothrombocytopenia and defective platelet activation in hemostasis and thrombosis. *Blood*. 2011;119 (4):1054-1063.
137. Dowal L, Flaumenhaft R. Targeting platelet G-protein coupled receptors (GPCRs): looking beyond conventional GPCR antagonism. *Curr Vasc Pharmacol*. 2010;8(2):140-154.
138. Bergmeier W, Rackebrandt K, Schroder W, Zirngibl H, Nieswandt B. Structural and functional characterization of the mouse von Willebrand factor receptor GPIb-IX with novel monoclonal antibodies. *Blood*. 2000;95(3):886-893.
139. Nieswandt B, Bergmeier W, Rackebrandt K, Gessner JE, Zirngibl H. Identification of critical antigen-specific mechanisms in the development of immune thrombocytopenic purpura in mice. *Blood*. 2000;96(7):2520-2527.
140. Levine RF, Hazzard KC, Lamberg JD. The significance of megakaryocyte size. *Blood*. 1982;60(5): 1122-1131.
141. Salic A, Mitchison TJ. A chemical method for fast and sensitive detection of DNA synthesis in vivo. *Proc Natl Acad Sci U S A*. 2008;105(7):2415-2420.
142. Nugent D, McMillan R, Nichol JL, Slichter SJ. Pathogenesis of chronic immune thrombocytopenia: increased platelet destruction and/or decreased platelet production. *British Journal of Haematology*. 2009;146(6):585-596.
143. Chang M. Immune thrombocytopenic purpura (ITP) plasma and purified ITP monoclonal autoantibodies inhibit megakaryocytopoiesis in vitro. *Blood*. 2003;102(3):887-895.
144. Lichtman MA, Chamberlain JK, Simon W, Santillo PA. Parasinusoidal location of megakaryocytes in marrow: a determinant of platelet release. *Am J Hematol*. 1978;4(4):303-312.
145. Schulze H, Gaedicke G. Immune thrombocytopenia in children and adults: what's the same, what's different? *Haematologica*. 2011;96(12):1739-1741.
146. Rajantie J, Zeller B, Treutiger I, Rosthoj S. Vaccination associated thrombocytopenic purpura in children. *Vaccine*. 2007;25(10):1838-1840.
147. Semple JW, Provan D. The immunopathogenesis of immune thrombocytopenia: T cells still take center-stage. *Curr Opin Hematol*. 2012;19(5):357-362.
148. Katsman Y, Foo AH, Leontyev D, Branch DR. Improved mouse models for the study of treatment modalities for immune-mediated platelet destruction. *Transfusion*. 2010;50(6):1285-1294.
149. Ucar C, Oren H, Irken G, et al. Investigation of megakaryocyte apoptosis in children with acute and chronic idiopathic thrombocytopenic purpura. *Eur J Haematol*. 2003;70(6):347-352.
150. Kienast J, Schmitz G. Flow cytometric analysis of thiazole orange uptake by platelets: a diagnostic aid in the evaluation of thrombocytopenic disorders. *Blood*. 1990;75(1):116-121.

151. Briggs LC, Ashton RM, Metcalf P. Development of a highly sensitive screen for influenza A in guano and its application in the search for ancient RNA preserved under Antarctic Adelie penguin colonies. *Avian Dis*. 2003;47(3 Suppl):1200-1202.
152. Strauss G, Vollert C, von Stackelberg A, Weimann A, Gaedicke G, Schulze H. Immature platelet count: a simple parameter for distinguishing thrombocytopenia in pediatric acute lymphocytic leukemia from immune thrombocytopenia. *Pediatr Blood Cancer*. 2011;57(4):641-647.
153. Rinder HM, Tracey JB, Recht M, et al. Differences in platelet alpha-granule release between normals and immune thrombocytopenic patients and between young and old platelets. *Thromb Haemost*. 1998;80(3):457-462.
154. Harker LA, Slichter SJ. The bleeding time as a screening test for evaluation of platelet function. *N Engl J Med*. 1972;287(4):155-159.
155. Slichter SJ. Relationship between platelet count and bleeding risk in thrombocytopenic patients. *Transfus Med Rev*. 2004;18(3):153-167.
156. Crow AR, Song S, Semple JW, Freedman J, Lazarus AH. IVIg inhibits reticuloendothelial system function and ameliorates murine passive-immune thrombocytopenia independent of anti-idiotype reactivity. *Br J Haematol*. 2001;115(3):679-686.
157. Newman PJ, Newman DK. Signal transduction pathways mediated by PECAM-1: new roles for an old molecule in platelet and vascular cell biology. *Arterioscler Thromb Vasc Biol*. 2003;23(6):953-964.
158. Reedquist KA, Ross E, Koop EA, et al. The small GTPase, Rap1, mediates CD31-induced integrin adhesion. *J Cell Biol*. 2000;148(6):1151-1158.
159. Patil S, Newman DK, Newman PJ. Platelet endothelial cell adhesion molecule-1 serves as an inhibitory receptor that modulates platelet responses to collagen. *Blood*. 2001;97(6):1727-1732.
160. Turner RR, Beckstead JH, Warnke RA, Wood GS. Endothelial cell phenotypic diversity. In situ demonstration of immunologic and enzymatic heterogeneity that correlates with specific morphologic subtypes. *Am J Clin Pathol*. 1987;87(5):569-575.
161. Kumar S, West DC, Ager A. Heterogeneity in endothelial cells from large vessels and microvessels. *Differentiation*. 1987;36(1):57-70.
162. Lagrue-Lak-Hal AH, Debili N, Kingbury G, et al. Expression and function of the collagen receptor GPVI during megakaryocyte maturation. *J Biol Chem*. 2001;276(18):15316-15325.
163. Savage B, Saldivar E, Ruggeri ZM. Initiation of platelet adhesion by arrest onto fibrinogen or translocation on von Willebrand factor. *Cell*. 1996;84(2):289-297.
164. Leven RM, Tablin F. Extracellular matrix stimulation of guinea pig megakaryocyte proplatelet formation in vitro is mediated through the vitronectin receptor. *Exp Hematol*. 1992;20(11):1316-1322.
165. Takahashi R, Sekine N, Nakatake T. Influence of monoclonal antiplatelet glycoprotein antibodies on in vitro human megakaryocyte colony formation and proplatelet formation. *Blood*. 1999;93(6): 1951-1958.
166. Nilsson SK, Debatis ME, Dooner MS, Madri JA, Quesenberry PJ, Becker PS. Immunofluorescence characterization of key extracellular matrix proteins in murine bone marrow in situ. *J Histochem Cytochem*. 1998;46(3):371-377.
167. Kleinman HK, McGarvey ML, Liotta LA, Robey PG, Tryggvason K, Martin GR. Isolation and characterization of type IV procollagen, laminin, and heparan sulfate proteoglycan from the EHS sarcoma. *Biochemistry*. 1982;21(24):6188-6193.
168. Vogel V. Mechanotransduction involving multimodular proteins: converting force into biochemical signals. *Annu Rev Biophys Biomol Struct*. 2006;35:459-488.
169. Sternlicht MD, Lochter A, Sympson CJ, et al. The stromal proteinase MMP3/stromelysin-1 promotes mammary carcinogenesis. *Cell*. 1999;98(2):137-146.
170. Zitka O, Kukacka J, Krizkova S, et al. Matrix metalloproteinases. *Curr Med Chem*. 2010;17(31): 3751-3768.
171. Rodriguez D, Morrison CJ, Overall CM. Matrix metalloproteinases: what do they not do? New substrates and biological roles identified by murine models and proteomics. *Biochim Biophys Acta*. 2010;1803(1):39-54.
172. Janowska-Wieczorek A, Marquez LA, Nabholtz JM, et al. Growth factors and cytokines upregulate gelatinase expression in bone marrow CD34(+) cells and their transmigration through reconstituted basement membrane. *Blood*. 1999;93(10):3379-3390.
173. Jepsen KJ. Systems analysis of bone. *Wiley Interdiscip Rev Syst Biol Med*. 2009;1(1):73-88.

7. Appendix

7.1. Eidesstattliche Erklärung

Ich versichere, dass ich diese Arbeit selbständig verfasst und keine anderen, als die angegebenen Quellen und Hilfsmittel benutzt habe. Diese Arbeit hat in gleicher oder ähnlicher Form noch keiner Prüfungsbehörde vorgelegen. Aus Prioritätsgründen wurden weite Teile dieser Arbeit bereits veröffentlicht. Kapitel 2.1, 2.2 und 3.1 wurden aus den Publikationen *Blood.*114:5532 (http://dx.doi.org/10.1182/blood-2009-04-216804)und *Blood*. 120:3594 (http://dx.doi.org/10.1182/blood-2012-01-401737) übernommen. Daten in Abbildungen, die in Zusammenarbeit entstanden sind, wurden als solche gekennzeichnet.

Berlin, im September 2012

_____

Imke Meyer

7.2. Curriculum Vitae

For reasons of data protection, the curriculum vitae is not included in the online version.

Supplementary Videos:

Video 1

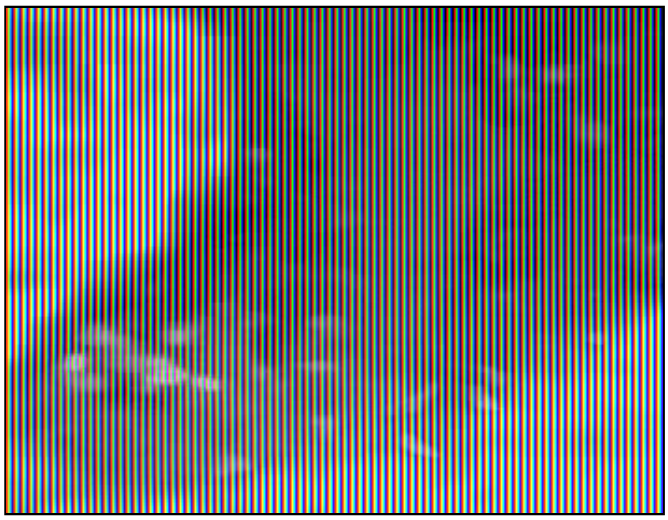

Video 2

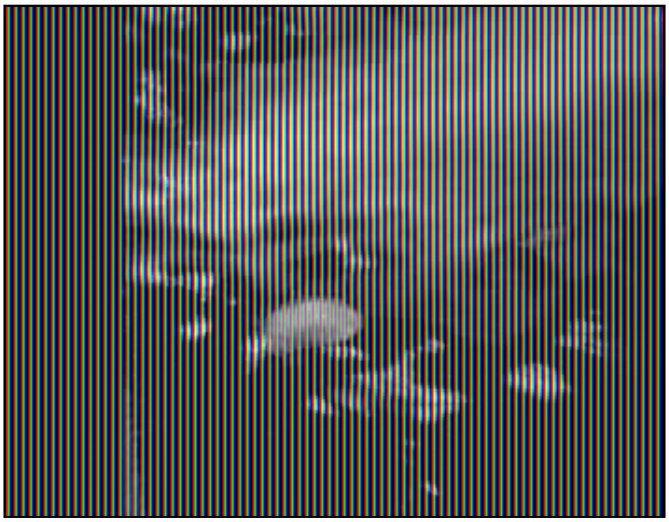

Video 3

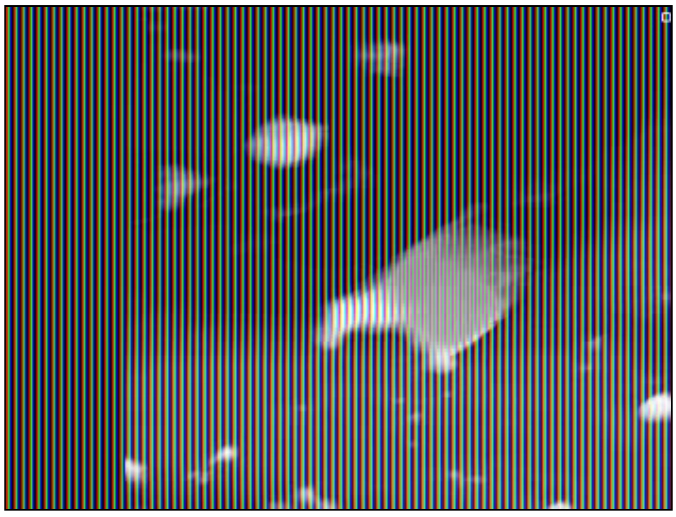

Video 4

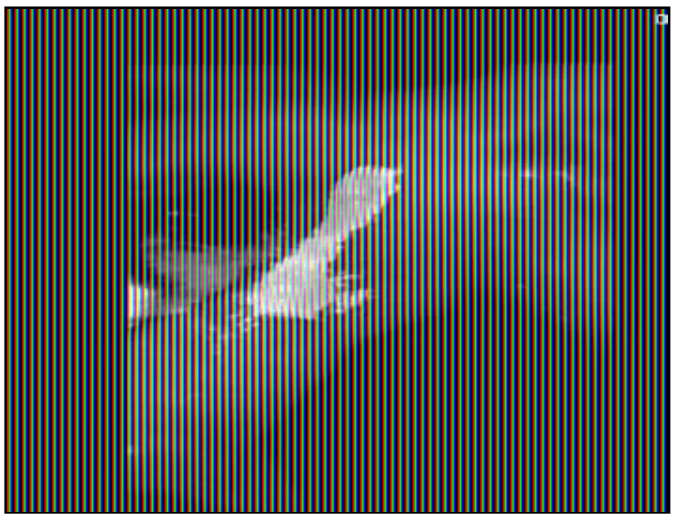

Video 5

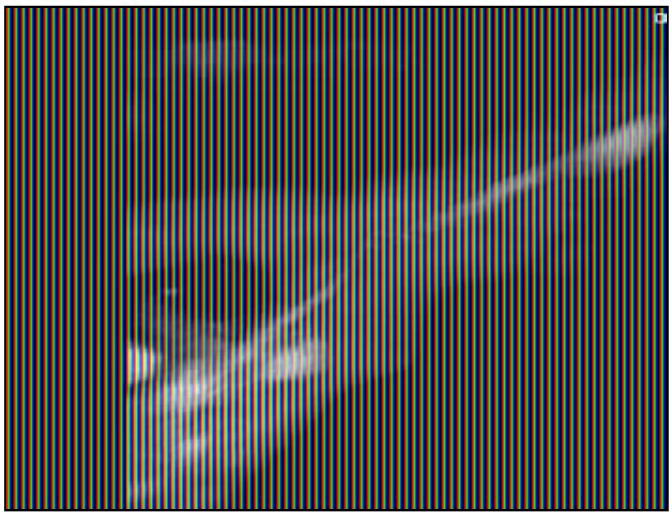

Video 6

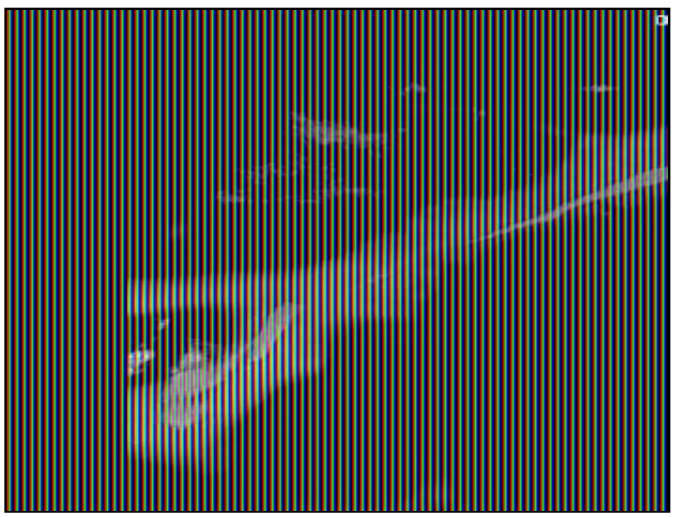

Condicio sine qua non